

When Robotics Meets Wireless Communications: An Introductory Tutorial

Daniel Bonilla Licea⁺ *Member, IEEE*, Mounir Ghogho^{†*}, *Fellow Member, IEEE*, and Martin Saska⁺,

⁺Czech Technical University in Prague, Czech Republic

[†]International University of Rabat, College of Engineering & Architecture, TICLab, Morocco

^{*} School of Electronic and Electrical Engineering, University of Leeds, UK

bonildan@fel.cvut.cz, m.ghogho@ieee.org, martin.saska@fel.cvut.cz

Abstract—The importance of ground Mobile Robots (MRs) and Unmanned Aerial Vehicles (UAVs) within the research community, industry, and society is growing fast. Nowadays, many of these agents are equipped with communication systems that are, in some cases, essential to successfully achieve certain tasks. In this context, we have begun to witness the development of a new interdisciplinary research field at the intersection of robotics and communications. This research field has been boosted by the intention of integrating UAVs within the 5G and 6G communication networks, and will undoubtedly lead to many important applications in the near future. Nevertheless, one of the main obstacles to the development of this research area is that most researchers address these problems by oversimplifying either the robotics or the communications aspects. Doing so impedes the ability to reach the full potential of this new interdisciplinary research area. In this tutorial, we present some of the modelling tools necessary to address problems involving both robotics and communication from an interdisciplinary perspective. As an illustrative example of such problems, we focus on the issue of communication-aware trajectory planning in this tutorial.

Index Terms—Communication, control, trajectory planning, robot, UAV.

I. INTRODUCTION

Interdisciplinary research involving communications and robotics is gaining momentum, as evidenced by the steady increase in publications from the robotics [1], [2], [3], [4], control [5], [6], [7], [8], [9], and communications [10], [11], [12], [13], [14], [15], [16], [17] communities, which are dealing with Mobile Robots (MRs) and communications issues. Some reasons behind the growing interest include the emergence of 5G technology that aims to integrate Unmanned Aerial Vehicles (UAVs) into the cellular communication network [18], [19] and the growing importance of robotic swarms [20]. From an application perspective, we can divide these interdisciplinary problems into two categories: Robotics-assisted Communications (RaC) and Communications-assisted Robotics (CaR).

In RaC applications, generally one or multiple MRs are incorporated into a communication network with the intent to improve the performance of the latter; the MRs typically operate as mobile relays, data ferries, or mobile flying Base

This work was partially funded by the European Union's Horizon 2020 research and innovation programme AERIAL-CORE under grant agreement no. 871479.

Stations (BSs) on-board UAVs. The main objective of RaC is to control the behavior of the added MR in order to improve the performance of the communications network. In traditional mobile communications, the transceiver's position is considered *uncontrollable* and random. In RaC, the transceiver's position is *controllable*, and thus constitutes an additional communication system parameter to be optimized. This small, but important difference opens up new and exciting possibilities in the design of communication systems involving MRs. For example, in the context of diversity techniques for the small-scale fading compensation, it is widely accepted that designing the diversity branches in such a way as to make the channels statistically independent maximizes the diversity gain and, therefore, the performance. By analyzing the same problem while considering a transceiver mounted on an MR, we demonstrated in [21] that by controlling and adapting the MR's position, we can obtain diversity branches that yield a higher diversity gain than that which is obtained with statistically independent branches. This short example provides a brief glimpse into the possibilities of going beyond the old theoretical bounds stated in classical communication problems if we treat the controlled mobility of the transceiver as an additional parameter of the communications system.

In CaR applications, the communication capabilities of the MR are leveraged to help the robotic system to better perform tasks. Communication is an essential component that enables multi-robot applications [22] and UAV swarms [20], [23], [3]. Communication between the MRs allows the exchange of different types of information, such as: relative localization, allowing for the creation of formations or the navigation of surroundings in a coordinated manner; sensing data, which could be used in mapping applications; and signalisation data to coordinate the behaviour of the team, among others. Often in CaR applications, the MRs must execute certain robotic tasks while considering the communication quality and swarm connectivity to ensure adequate behaviour of the robotic team.

To efficiently address the problems encountered in RaC and CaR applications, we argue that a good understanding of *both* communications and robotics is required. Indeed, as will be described later, there is often a deep entanglement between the communications and robotics aspects in such problems. Considering only the communications aspects and oversimplifying the MR's model might produce an energy inefficient solution that wastes too much energy in motion, or

even an unfeasible solution for a real MR due to a breach of its own mechanical constraints. On the other hand, focusing on the robotics aspects and oversimplifying the communication model may lead the MR to fail to complete its task due to unexpected communication failures, which may arise from poorer connectivity or a lower bit rate than that expected with the oversimplified model. Therefore, an interdisciplinary approach is essential when dealing with CaR and RaC problems in order to propose functionally adequate solutions and to fully exploit all underlying opportunities in this new research area. The importance of such an interdisciplinary approach has also been recently recognized in [24], [25], where the authors proposed a simulation framework that allows for coordinating a robotics simulator (e.g. Robot Operating System (ROS)), a communications network simulator, and an antenna simulator. This enables accurately simulating the dynamics of the robot and the communications channel.

In the literature, however, CaR and RaC problems are often not addressed with such an interdisciplinary approach. Indeed, oversimplified models are often adopted for either the communications or the robotics aspects. This oversimplification causes the researchers to miss interesting results and opportunities, or even to derive techniques that would fail when tested on real robots equipped with real communication systems. Some tutorials have recently been published on communications-aware robotics problems, however they still simplify either the robotics or communications aspects. For instance, the tutorial [19] discusses UAV communications with great detail from the communications perspective, but treats the control and robotics aspects in a superficial manner. The authors in [19] mention that, to the best of their knowledge, no rigorous expression for the UAV energy consumption for a given trajectory has been derived. As we will show in subsection II-B, such a statement is imprecise and comes from a lack of understanding of the UAV dynamic models and control theory. On the other hand, the robotics community generally oversimplifies the communication model. For instance, the authors of [26] consider the problem of a team of data-gathering MRs and assume a binary disk model [27] for the communication channel. In this model, the communication is perfect as long as two MRs remain within a certain distance of each other, although this model is far from reality, as we shall see in section III-A.

To our knowledge, in the literature, there are no surveys or tutorials which have taken an interdisciplinary approach to address CaR or RaC problems. The aim of this tutorial is to contribute to closing this gap and raising awareness of the importance of an interdisciplinary approach when tackling these problems. To illustrate the opportunities and challenges of this approach, we focus on the important problem of Trajectory Planning (TP) within the context of CaR and RaC applications, henceforth referred to as Communications-aware Trajectory Planning (CaTP). We hope that this tutorial will contribute to the quality and quantity of new research done in this exciting and promising, yet underdeveloped, research area.

This tutorial is organized as follows. In section II, we describe in detail the basic and crucial mobile robotics aspects

and models. Section III describes the different aspects of communications systems that are relevant to CaTP problems and discusses modelling the wireless communication channels. In section IV, the general structure of various CaTP problems, different types of cost functions, and constraints involved in these problems are described. Finally, section V provides conclusions and discusses some open research problems and opportunities.

II. MOBILE ROBOT MODELING

Mathematically modelling a phenomenon or object consists of describing it in terms of certain aspects of interest and under certain conditions. We can divide the model into four components:

- 1) **Object representation:** in our case, the object to be modelled is the MR. The object representation is a mathematical abstraction of the physical MR that describes properties that are relevant for the problem at hand. In the context of trajectory planning problems, the MR can be described as a single point¹ with orientation, even if the real object itself occupies non-zero physical space. This is a suitable representation of the MR for trajectory planning problems, although it may be inadequate for other problems, such as the mechanical analysis of the MR's frame.
- 2) **Model Input:** the model input is a set containing all controllable variables and whose effect on the object representation will be captured by the mathematical model. There might be other controllable variables which affect the object representation, but the model input includes only the variables considered in the mathematical model.
- 3) **Range of validity:** this consists of all of the conditions under which the model will adequately describe the behaviour of the object representation, e.g. the assumptions on the considered scenarios and ranges of variations for the variables forming the model input. Note that, the model input together with the range of validity provides us the **model input space**. This space is the set of all valid values that the model input can take.
- 4) **Input-to-object relation:** this is the mapping rule that relates any element within the model input space to a corresponding element within the **object representation space**. In the case of analytical models, this relation can take the form of explicit mathematical equations, while in the case of numerical methods, it can take the form of numerical-lookup tables or neural networks.

Simplicity is always a desirable property in modelling as it brings tractability, facilitates mathematical analysis, lowers computational requirements, and allows for better problem understanding. One of the fundamental problems in modelling is finding a compromise between simplicity and accuracy that reflects the difference between the behaviour of the mathematical model and the real object. Simple models tend to be highly inaccurate and have reduced ranges of validity; highly accurate models with large ranges of validity tend to be very complex

¹This holds only if the obstacles and the other MRs are dilated to avoid collisions with the considered MR.

and have little tractability, hence the importance of selecting an adequate level of model complexity. Oversimplification of the model occurs when it is used beyond its range of validity or when variables that have a significant impact on the object representation are disregarded.

Let us analyse this problem in more detail by discussing two important consequences of using oversimplified models for robots in the context of CaTP:

- 1) *Involuntary energy waste*: Oversimplifying the motion-induced energy consumption model while searching for minimum energy trajectories may significantly degrade performance. This is illustrated with the scenario described in [28], where a rotary-wing UAV (i.e. with propellers and, therefore, hovering capability) has to collect data from a sensor network. The authors optimize the UAV trajectory to accomplish this task in minimum time and assume that the energy consumed by the UAV is proportional to the time that the UAV spends in the air. In other words, the authors implicitly model the UAV energy consumption as being proportional to the flying time, thus expecting that a real UAV following the trajectory optimized according to the assumed energy model would indeed accomplish its assigned task while draining the minimum energy from its battery.

For those who are unfamiliar with aeronautics or with aerial robotics, the energy model mentioned above might seem reasonable. However, in [29], the authors present an aerodynamic power consumption model for a rotary-wing UAV that shows that the power consumption also depends on the horizontal speed of the UAV. This model contains a term that increases with the horizontal UAV speed due to the blade's drag. Hence, a UAV executing the minimum time trajectory will travel as fast as possible and consume a large amount of energy instead of minimizing energy consumption.

- 2) *Unfeasibility of designed trajectory*: another problem of oversimplified models is the possibility of obtaining a trajectory that does not satisfy robot motion constraints. This may lead to collisions with obstacles or among robots, as well as failures to perform the planned tasks. This occurs when the MR's motion model disregards the specific kinematic or dynamic constraints of the MR under consideration.

Let us illustrate this with the following example. Assume that we want to design a trajectory for a car-like MR to pass in a predefined order through a set of points of interest $\{\mathbf{o}_k\}_k^K$ in a minimum time. We first model the car-like MR with a single integrator, i.e. the position $\mathbf{p}(t)$ of the robot at time t is described by:

$$\mathbf{p}(t) = \mathbf{p}(0) + \int_0^t \mathbf{v}(\tau) \tau, \quad (1)$$

where $\mathbf{p}(0)$ is the MR's initial position and $\mathbf{v}(\tau)$ is its velocity, which can be directly controlled. To make the model more realistic, we take into account the maximum translational speed of the robot, and thus add the following constraint $\|\mathbf{v}(\tau)\|_2 < V_{max}$. According to this model, the optimum trajectory that allows the MR

to pass through all the points of interest in the minimum time is a piece-wise linear path linking consecutive points of interest, requiring the MR to use the maximum linear speed possible, V_{max} , at all times.

Following this piece-wise linear path continuously at a constant linear speed without stopping until reaching the end of the path would require, in general, that the MR instantaneously changes direction at each point of interest without stopping. However, this is an impossible manoeuvre for a car-like MR due to its dynamic and kinematic constraints. Its dynamic constraints will not allow abrupt changes in velocity (whether the change is in direction or in magnitude) and its kinematic constraints will limit the curvature of the turns it can execute. Now, assume that we allow the MR to stop at each point of interest of the piece-wise linear path. This would now require the robot to rotate on the spot at each point of interest in order to change direction and then continue its path. Yet, this manoeuvre is also impossible for the car-like MR due to the kinematic constraints imposed by its own physical geometry.

Clearly, the model (1) used in this example oversimplifies the motion capabilities of the car-like MR. Thus, the solution for the trajectory planning problem derived from such a model results in an unfeasible trajectory for the real car-like MR. Some post-processing, e.g. smoothing the path, could be done on the resulting trajectory to make it feasible for the real MR, however this would still require considering the MR's kinematic and/or dynamic constraints.

In some cases, increasing the complexity of the MR models may bring only small benefits. For instance, in [30] the authors considered a three wheeled omnidirectional MR and compared two approaches of finding a minimum energy trajectory. The first trajectory was optimized using a certain dynamic model of the robot; the second trajectory used the same dynamic model of the robot, except that it neglected the term accounting for the Coriolis force. Both trajectories were then tested on a real MR. The results showed that when the robot tracked the second trajectory (optimized with the simpler dynamic model), it consumed just slightly more energy than when it tracked the first one.

As we have explained above, the oversimplification of MR models can have serious consequences, thus the importance of selecting an adequate model complexity. In order to help researchers with no (or little) robotics background, the rest of this section provides a general description of mathematical models describing the motion and energy consumption for two popular MRs: ground wheeled robots and aerial rotary-wing(s) robots. We will present an overview of the different types of models, their implications, and their limitations. This does not constitute an exhaustive list of all the mathematical models associated with these MRs, but rather an introductory presentation for common models used in trajectory planning. Readers familiar with this research area can skip to section III where we discuss the modelling of communication systems and the wireless channel.

Before moving to the next subsection, we must mention

that selecting the appropriate complexity of the models is not always an easy task and sometimes does not have a clear, or even a unique *correct* answer. This is highly dependent on the particular and specific conditions of the problem to be solved. In this tutorial, we aim to raise awareness about the problems related to oversimplification, while underlining that the solution to the latter is not an overcomplexification. Indeed, overly complex models might solve some issues due to oversimplification, but may also cause other problems, such as a lack of tractability and the high computational load of the solutions.

A. Wheeled Mobile Robots (WMRs)

WMRs [31] can be implemented in a simple and relatively inexpensive way, making them highly popular for numerous applications, particularly in the context of trajectory planning. They can be classified according to the number of wheels, their wheel type, and spatial configuration within the WMR's frame. These aspects determine the kinematic constraints of the robot. Therefore, before discussing the kinematic model, we briefly present the wheels used in typical WMRs. Some common types include [32]:

- 1) Conventional wheels: these wheels have two degrees of freedom (DOFs), including rotation around its axis line and rotation around its contact point with the floor.
- 2) Omnidirectional wheels: this is a special type of wheel constructed using a main conventional wheel with embedded small rollers whose orientation is not aligned with that of the main wheel. This special configuration allows the omnidirectional wheel to operate not only as a conventional wheel, but also to advance along the direction orthogonal to the main wheel's orientation. These wheels can be actuated (i.e. mechanically coupled directly or indirectly to a motor's shaft).

Kinematics is the field of mechanics that studies the motion of objects without considering the effect of forces. WMR kinematic models describe the relationship between the angular speed of the WMR's actuated wheels and the velocity of the WMR's object representation, i.e., the translational and angular velocities of \mathbf{p} . There are two types of kinematic models: the forward kinematic model and the inverse kinematic model. Forward kinematic models describe the WMR's velocities in terms of the angular speeds of the wheels, i.e. the wheels' angular speeds are the model's inputs, and the WMR's velocities are the model's output. Inverse kinematic models describe the opposite relation: the WMR's velocities are the model's inputs, and the angular speeds of the wheels are the model's outputs. The forward kinematic model is useful for analyzing the movement of the WMR generated by a particular control signal applied to its motors. The inverse kinematic model is useful to make the WMR's controller track a desired trajectory (i.e. the model's input is the desired trajectory and the model's output is the required wheels' angular speeds).

In the following sections, we will discuss the above-mentioned kinematic models for various WMRs.

1) *Forward Kinematic Model*: As mentioned before, although WMRs are not single points in the plane, but rather

systems that cover a certain area, their object representation consists of their horizontal position \mathbf{p} and orientation ϕ (WMRs usually operate in 2D). The point \mathbf{p} is a point on the WMR's frame whose exact location is selected to facilitate kinematic and dynamic analysis. For instance, in the Three Wheeled Omnidirectional Robot (TOMR) of Fig. 2, the point \mathbf{p} is chosen to be the geometrical center of the MR, but in the Differential Drive Robot (DDR), the point \mathbf{p} is the center of the axis-line of the actuated wheels, rather than the geometrical center of the robot, see Fig. 1. Other choices for \mathbf{p} are also possible, but these would complicate the mathematical analysis of the motion models.

Each type of wheel and their location within the WMR's frame determines the forward kinematic model, and each type imposes different constraints. For instance, a conventional wheel is allowed rotational slippage around its contact point with the floor, but is not allowed translational slippage. The key hypotheses in the kinematic model derivation are the following: (i) the WMR's frame is solid and suffers no deformation; (ii) all the wheels are in contact with the floor at all times, which implies the consideration of a flat floor; (iii) each wheel is in contact with the floor only at a single point. For more details about the derivations of forward kinematic models, the interested reader can consult [32].

In terms of number of wheels, the unicycle is the simplest WMR whose kinematic model of the unicycle is described in [33]. Then we have bicycle which is a vehicle that has a back conventional wheel and a front steerable conventional wheel. Its kinematic model will depend if the driving wheel is the front wheel or the back wheel, see [33] for more details.

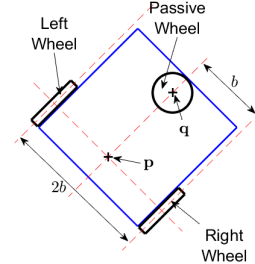


Figure 1: Differential Drive robot diagram.

Now, we consider the DDR, see Fig. 1. This robot has two conventional wheels, of radii r , which are actuated by separate motors. The horizontal position of the DDR is determined by the point \mathbf{p} located in the center of the line linking the points of contact of both wheels with the floor. The distance between these points is $2b$. A third unactuated wheel making contact with the floor at point \mathbf{q} provides mechanical stability; it is chosen so that it does not impose any kinematic constraints. The corresponding kinematic model for the DDR is [34]:

$$\begin{bmatrix} \dot{x} \\ \dot{y} \\ \dot{\theta} \end{bmatrix} = \frac{r}{2} \begin{bmatrix} \cos(\theta) & \cos(\theta) \\ \sin(\theta) & \sin(\theta) \\ \frac{1}{b} & -\frac{1}{b} \end{bmatrix} \begin{bmatrix} \omega_R \\ \omega_L \end{bmatrix}, \quad (2)$$

where $\omega_R \in \mathbb{R}$ and $\omega_L \in \mathbb{R}$ are the angular speeds of the right and left wheels, x and y are the x and y positions of the DDR, respectively, and θ is its orientation. The model input vector in (2) is two dimensional, while the DDR configuration (i.e.

the output vector) is three dimensional. This implies that the DDR translational velocity (i.e. $[\dot{x}, \dot{y}]$) and its angular speed $\dot{\theta}$ cannot be controlled independently. The DDR translational speed (i.e. the magnitude of the DDR translational velocity) and its angular speed are expressed as:

$$\begin{bmatrix} v \\ \dot{\theta} \end{bmatrix} = \frac{r}{2} \begin{bmatrix} 1 & 1 \\ 1 & -1 \end{bmatrix} \begin{bmatrix} \omega_R \\ \omega_L \end{bmatrix}. \quad (3)$$

Another common WMR is the car-like robot. It has two rear conventional wheels which are mechanically coupled to the same motor, and also has two conventional steerable front wheels which are mechanically coupled. Its kinematic model is described in [35].

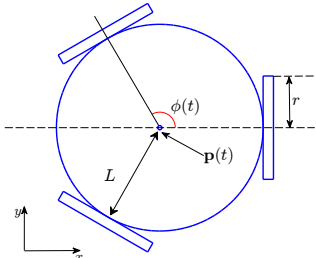


Figure 2: Three-wheeled omnidirectional robot diagram.

Another class of WMR includes omnidirectional robots. They have the particularity of using omnidirectional wheels to enable the robot's omnidirectional motion, i.e., moving in any direction at any time. One popular MR belonging to this class is the TOMR, see Fig. 2. Its kinematic model is [36]:

$$\begin{bmatrix} \dot{x} \\ \dot{y} \\ \dot{\phi} \end{bmatrix} = r \begin{bmatrix} 0 & 1 & L \\ -\sin\left(\frac{\pi}{3}\right) & -\cos\left(\frac{\pi}{3}\right) & L \\ \sin\left(\frac{\pi}{3}\right) & -\cos\left(\frac{\pi}{3}\right) & L \end{bmatrix}^{-1} \begin{bmatrix} \omega_1 \\ \omega_2 \\ \omega_3 \end{bmatrix}, \quad (4)$$

where r is the radii of the omnidirectional wheels, ω_i is the angular speed of the i th wheel, and L is the distance from the wheels to the robot's center. Unlike the kinematic models of the DDR and of the car-like robot, that of the TOMR is fully invertible analytically. Hence, we can always independently determine the translational velocity and the angular speed of the MR to find the corresponding exact angular speed of each wheel. Therefore, the TOMR does not present any kinematic restriction on its motion, but dynamic constraints still need to be considered, as will be described in section II-A3.

2) *Inverse Kinematic Model*: As explained in the previous section, the forward kinematic model is obtained by analysing the MR's geometry and applying the motion constraints imposed by the wheels. The inverse kinematic models are obtained by inverting the forward kinematic model.

In some cases, the derivation of the inverse kinematic model is straightforward. For instance, consider the kinematic model of the TOMR (4). This is a linear model involving an invertible matrix, and thus the inverse kinematic model for the three-wheeled omnidirectional MR is:

$$\begin{bmatrix} \omega_1 \\ \omega_2 \\ \omega_3 \end{bmatrix} = \frac{1}{r} \begin{bmatrix} 0 & 1 & L \\ -\sin\left(\frac{\pi}{3}\right) & -\cos\left(\frac{\pi}{3}\right) & L \\ \sin\left(\frac{\pi}{3}\right) & -\cos\left(\frac{\pi}{3}\right) & L \end{bmatrix} \begin{bmatrix} \dot{x} \\ \dot{y} \\ \dot{\phi} \end{bmatrix}. \quad (5)$$

Similarly, the inverse kinematic model for the DDR can be derived from inverting (3):

$$\begin{bmatrix} \omega_R \\ \omega_L \end{bmatrix} = \frac{b}{r} \begin{bmatrix} \frac{1}{b} & 1 \\ \frac{1}{b} & -1 \end{bmatrix} \begin{bmatrix} v \\ \dot{\theta} \end{bmatrix}. \quad (6)$$

Finally, some MRs have complex forward kinematic models that are difficult to invert analytically due to nonlinearities and singularities. In such cases, alternatives for the derivation of the inverse kinematic model are based on machine learning techniques [37].

3) *Dynamic Model*: Dynamic models consider the forces exerted by the robot on its environment. They relate the WMR motion to the torque exerted by each motor and the electric signals producing it. WMR can be modelled as a nonlinear dynamic system whose general form is [38]:

$$\dot{\mathbf{z}} = f(\dot{\mathbf{z}}, \mathbf{u}), \quad (7)$$

where \mathbf{z} is the *state vector* of the WMR², where \mathbf{u} is the input signal vector and $f(\cdot)$ is a general function, which can be linear or non-linear. Let us begin the discussion of dynamic models with the popular *pure integrator model*:

$$\frac{d^n \mathbf{p}(t)}{dt^n} = \mathbf{u}(t), \quad n \in \mathbb{N}^+, \quad (8)$$

where \mathbf{u} is the control signal and \mathbf{p} is the WMR position. (8) models a generic omnidirectional robot. It is also a very popular model due to its simplicity, which eases the theoretical analyses. This allows analytical results to be derived with less effort than with the use of more elaborate dynamic models (at the expense of accuracy, however).

Next, we discuss the order n in the model (8). If $n = 1$, we obtain the *single integrator model*, which allows for abrupt velocity changes. This model can describe with some accuracy the WMR motion under any of the following conditions: (i) the WMR speed is constant or changes slowly; (ii) the WMR dynamics is fast enough to follow the input. In [22], the authors used this model to design trajectories, which were then tested experimentally on real WMRs.

The model (8) with $n = 2$, which is referred to as the *double integrator model*, limits the WMR acceleration. It is also a very common model in mobile robotics [5], [39].

The *pure integrator model* is a very simple general model used to describe a variety of WMRs, but greatly lacks accuracy. We will now begin to discuss more complex and specific dynamic models.

Most WMRs use Direct Current (DC) motors to drive their wheels [34] as they are cheap, easy to control, and efficient. The WMR's dynamic model can be derived by first modeling the DC motor and then by combining the motor models while

²The state vector is a vector composed of a set of state variables. Broadly speaking, a set of state variables is the minimum set of variables required (in addition to the input) to uniquely determine the state vector. For more information on the subject, see [38].

considering the MR frame. Following such a procedure, a dynamic model for the DDR is found to be [34]:

$$\dot{\mathbf{z}} = \mathbf{A}\mathbf{z} + \mathbf{B}\mathbf{u}, \quad (9)$$

$$\dot{\mathbf{p}} = \begin{bmatrix} \cos(\phi) & \sin(\phi) & 0, \\ 0 & 0 & 1, \end{bmatrix}^T \mathbf{z}, \quad (10)$$

$$\mathbf{z} = \mathbf{T}_q \begin{bmatrix} \omega_R \\ \omega_L \end{bmatrix}, \quad (11)$$

$$\mathbf{T}_q = \frac{r}{2} \begin{bmatrix} 1 & 1 \\ b^{-1} & -b^{-1} \end{bmatrix}, \quad (12)$$

$$\mathbf{p} = [\mathbf{x}, \mathbf{y}, \phi]^T, \quad (13)$$

$$\mathbf{z} = [v, \dot{\phi}]^T, \quad (14)$$

$$\mathbf{u} = [u_R, u_L]^T, \quad (15)$$

where u_R and u_L are the normalized input DC voltage to the motors (i.e. $|u_R| \leq 1$ and $|u_L| \leq 1$); ω_R and ω_L are the angular speeds of the right and left wheels, respectively; \mathbf{p} is the pose of the WMR (i.e. the WMR's horizontal position and orientation); v and $\dot{\phi}$ are the translational speed and the angular speed (around its center) of the WMR, respectively. The matrices \mathbf{A} and \mathbf{B} contain information related to the inertia of the MR, its weight, the friction, the battery voltage level, and other electromechanical parameters of the used motors.

From this dynamic model, we observe that:

- 1) The DDR's state vector \mathbf{z} is linear w.r.t. the control input \mathbf{u} , see (9), however the pose is nonlinear w.r.t. the state, see (10).
- 2) The DDR's velocity, encoded in \mathbf{z} , is related to the input \mathbf{u} by a first-order linear system and its pose is related to \mathbf{u} by a second-order nonlinear system. This implies that the input \mathbf{u} controls the DDR's acceleration, and so the state \mathbf{z} cannot change abruptly. As a consequence, the WMR has the following limitations: (i) it cannot change the speed abruptly, thus requiring a non-zero deceleration time to stop; (ii) it cannot change direction abruptly.
- 3) If $\dot{\mathbf{z}}$ in (9) is significantly small, then $\mathbf{z} \approx -\mathbf{A}^{-1}\mathbf{B}\mathbf{u}$. In other words, if the DDR's acceleration is significantly small, then the WMR state \mathbf{z} almost becomes linear w.r.t. the control signal \mathbf{u} . As such, the dynamic DDR motion model (9)-(13) does not add additional constraints and can be sufficiently modelled by the kinematic model.

The dynamic model of the TOMR is [30]:

$$\dot{\mathbf{z}} = \mathbf{A}(\phi, \dot{\phi})\mathbf{z} + \mathbf{B}\mathbf{u}, \quad (16)$$

$$\mathbf{p} = [\mathbf{I}_{3 \times 3} \quad \mathbf{0}_{3 \times 3}] \mathbf{z}, \quad (17)$$

$$\mathbf{z} = [\mathbf{x}, \mathbf{y}, \phi, \dot{\mathbf{x}}, \dot{\mathbf{y}}, \dot{\phi}]^T, \quad (18)$$

$$\mathbf{u} = [u_1, u_2, u_3]^T, \quad (19)$$

where:

$$\mathbf{A}(\phi, \dot{\phi}) = \begin{bmatrix} \mathbf{0}_{3 \times 3} & \mathbf{I}_{3 \times 3} \\ \mathbf{0}_{3 \times 3} & \mathbf{R}(\phi)\dot{\mathbf{R}}^T(\phi)\dot{\phi} - \mathbf{C} \end{bmatrix}, \quad (20)$$

$$\mathbf{R}(\phi) = \begin{bmatrix} \cos(\phi) & -\sin(\phi) & 0, \\ \sin(\phi) & \cos(\phi) & 0, \\ 0 & 0 & 1, \end{bmatrix}. \quad (21)$$

The matrices \mathbf{B} and \mathbf{C} in (16) and (20), respectively, depend on the electromechanical characteristics of the particular TOMR. The matrix $\mathbf{R}(\phi)\dot{\mathbf{R}}^T(\phi)\dot{\phi}$ is related to the Coriolis force.

As opposed to the DDR, where the dynamic model described in (9) is linear, the TOMR dynamic model in (16)-(21) is nonlinear w.r.t. the input. The nonlinearity comes from $\mathbf{A}(\phi, \dot{\phi})$ and, in particular, from the component $\mathbf{R}(\phi)\dot{\mathbf{R}}^T(\phi)\dot{\phi}$ in (18) produced by the Coriolis force.

After having discussed some dynamic models for WMRs, we continue to discuss the models used for describing their energy consumption due to motion.

4) *Energy Consumption model:* Most MRs draw their energy from a battery. Due to the limited capacity of the battery, it is important to calculate the MR energy consumption to determine their operation time. There are various approaches to derive energy consumption models, but we will discuss only some of the most common ones.

- 1) **Electric model.** Most WMRs use DC motors to actuate their wheels because of their advantages in comparison to other types of motors, as explained in [34]. In this approach, we first calculate the energy consumed by the k th motor as a function of the instantaneous electric power:

$$E_k = \int_t p_k(t) dt, \quad (22)$$

$$p_k(t) = i_k(t)v_k(t), \quad (23)$$

where $p_k(t)$ is the instantaneous electric power consumed by the k th motor, $i_k(t)$ is the input current, and $v_k(t)$ is the DC input voltage to the k th motor. Since this is a DC motor, the input variable controlling it is the DC input voltage (controlled using Pulse-Width Modulation (PWM)), which is given as:

$$v_k(t) = u_k(t)V_s, \quad (24)$$

where V_s is the amplitude of the PWM signal and $u_k(t) \in [-1, 1]$ is the normalized control signal. Circuit theory and electromechanical equations are then used to derive the equations relating the input current $i_k(t)$ to the angular speed ω_k of the wheel that is mechanically coupled with the motor's shaft. Thereafter, the dynamic model is used to relate the WMR state vector to the wheel's angular speed. Finally, these equations are combined to obtain an equation relating the WMR energy consumption to the input vector \mathbf{u} and the WMR state vector. To illustrate this method, we briefly present the energy consumption models of a DDR and of a TOMR. According to [40], the DDR's energy consumption model is:

$$E = \int_t \mathbf{i}^T(t)\mathbf{v}(t) dt, \quad (25)$$

$$= \int_t (k_1 \|\mathbf{u}(t)\|^2 - k_2 \mathbf{z}^T(t)\mathbf{T}_q^{-T}\mathbf{u}(t)) dt,$$

where the parameters k_1 and k_2 depend on electromechanical properties of the motors. Variables \mathbf{u} , \mathbf{z} , and \mathbf{T}_q have the same definition as in (9)-(13). The energy consumption model for the three-wheeled omnidirectional MR is given in [30] as:

$$\begin{aligned} E &= \int_t \mathbf{i}^T(t) \mathbf{v}(t) dt, \\ &= \int_t (k_1 \|\mathbf{u}(t)\|^2 - k_2 \dot{\mathbf{p}}^T(t) \mathbf{R}(\phi) \mathbf{B} \mathbf{u}(t)) dt, \end{aligned} \quad (26)$$

where $\mathbf{u}(t)$, $\mathbf{p}(t)$, and \mathbf{T}_q have the same definition as in (16), while k_1 and k_2 depend on the motor's electromechanical characteristics. In [41], the authors present an energy consumption model for a car-like robot derived using the same method, however neglecting the energy required to steer.

This model describes the electrical energy consumed at the input of the motors and takes into account the energy lost as heat within the motor. (25) and (26) are quadratic functions of the normalized control signal $\mathbf{u}(t)$.

2) **Physics approach.** Another approach to describe the WMR energy consumption is to analyze the system from an external perspective and calculate the WMR's kinetic energy and the energy required to overcome the floor's friction. To illustrate this type of model, let us consider the energy consumption model of the DDR presented in [42]:

$$E_{\text{motors}} = E_{\text{kin}} + E_{\text{res}}, \quad (27)$$

where E_{kin} is the kinetic energy, E_{res} is the energy consumed by the motors to overcome the traction resistance presented by the friction of the floor, and E_{motors} is the energy consumed by the motors, which is *observable* from an external point of view, i.e., without taking into account the internal losses. The kinetic energy is given by:

$$\begin{aligned} E_{\text{kin}} &= \frac{1}{2} m v^2(t) + I \omega^2(t), \\ &= \int_t \{m v(t) a(t) + I \omega(t) \beta(t)\} dt, \end{aligned} \quad (28)$$

where m is the total WMR's mass; I is the total WMR's rotational inertia; v and ω are the translational and rotational speeds, respectively; and $a(t)$ and $\beta(t)$ are the translational and rotational accelerations, respectively. The products $v(t)a(t)$ and $\omega(t)\beta(t)$ in (28) can be negative when the WMR stops, meaning that the WMR's motors get some power back that **could** be recovered by the WMR's electrical system. However, most WMR's do not have the electric systems needed to recover such power and thus, considering this limitation, (28) becomes:

$$E_{\text{kin}} = \int_t \{m \max(v(t)a(t), 0) + I \max(\omega(t)\beta(t), 0)\} dt. \quad (29)$$

The term describing the energy consumed to overcome friction in (27) is:

$$E_{\text{res}} = 2\mu mg \int_t \max(|v(t)|, b|\omega(t)|) dt. \quad (30)$$

The distance travelled by the DDR is approximately $\int_t |v(t)| dt$. The advantage of this model lies with its independence to the type of motor used by the WMR. It requires only the mass m and the rotational inertia I of the WMR, which can be estimated. The disadvantage is that it only considers the energy expenditure observed from the outside and does not take into account the internal losses of the motors and the circuitry.

3) **Data-driven Model.** The energy consumption models mentioned above are derived from physical principles. Those theoretical models, for the sake of tractability, often ignore certain effects, such as nonlinearities of the motor or the influence of temperature on the electric resistances. Another approach consists of measuring the electric consumption of the WMR under different conditions, creating a dataset, and then training numerical models. The authors of [43] present a simple implementation of this approach by measuring the power consumed by DC motors at different angular speeds. The authors note that a suitable model for the power consumption of the k th motor is:

$$P_k = \sum_{j=0}^6 a_j \omega_k^j, \quad (31)$$

where ω_k is the angular speed of the k th motor and $\{a_j\}_{j=0}^6$ are experimentally determined coefficients. The model in (31) is then combined with the kinetic model, which relates the velocity of the WMR to the angular speed of the wheels ω_k in order to obtain the power consumed by the WMR. After integration over time, we obtain the consumed energy.

In [44], there are two examples of this type of energy consumption model. First, the authors measure the power consumption of the PPRK (a commercial TOMR moving at a constant linear speed v). The measurements are done at different linear speeds up to a maximum value. After a numerical analysis of the measurements, the authors observed that the power consumed by the PPRK can be well-modelled by a fourth order polynomial function of the linear speed. Next, the authors did the same for the Pioneer 3DX (a commercial DDR) and measured its energy consumption while moving at a constant speed on a straight line. Due to limitations in the robot's internal system, the Pioneer 3DX could not be operated at its maximum linear speed. The experimental results showed that the power consumption of this robot can be modelled with an affine function of the linear speed.

The derivation of this type of model can require significant time to gather data in the laboratory. Additionally, the generalisation of the derived models to conditions different from those of the modeling phase might exhibit an uncertain accuracy, e.g. when trying to use the model in [44] to predict the energy consumption of the Pioneer 3DX while moving along curves or at variable linear speed. On the other hand, one advantage of this type of model is that they do not require deep

theoretical knowledge. Also, they can implicitly consider the various complex processes involved in energy consumption, which may be complicated to take into account in the theoretical models. For example in [43], the authors mention that DC motors can be modelled with a second-order polynomial of the angular speed ω from electromagnetic theory. Yet, measurements show that such a model is insufficient. For example, the sixth-order polynomial model introduced in (31) exhibited a much better fit on real measurements. This may be due to the fact that the second-order model derived from theory overlooks certain processes, while the model in (31) took them into account implicitly through the fitting process.

4) **Restricted Domain Models.** Some simple energy consumption models are derived from more complex models by constraining their range of validity. To illustrate this, let us consider the work in [45] where the authors use an electric energy consumption model for a DDR, similar to the one used in (25). They restrict the DDR to move within a straight line with a trapezoidal linear speed profile. For such a trajectory, they analytically calculate the energy consumption starting from the electric energy consumption model to obtain the following expression:

$$E = \sum_{j=-1}^3 a_j \omega^j, \quad (32)$$

where ω is the angular speed of the DDR wheels. The model (32) exposes an interesting phenomenon that is sometimes overlooked: motors can be inefficient when operated at very low speeds. As the motor's speed decreases, the term ω^{-1} in (32) dominates the energy consumption and grows very quickly. After the optimization of the trapezoidal speed profile, the authors found that the energy consumption is proportional to the distance travelled when the total duration of movement remains constant. Based on the result in (32), the authors of [46] modeled the energy consumption as being proportional to the distance D travelled by the WMR:

$$E = kD, \quad (33)$$

where k is a proportionality factor. The model (33) has been adopted by many authors for simplicity and is sometimes derived in a similar manner in different papers, or sometimes just assumed as it is *intuitive* and simple (see for example [47] and [48]).

These types of models are, in general, simplifications of other more complex models under certain conditions. When choosing a model, we must take into consideration where it comes from and how it was derived in order to see if the application in which we intend to use it is close enough to the conditions under which the model was derived. This is done so as to ensure that we do not operate the model outside its range of validity. Otherwise, if we neglect this aspect, then the model selected might deviate significantly from the true energy consumption. For example, while the model introduced

in (33) is appropriate when a WMR is moving at a constant speed, it may be quite inaccurate when the speed varies considerably over time.

5) **Square norm.** Lastly, another popular approach within the control theory community is to assume that the energy consumption is given by:

$$E = \int_0^t \|\mathbf{u}(\tau)\|^2 \tau, \quad (34)$$

where \mathbf{u} is the control signal of the WMR dynamic model. This is notably a simplification of the energy consumption models derived through circuit theory presented in (25) and (26). The model in (34) becomes closer to the models (25) and (26) when the WMR operates at low speeds and/or the coefficient k_2 of those models is small.

Although motion consumes a significant part of the energy in WMRs, there are also other processes which consume a non-negligible amount of energy. In [49], the authors empirically evaluated the contribution of different processes to the energy consumption of a DDR and found that the sensors and microcontrollers also contribute significantly to energy consumption. The microcontroller's power consumption can be modelled as constants, since they usually perform low level tasks which are repetitive and relatively stable. On the other hand, the power consumption of the embedded computers can be modelled as a stochastic process as they usually perform tasks which depend more on exogenous inputs, and thus have a more variable behaviour.

B. Rotary-wing UAVs

The study of the motion of aerial vehicles is a complex subject that has been investigated since the early appearance of the first airplanes. There is a large body of literature on the aerodynamic aspects of these vehicles and their modeling. In this section, we will discuss the quadrotor aerial robot, which is a basic type of multirotor UAV.

Multirotor aerial robots (also called rotary-wing aerial robots) are one of the most popular types of aerial robots nowadays. One of the most common type of these UAVs is the quadrotor, which is the subject of this section.

The WMRs discussed in the previous section operate in 2D and their configuration is fully described by their horizontal position and orientation. In contrast, UAVs operate in 3D. To fully describe their configuration, we need to specify their 3D position, as well as their attitude³, which can be expressed using either Euler angles or quaternions [50], [51]. In this tutorial, we will limit the discussion to models representing the attitude using Euler angles; details about the utilisation of quaternions to represent the attitude can be found in [52].

The configuration of the UAV can be described using Euler angles as:

$$\mathbf{p}(t) = [x, y, z, \theta, \phi, \psi]^T, \quad (35)$$

where $[x, y, z]^T$ is the UAV center of mass and θ, ϕ , and ψ are the Euler angles of roll, pitch, and yaw, respectively,

³The attitude, not to be confused with the altitude, is the equivalent of the orientation for the ground WMRs.

which describe the orientation of the UAV (see [53] for a more detailed geometrical description of these angles). Note that $[x, y, z]^T$ is represented in a static coordinate frame attached to the world and not to the UAV itself, and $[\theta, \phi, \psi]^T$ are represented in a coordinate frame attached to the center of mass of the UAV oriented in the same manner as the inertial coordinate frame. Before discussing the quadrotor dynamic model, we will briefly discuss the physical principles that allow it to fly. In a classic quadrotor, the four propellers lie in the same plane and are oriented vertically. When the propeller rotates, it creates thrust in the same direction as its orientation and with a sense opposing the gravity. The faster the propeller turns, the greater the thrust generated. When all four propellers produce the same thrust, the plane containing all four propellers is parallel to the floor, and the resulting thrust is vertical. If this thrust equals the gravitational force, then the quadrotor remains in the air hovering. When one propeller turns faster or slower than the other, the quadrotor tilts and the resulting thrust presents a horizontal component, making the UAV move in the horizontal plane.

Just as the dynamic models of the WMRs were derived starting from the electrical analysis of their motors, the derivation of the dynamic model for multirotors begins in the same way. Consider a dynamic model for the quadrotor that is used by many roboticists [54]:

$$\begin{bmatrix} \frac{d^2x}{dt^2} \\ \frac{d^2y}{dt^2} \\ \frac{d^2z}{dt^2} \end{bmatrix} = \begin{bmatrix} c(\phi)s(\theta)c(\psi) + s(\phi)s(\psi) \\ c(\phi)s(\theta)s(\psi) - s(\phi)c(\psi) \\ c(\phi)c(\theta) \end{bmatrix} \frac{u_z}{m} - \begin{bmatrix} 0 \\ 0 \\ g \end{bmatrix}, \quad (36)$$

$$\begin{bmatrix} \frac{d^2\phi}{dt^2} \\ \frac{d^2\theta}{dt^2} \\ \frac{d^2\psi}{dt^2} \end{bmatrix} = \begin{bmatrix} \left(\frac{I_y - I_z}{I_x}\right) \frac{d\theta}{dt} \frac{d\psi}{dt} - \frac{J}{I_x} \frac{d\theta}{dt} q_w \\ \left(\frac{I_z - I_x}{I_y}\right) \frac{d\phi}{dt} \frac{d\psi}{dt} + \frac{J}{I_y} \frac{d\phi}{dt} q_w \\ \left(\frac{I_x - I_y}{I_z}\right) \frac{d\phi}{dt} \frac{d\theta}{dt} \end{bmatrix} + \begin{bmatrix} \frac{\ell u_y}{I_x} \\ \frac{\ell u_x}{I_y} \\ \frac{u_\psi}{I_z} \end{bmatrix}, \quad (37)$$

$$\begin{bmatrix} u_x \\ u_y \\ u_z \\ u_\psi \end{bmatrix} = \begin{bmatrix} -\kappa_b & 0 & \kappa_b & 0 \\ 0 & \kappa_b & 0 & -\kappa_b \\ \kappa_b & \kappa_b & \kappa_b & \kappa_b \\ \kappa_\tau & -\kappa_\tau & \kappa_\tau & -\kappa_\tau \end{bmatrix} \begin{bmatrix} \omega_1^2 \\ \omega_2^2 \\ \omega_3^2 \\ \omega_4^2 \end{bmatrix}, \quad (38)$$

$$q_w = \omega_1 - \omega_2 + \omega_3 - \omega_4, \quad (39)$$

where $u_x(t)$, $u_y(t)$, $u_z(t)$, and $u_\psi(t)$ denote the control signals for the drone; $\omega_j(t)$ is the angular velocity of the j th motor; m is the total mass of the drone; g is the gravitational constant; ℓ is the distance from the center of the quadrotor to each motor; I_x , I_y , and I_z are the rotational inertia components; J is the total inertia of the motors; and κ_b and κ_τ are the thrust and aerodynamic drag factors of the propellers, respectively. In (38), the matrix relating the vector inputs $[u_z \ u_y \ u_x \ u_\psi]^T$ with the square angular velocities vector $[\omega_1^2(t) \ \omega_2^2(t) \ \omega_3^2(t) \ \omega_4^2(t)]^T$ is not singular.

Equation (37) describes the drone's Euler angles (roll (ϕ), pitch (θ), and yaw (ψ)) measured with respect to the axes o_Bx_B , o_By_B , and o_Bz_B , with $(o_Bx_By_Bz_B)$ being the body axis system whose origin o_B is given by the geometric centre of the quadrotor.

The quadrotor motion given by the model in (36)-(39) is described w.r.t. to a fixed orthogonal axis set $(oxyz)$, where oz points vertically up the gravity vector $[0 \ 0 \ -g]^T$ (earth axes). The origin o is located at a desired height \bar{z} with respect to the ground level. The coordinates x , y , and z in (36) refer to the position of the centre of gravity of the quadrotor in the space where z is its altitude [55]. In the literature, we find different axis configurations in which the quadrotor motion can be described and each axis configuration provides slightly different models.

The time dependence of the variables in equations (36) and (37) is not explicitly shown in order to lighten the notation. Further, due to the symmetry of the quadrotor, we have $I_x = I_y = I$.

More complex models are also possible, which consider external disturbances, such as the wind. Regarding the energy consumption of the quadrotor, there are electric models and physics-based models that are derived using approaches similar to those used for the WMR. In [54], the energy consumption of a quadrotor is modeled as:

$$E = \sum_{j=1}^4 \int_t^4 \left[\left(\sum_{k=0}^4 c_k \omega_j^k(t) \right) + c_6 \dot{\omega}_j(t) + c_7 \dot{\omega}_j^2(t) \right. \\ \left. + c_8 \omega_j(t) \dot{\omega}_j(t) + c_9 \omega_j^2(t) \dot{\omega}(t) \right] dt, \quad (40)$$

where the coefficients $\{c_k\}_0^9$ depend on the parameters of the quadrotor's motors and the geometry of the propellers.

In [56], the authors present the following hybrid energy consumption model, which is based on basic mechanics and completed with some correction factors obtained experimentally:

$$E_c = \int_{t_0}^{t_f} \sum_{j=1}^4 \tau_j(t) \omega_j(t) dt, \quad (41)$$

$$= \int_{t_0}^{t_f} \sum_{j=1}^4 (\dot{\omega}_j(t) + \mathcal{K}_\tau \omega_j^2(t) + D_v \omega_j(t)) \omega_j(t) dt,$$

where (41) is the energy consumed by the four motors of the quadrotor. In other words, (41) only describes the amount of energy that is translated into mechanical energy, but disregards the efficiency of the motors.

C. Fixed-wing UAVs

In this section, we briefly discuss fixed-wing UAVs and present a simple, but useful dynamic model for CaTP problems. Fixed-wing UAVs fly using principles that are different from those used by multirotor UAVs and are consequently modelled in a different manner with different characteristics.

In general, fixed-wing UAVs are more energy-efficient than multirotor UAVs mainly because of their ability to glide.

They also fly for longer times, longer distances, and at higher speeds. However, they are less agile and cannot land or take-off vertically. As opposed to multirotor UAVs, fixed-wing UAVs are generally not designed to hover. Nevertheless, some special types of fixed-wing UAVs having high thrust-to-weight ratios can hover using complex control techniques [57].

Fixed-wing UAV are controlled by the thrust generated by its propeller(s) and by controlling surfaces (aileron, elevator, and rudder). Micro fixed-wing UAVs usually drive their propellers with an electric motor, while small fixed-wing UAVs can drive it using gas powered motors.

The fixed-wing UAV center of mass position is sometimes described in the North-East-Down (NED) coordinate system, where the down axis points towards the center of the Earth and is aligned with the force of gravity. In this case, the altitude is measured in the opposite direction of the down axis. The attitude of the fixed-wing airplane is expressed using Euler angles in the body frame defined as follows: its origin lies in the center of gravity of the airplane, the x axis points to the nose of the plane, the y axis points to the right wing, and the z axis is orthogonal to those two axes and follows the right-hand rule. The roll ϕ describes the rotation about the x axis, the pitch θ describes the rotation about the y axis, and the yaw ψ describes the rotation about the z axis.

The aerodynamics of airplanes are significantly more complex and nonlinear. Since this is an elementary tutorial, we will present only a high-level simplified dynamic model that can be used for trajectory planning, as well as one linearized dynamic model. In the absence of wind, a simplified nonlinear dynamic model describing the fixed-wing UAV motion is [58]:

$$\begin{bmatrix} \dot{p}_n \\ \dot{p}_e \\ \dot{h} \end{bmatrix} = V_a \begin{bmatrix} \cos(\psi) \cos(\gamma) \\ \sin(\psi) \cos(\gamma) \\ \sin(\gamma) \end{bmatrix} \quad (42)$$

$$\begin{bmatrix} \dot{\psi} \\ \dot{\gamma} \end{bmatrix} = \begin{bmatrix} \frac{F_{lift} \sin(\phi)}{mV_a \cos(\gamma)} \\ \frac{F_{lift}}{mV_a} \cos(\phi) - \frac{g}{V_a} \cos(\gamma) \end{bmatrix} \quad (43)$$

$$\begin{bmatrix} F_{lift} \\ F_{drag} \end{bmatrix} = \frac{1}{2} \rho V_a^2 S \begin{bmatrix} C_L \\ C_{D_0} + KC_L^2 \end{bmatrix} \quad (44)$$

$$\dot{V}_a = \frac{F_{thrust}}{m} - \frac{F_{drag}}{m} - g \sin(\gamma) \quad (45)$$

where g is the gravitational constant, S is the planform area of the wing, C_{D_0} is the zero lift drag, K is the induced drag factor, m is the mass of the airplane, and ρ is the air density. The input to this model is the lift coefficient⁴ C_L , the thrust F_{thrust} , and the roll ϕ . \dot{p}_n and \dot{p}_e are the speeds along the north and east axes, respectively, and \dot{h} is the altitude speed measured w.r.t. to the negative direction of the down axis. F_{lift} and F_{drag} are the lift and drag forces experienced by the plane. Finally, V_a is the air speed of the airplane.

The constant altitude and the airspeed scenario (i.e. $\dot{h} = 0$ and $\dot{V}_a = 0$) are common and of particular importance for CaTP applications. In this case, we have $\gamma = 0$, $\dot{\gamma} = 0$, and

⁴Note that the physical fixed-wing UAV is controlled via its thrust and the three control surfaces (aileron, elevator, and rudder). Hence, even if C_L constitutes the input to the model, in practice it is not directly controlled.

$F_{thrust} = F_{drag}$. The dynamic model (42) reduces to the kinematic model:

$$\begin{bmatrix} \dot{p}_n \\ \dot{p}_e \end{bmatrix} = V_a \begin{bmatrix} \cos(\psi) \\ \sin(\psi) \end{bmatrix} \quad (46)$$

$$\dot{\psi} = \frac{g}{V_a} \tan(\phi). \quad (47)$$

With this kinematic model, the paths are usually composed of straight lines and circular arcs [59]. The simplified models (42) and (46) are practical, but they do not describe the pitch angle θ . This can be an issue for some CaTP since the variations in the orientation of the antenna mounted on the fixed-wing UAV cannot be fully determined without the pitch θ .

Another simple type of dynamic model for the fixed-wing UAV are the linear models. These models are derived after linearizing more complex nonlinear aerodynamic models around small attitude variations. They are separated into two decoupled models, the longitudinal motion model and the lateral motion model, as follows:

$$\begin{bmatrix} \dot{u} \\ \dot{w} \\ \dot{q} \\ \dot{\theta} \\ \dot{h} \end{bmatrix} = \mathbf{A} \begin{bmatrix} u \\ w \\ q \\ \theta \\ h \end{bmatrix} + \mathbf{B} \begin{bmatrix} \delta_e \\ \tau \end{bmatrix} \quad (48)$$

where τ is the thrust and δ_e is the elevator angle. For the lateral model, we have that:

$$\begin{bmatrix} \dot{v} \\ \dot{p} \\ \dot{r} \\ \dot{\phi} \\ \dot{\psi} \end{bmatrix} = \mathbf{C} \begin{bmatrix} v \\ p \\ r \\ \phi \\ \psi \end{bmatrix} + \mathbf{D} \begin{bmatrix} \delta_a \\ \delta_r \end{bmatrix} \quad (49)$$

where δ_a and δ_r are the action of the aileron and the rudder, respectively. The matrices \mathbf{A} , \mathbf{B} , \mathbf{C} , and \mathbf{D} depend on the particular airplane. Since this is an elementary tutorial, we did not consider the effect of wind on the fixed-wing UAV motion models, but the interested reader can look into [60], [61], [62], [63] for more information regarding this subject.

It can be demonstrated from physical principles that the energy consumption for the fixed-wing UAV can be expressed as follows [10]:

$$\begin{aligned} E = & \int_0^T \left(c_1 \|\mathbf{v}\|^3 + \frac{c_2}{\|\mathbf{v}\|} \left(1 + \frac{\|\mathbf{a}\|^2 - \frac{\mathbf{a}^T \mathbf{v}}{\|\mathbf{v}\|^2}}{g^2} \right) \right) dt \\ & + \frac{m}{2} (\|\mathbf{v}\|^2(T) - \|\mathbf{v}\|^2(0)) \end{aligned} \quad (50)$$

where \mathbf{v} is the velocity and \mathbf{a} is the acceleration vector of the fixed-wing UAV.

D. Final Comments on Models for Robots

We have presented an overview of some relevant MR's models that are useful for CaTP problems, but have omitted some important observations. The models presented in this section are all in continuous time, but it is possible to transform them into discrete time models by transforming differential equations into difference equations. Continuous-time models

allow for the utilisation of many analytical tools based on derivatives, such as calculus of variations. On the other hand, discrete-time models allow for numerical techniques like dynamic programming or other related techniques. It is important to mention that, in practice, the control signals for the ground MRs and the UAVs are executed in digital computers on board, and thus the control system is implemented in discrete time.

Finally, all the kinematic and dynamic models described in this section have an analytical form and are mostly derived from physics. However, there are other types of motion models derived through experimentation and machine learning techniques [64].

III. COMMUNICATIONS SYSTEM

This section mainly addresses researchers who desire to work on CaTP, but lack the background in communications systems. Those familiar with the topic can skip this section and directly proceed to section IV.

In this section, we introduce the reader to the basic concepts of communication systems and wireless channel models required to study CaTP problems. We begin by introducing a common communication system: **transceiver**. This is a device composed of a transmitter and a receiver. When a communications link is established between two entities, it can take three different forms:

- 1) **Simplex Link**: one entity operates exclusively as a transmitter and the other operates exclusively as a receiver. The data flow is always unidirectional.
- 2) **Full-Duplex Link**: both entities receive and transmit simultaneously. Two independent data flows in opposite directions occur simultaneously.
- 3) **Half-Duplex Link**: both entities receive and transmit in turns, where two independent data flow in opposite directions, but only one is active at a time. This can be implemented using **time duplexing**, where during an interval of time, one entity transmits and the other receives. During the following interval of time, the roles are swapped. This process is periodically repeated.

We now provide a brief overview of the digital transmission. The **source node** generates data as blocks of bits or as a continuous stream of bits. This data is then divided in small groups, which are inserted into packets to form the payload⁵. Each packet has a **header** that contains information such as the destination and/or checkup bits to evaluate the integrity⁶ of the packet at the receiver. There are two main strategies to exploit the checkup bits in the packet's header:

- 1) **Retransmission**: if the receiver does not detect any error in the received data packet, it transmits a confirmation packet back to the source node (containing no payload), indicating that the data packet was correctly received. Thereafter, the source node can transmit new data packets (containing new payload). However, if the receiver detects an error in the received data packet, it does not send back the confirmation packet. When the

⁵The payload's size can be constant or variable depending on the communications protocol selected.

⁶In other words checking if the packet has been received with errors.

source node realizes that it did not receive a confirmation packet, it assumes that an error occurred and re-transmits the same data packet. The number of retransmissions will depend on the particular communications protocol.

- 2) **No-retransmission**: if the receiver detects an error in the data packet, it discards the payload. On the other hand, if the packet is correctly received, the receiver does not transmit any confirmation to the source node and simply waits for the next packet. The source node continues to transmit data packets.

The retransmission strategy provides robustness to the transmission of data at the cost of a lowered bit rate and increased latency due to the time spent in confirmation and retransmission of data packets. The no-retransmission strategy can achieve a higher bit rate and lower latency at the cost of more erroneous or missing data. The selection of the transmission strategy will depend on the particular application requirements.

After forming the packets, the transmitter modulates the sequence of bits with a carrier signal of high frequency f_c suitable to be radiated as an electromagnetic waves, which are then radiated through the antenna. The propagation environment modifies the radiated wave before arriving to the receiver's antenna, where it is converted back to an electric signal and processed. The wireless channel model describes the effect that the propagation environment has on the transmitted signal until it reaches the receiver.

A. Wireless channel modelling

In the context of CaTP, oversimplified wireless channel models can lead the designer to overestimate the communications channel quality and to overlook certain channel behaviours that the MR will encounter in real operating conditions. In such cases, the MR might underperform or fail to complete its task due to unexpectedly poor communication quality.

To provide the researcher with the *basic* knowledge of communications for CaTP problems, we will limit the discussion to the simplest type of communications systems: narrowband⁷, single-antenna, and single carrier communications systems. In addition, we will not address the issue of interference. The general channel model representing such systems is:

$$y(t) = \mathcal{H}(\mathbf{p}(t), \mathbf{q}(t), t)x(t) + n(t), \quad (51)$$

where $x(t)$ and $y(t)$ are the continuous-time transmitted and received complex signals, respectively; $n(t)$ is the noise generated at the receiver, which is usually modelled as a random complex circular white Gaussian process; $\mathbf{p}(t)$ and $\mathbf{q}(t)$ are the positions of the transmitter and the receiver, respectively, at time t ; and $\mathcal{H}(\mathbf{p}(t), \mathbf{q}(t), t)$ is the complex channel gain. CaTP problems require models that describe the spatio-temporal channel gain $\mathcal{H}(\mathbf{p}(t), \mathbf{q}(t), t)$. We further discuss different common models to describe the spatial variations of the channel gain.

To model $\mathcal{H}(\mathbf{p}(t), \mathbf{q}(t), t)$, deterministic, stochastic, and machine learning approaches can be used.

⁷This means that the bandwidth of the modulated signal is significantly smaller than the carrier frequency f_c .

1) *Deterministic Models*: In the deterministic approach [65], the wireless channel models are often derived from physical principles. One of the simplest and yet most important channel models is the *power loss model*. It is the base for many more sophisticated channel models and describes how the mean received signal power varies with the transmitter-receiver distance. It is modelled as [66]:

$$\mathcal{H}(\mathbf{p}(t), \mathbf{q}(t), t) = L_P^{-1}(\mathbf{p}(t), \mathbf{q}(t)), \quad (52)$$

$$L_P(\mathbf{p}(t), \mathbf{q}(t)) = K_0 \left(\frac{d(t)}{d_0} \right)^{\alpha/2}, \quad (53)$$

$$d(t) = \|\mathbf{q}(t) - \mathbf{p}(t)\|_2, \quad (54)$$

where α is the power path loss coefficient, d_0 is a reference distance, and K_0 is the path loss observed at distance d_0 that must be in the far field region [67]. This model is valid for distances larger than d_0 , and is used at distances larger than the radiated signal's wavelength and the physical antenna's dimensions [65]. Under *free space* conditions, the power path loss coefficient becomes $\alpha = 2$, but experimental results have reported path loss coefficients as low as $\alpha = 1.6$ [68], [69] in some urban environments, buildings, and underground mines. This occurs because some hallways and tunnels behave as *giant waveguides* due to their geometry and the presence of metallic objects that act as reflectors.

Experiments have shown that the power path loss coefficient can change after certain distances. This phenomenon is modelled using break points [68] after which the path loss changes.

Another deterministic extension to the model in (53) is the two-ray model [66], which takes into consideration only the Line of Sight (LoS) wave and the wave that reaches the receiver's antenna after only one reflection on the floor. This model was originally derived in the context of cellular network communications [70]. It has been tested for scenarios with a transmitter of less than 50m altitude; this model makes the assumption that the distance between the transmitter and the receiver is such that the curvature of the earth can be neglected, and thus the floor is considered flat.

If we consider multiple waves beside the LoS and the reflected wave of the two-ray channel model, then we obtain the ray tracing model [71], [72], [73]. This method determines the interaction of multiple radiated waves with the environment (e.g. buildings, floor, walls) before arriving to the receiver's antenna and requires a computational map of the area in which both the transmitter and the receiver operate. The accuracy of the ray tracing model increases when the map is more detailed and when more electromagnetic interactions are considered (e.g. reflection, refraction, diffraction). However, this also increases the computational load.

Let us discuss another deterministic channel model which has been specially devised for indoor operations, and which also requires a map of the building as well as the positions of both transceivers. This model draws a straight line between both nodes, counts the number of walls and floors crossed [74], and then represents the losses due to those walls and floors as described in [75].

2) *Stochastic Models*: Stochastic models describe the channel in terms of its mean, variance, and correlation functions, rather than trying to predict the exact channel value, unlike deterministic models. Stochastic models are usually simple and can describe the average behaviour of the channel models accurately. Their simplicity allows for mathematical analysis that can provide useful insights in many application domains, including CaTP problems. Using this approach, $\mathcal{H}(\mathbf{p}(t), \mathbf{q}(t), t)$ is modelled as a multi-scale spatial and time-varying stochastic process [76] composed of three terms [76], [77]:

$$\mathcal{H}(\mathbf{p}(t), \mathbf{q}(t), t) = \frac{s(\mathbf{p}(t), \mathbf{q}(t))h(\mathbf{p}(t), \mathbf{q}(t), t)}{L_P(\mathbf{p}(t), \mathbf{q}(t))}, \quad (55)$$

where $s(\mathbf{p}(t), \mathbf{q}(t))$ represents the shadowing [78], [79], $h(\mathbf{p}(t), \mathbf{q}(t), t)$ represents the small-scale fading [67], and $L_P(\mathbf{p}(t), \mathbf{q}(t))$ represents the path loss [66]. We proceed to discuss the physical meaning of these components and their most relevant mathematical models from the perspective of CaTP applications.

- **Path-loss**: this describes a deterministic component that models the mean power loss variations due to distance between the transmitter and the receiver. It usually takes the form of (53). There are also experimentally derived models for the path loss models, such as the Okumura-Hata model [80].
- **Shadowing**: this is a random process that models the signal power reduction due to obstructions caused by large objects⁸, such as buildings. It is a time-invariant term and depends on the transmitter and receiver positions. The shadowing has been experimentally characterized [78] and is generally modelled as a log-normal real random process with variance σ and mean μ . Its spatial autocorrelation has been found experimentally to follow an exponential function [76]⁹:

$$r(d(t)) = \exp(-d(t)/\beta), \quad (56)$$

where β is the decorrelation distance that is usually in the order of 10λ , and is thus also called large-scale fading. For small distances (smaller than β), the shadowing is often considered constant. To give more flexibility to the shadowing model, σ and mean μ can be made dependent on the geographical region [77]. The shadowing effect can thus be simulated numerically using mathematical models [82].

- **Multipath-fading**: the electromagnetic wave radiated by the transmitter reaches the receiver's antenna after travelling through multiple random paths. These multiple components interact with the environment through reflection, diffraction, and refraction before arriving, with different phases, to the receiver's antenna where they are combined. As a consequence, the receiver observes constructive interference in some locations and destructive interference in others. This results in a random spatial process with large signal strength variations over

⁸Large w.r.t. the wavelength.

⁹Although this spatial correlation model fits many scenarios, it is by no means a universal model for the shadowing process, see [81]

small distances (smaller than one wavelength). This phenomenon is called small-scale fading or multi-path fading [65], [83].

Small-scale fading $h(\mathbf{p}(t), \mathbf{q}(t), t)$ is modelled as a random spatial-temporal process with a certain distribution and spatio-temporal correlations dependent on the environment. The study of small-scale fading is a complex subject. In this elementary tutorial, we focus only on the basic models used in CaTP problems.

Three elements influence $h(\mathbf{p}(t), \mathbf{q}(t), t)$: the position of the receiver $\mathbf{p}(t)$, the position of the transmitter $\mathbf{q}(t)$, and the environment. Any change in any of these elements changes the experienced small-scale fading. In traditional mobile communications, $\mathbf{p}(t)$ and $\mathbf{q}(t)$ are considered uncontrollable time-variant random variables. In that context, $h(\mathbf{p}(t), \mathbf{q}(t), t)$ is considered time variant if the environment varies or if the position of the transceivers changes over time. On the other hand, in CaTP, $h(\mathbf{p}(t), \mathbf{q}(t), t)$ is considered time invariant if $h(\mathbf{p}, \mathbf{q}, t_1) = h(\mathbf{p}, \mathbf{q}, t_2)$ for any $t_1 \neq t_2$ and for any positions \mathbf{p} and \mathbf{q} . In CaTP, the small-scale fading is time-variant only if the environment is dynamic. Otherwise, is it considered time-invariant.

When the small-scale fading is time variant, the temporal variation can be characterized with the coherence time τ , which indicates the maximum duration over which the small-scale fading term remains almost constant. One common way to model the temporal variation of small-scale fading is as follows: $h(\mathbf{p}, \mathbf{q}, t) = h_k$, for $t \in [k\tau, (k+1)\tau]$ with $\{h_k\}_k$ being a sequence of independent and identically distributed (i.i.d.) random variables. More dynamic environments have shorter coherence times τ . After discussing the concept of time-variance for small-scale fading in the context of CaTP, we now proceed to first discuss time-invariant small-scale fading models, and then briefly discuss time-variant models.

We start with the statistical distribution of small-scale fading. When there is no line of sight between the transceivers nor any particular strong wave due to some reflection, $h(\mathbf{p}, \mathbf{q}, t)$ is commonly modelled as a zero-mean complex circular Gaussian random variable. Hence, $|h(\mathbf{p}, \mathbf{q}, t)|$ is a Rayleigh distributed random variable, which explains why such a model is referred to as Rayleigh fading [67].

Alternatively, if there is a line of sight between both transceivers, then $h(\mathbf{p}, \mathbf{q}, t)$ can be modelled as a non-zero-mean complex circular Gaussian random variable:

$$h(\mathbf{p}, \mathbf{q}, t) = h_R + jh_I + L, \quad (57)$$

where h_R and h_I , which are zero-mean independent real Gaussian random variables with variance $1/2$, represent the ensemble of scattered waves arriving to the receiver's antenna, and L is a real number representing the strength of the line of sight component. The ratio $K = L^2/\text{var}(h_R + jh_I)$ is called the Rician factor. If $K \neq 0$, then we say that we have Rician fading [83] and the norm of $h(\mathbf{p}, \mathbf{q}, t)$ is a random variable with a Rician

probability distribution function. But, when $K = 0$, we have Rayleigh fading.

There are other common probabilistic distributions used to model $|h(\mathbf{p}, \mathbf{q}, t)|$, such as the Nakagami distribution. Unlike the Rayleigh and the Rician distributions, not all other models have physical interpretations, as some distributions are used only because they fit the experimental results well.

We now address the modeling of the spatial variations of small-scale fading. As the name indicates, the magnitude of $h(\mathbf{p}, \mathbf{q}, t)$ varies significantly over very small distances. Many experiments show that the small-scale fading coherence distance is usually lower than $\approx \lambda/2$. There is no universal model to describe its spatial correlation [84], but there is an important theoretical model derived by Jakes [85] for the case where the receiver is surrounded by a ring of uniformly distributed scatterers. In this scenario, the small-scale fading has a Rayleigh distribution and the following normalized spatial correlation:

$$r(\mathbf{p}, \mathbf{q}) = J_0 \left(\frac{2\pi \|\mathbf{p} - \mathbf{q}\|_2}{\lambda} \right), \quad (58)$$

where $J_0()$ is the Bessel function of the first kind and zero-th order. It is possible to simulate the 2D random field representing the small-scale fading with the Jakes model using numerical techniques such as those of [86]. If the conditions of the environment differ from those required in the Jakes model, (58) would not be a good model for the spatial correlation function. Alternative models have been developed in the literature see [83], but as with the Jakes model, the decorrelation distance is generally around $\lambda/2$.

3) *Data driven Models*: Another approach consists of using machine learning techniques to *learn* the communications channel. For instance in [87], in the context of an iterative CaTP problem, the authors use Gaussian processes to construct a radio map of the wireless channel. This radio map is iteratively updated with channel measurements. In [88], the authors predict the Received Signal Strength (RSS) of the link between a UAV and a BS using the ensemble method technique, which combines various machine learning models. In [89], the authors propose a machine learning technique to learn the channel map of a defined region using segmentation.

In [90], the authors developed a machine learning technique that uses satellite images, determines the position of trees, and then uses an artificial neural network to determine the channel loss depending on the transceivers' positions. Some other works also use artificial neural networks to predict the channel loss [91]. The radio maps constructed using machine learning techniques can be highly accurate in the regions where the measurements have been taken, but obtaining such measurements can be costly and time consuming. In addition, these are often numerical maps without analytical expressions, thus making them unsuitable for mathematical analysis that could provide useful insight into how to solve CaTP problems. In the rest of this section, we will focus on analytical channel

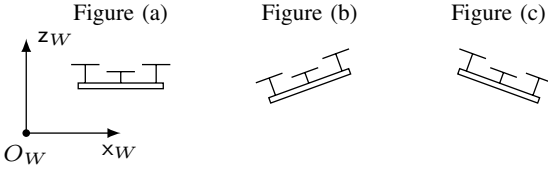


Figure 3: (a) quad-rotor hovering, (b) quad-rotor moving to the left, and (c) quad-rotor moving to the right.

models. The reader interested in machine learning techniques for channel modelling can find more information in [92].

B. UAV Channel Models

The channel models described in the previous section were originally developed for mobile communications considering ground users and are well-suited to ground MRs applications. In general, they are not appropriate for UAVs applications mainly because of the changing altitude of the UAV. Given the increasing attention being paid to the integration of UAVs into 5G networks [18], [19], for the sake of completeness of this tutorial, we next discuss briefly the modeling of UAV wireless channels, which is currently an active research topic [93], [94].

Before presenting the UAV channel models, let us discuss some particularities of UAV communications. For small-sized UAVs, the receiver is close to the UAV's power electronics and to the motors which run continuously. As a consequence, sometimes the UAV's motors generate electromagnetic noise that interferes with the UAV's own receiver [95].

Another phenomenon is airframe shadowing [93]. This occurs when the frame of the UAV itself partially blocks the LoS. Consider a multirotor UAV with an antenna on the top surface (i.e. the UAV's surface facing the sky) that is communicating with a ground station. Assume that the UAV moves away from the ground node. To do this, the multirotor UAV has to tilt in such a way that its bottom surface (i.e. the UAV's surface facing the ground) is slightly orientated towards the ground node, see Fig. 3. This can fully or partially block the LoS between the ground station's antenna and the UAV's antenna. In the case of fixed-wing UAVs, airframe shadowing can occur when the UAVs turn. In turning, they usually change their roll by controlling their ailerons. During this manoeuvre, one wing tilts up and the other tilts down. This wing tilting might temporarily block the LoS with other communication nodes. The severity of the airframe shadowing, for both types of UAVs, depends on the airframe or wings material, its size, its shape, antenna location on the UAV's frame, and UAV trajectories. This phenomenon has been observed in practice; however, as mentioned in [93], [94], it has not yet been fully studied.

The communications channel gain depends on the relative orientation of the transmitting and receiving antennas. During the flying phase, a multirotor UAV must tilt, thus changing its antenna orientation. As a consequence, the communication channel observed when a multirotor UAV hovers is different than when they move [96]. Furthermore, the contribution on

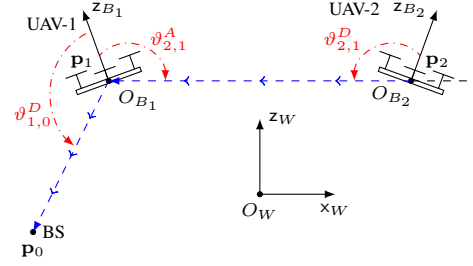


Figure 4: A chain of relays composed of two UAVs and one ground BS. In blue the LoS components, and in red the Angle of Arrival (AoA) and the Angle of Departure (AoD) for each UAV [97].

the antenna channel gain will vary with the motion of the UAV, see [97] for more details. Similarly, during turning manoeuvres, a fixed-wing UAV has to tilt, thus changing its antenna orientation, see Fig. 5. The communications channel observed when fixed-wing UAVs move on a straight line is different than when they are turning. We also note that the location and orientation of the antenna on the UAV has a significant impact on the communications channel, as shown experimentally in [98], [99], [100], [101].

The UAV channel models can be divided into two types. The first consists of air-to-ground channels, which characterize the channels between a UAV and ground users or ground BS. The second consists of air-to-air channels, which characterize the channels between flying UAVs.

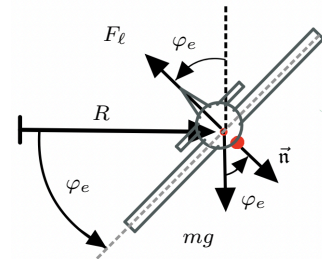


Figure 5: Fixed-wing UAV; the UAV antenna is indicated by a red dot. Front view of fixed-wing UAV performing a steady turn with a bank angle φ_e .

1) *Air-to-ground channels*: The air-to-ground channel communication models the link between a UAV and a ground user, such as a control station or a 5G BS. The properties of this channel depend not only on the distance between both nodes, but also on the UAV altitude and on the **elevation angle**¹⁰. As the elevation angle increases, the probability of LoS between both nodes also increases. As such, LoS links present lower losses than non-LoS links. As the UAV altitude increases, the elevation angle increases along with the distance between the nodes. For instance, one illustrative model that describes such

¹⁰The angle of vector $\mathbf{p}_{UAV} - \mathbf{p}_G$ measured w.r.t. the horizontal plane, where \mathbf{p}_{UAV} and \mathbf{p}_G is the position of the ground node.

effects is [102]:

$$\begin{aligned}\mathcal{H}(\mathbf{p}(t), \mathbf{q}(t)) [dB] &= -20 \log (4\pi\lambda \|\mathbf{p}(t) - \mathbf{q}(t)\|_2) \\ &+ \xi(\mathbf{p}(t), \mathbf{q}(t)),\end{aligned}\quad (59)$$

where the first term represents the average path loss and $\xi(\mathbf{p}(t), \mathbf{q}(t))$ represents the shadowing. If there is line of sight, then $\xi(\mathbf{p}(t), \mathbf{q}(t)) \sim \mathcal{N}(\mu_{LOS}, \sigma_{LOS}^2)$. Otherwise, $\xi(\mathbf{p}(t), \mathbf{q}(t)) \sim \mathcal{N}(\mu_{NLOS}, \sigma_{NLOS}^2)$. To complete this channel model, we must also consider the probability of having line of sight, which can be expressed as:

$$P_{LOS}(\mathbf{p}_{UAV}, \mathbf{q}) = \frac{1}{1 + a \exp \left(-b \left[\frac{180}{\pi} \sin^{-1} \left(\frac{z_{UAV}}{d_h} \right) - a \right] \right)}, \quad (60)$$

where z_{UAV} is the altitude of the UAV, d_h is the horizontal distance between \mathbf{p}_{UAV} and \mathbf{q} , and the coefficients a and b are environment-dependent.

The model (59)-(60) does not take into account small-scale fading. As mentioned in [94], small-scale fading in air-to-ground channels often follows a Ricean distribution whose properties depend on the UAV altitude and the surroundings of the ground node. There are also approaches which use 3D numerical maps of the region of operation to determine the channel model [103]. We refer the reader to the survey in [94] for more detailed information about the air-to-ground UAV communications channels.

2) *Air-to-air channels*: The modeling of ground-to-air channels is not yet well studied, but the situation for air-to-air channels (communications channels between flying UAVs) is worse still as there are fewer studies and measurement campaigns focusing on these types of channels [93]. When the altitude of two UAVs is low, the floor and other objects on the surface (e.g. hills, buildings, and trees) influence the channel. However, as the altitude of the UAVs increases, such influences weaken. As the altitude of both UAVs increases, the channel tends to consist of a LoS and tends to behave like the *free-space* channel described in section III-A1.

It has been observed experimentally that when the UAVs operate in an open field with a floor that is flat enough, the propagation channel follows a two-ray model [93]. As the altitude of the UAVs increases, the strength of the reflected path decreases. Further, when the UAVs are operating over bodies of water, such as lakes, the strength of the reflected path is stronger than when operating over land.

The constructive and destructive interference between the LoS and reflected waves described by the two-ray model can statistically be described with the small-scale fading. This is the approach taken in [104], where it was shown experimentally that the air-to-air channel model can be modelled as follows:

$$\mathcal{H}(\mathbf{p}(t), \mathbf{q}(t), t) = \frac{h(\mathbf{p}(t), \mathbf{q}(t), t)}{L_P(\mathbf{p}(t), \mathbf{q}(t))}, \quad (61)$$

where the pathloss term $L_P(\mathbf{p}(t), \mathbf{q}(t))$ follows the *free space* model, and the small-scale fading term is well described by a Rician distribution with the height-dependent parameters:

$$p_h(x) = \frac{x}{\sigma_0^2} \exp \left(\frac{-x^2 - \rho^2}{2\sigma_0^2} \right) I_0 \left(\frac{x\rho}{2\sigma_0^2} \right), \quad (62)$$

$$\sigma = ah^b + c, \quad (63)$$

where $x \geq 0$; ρ and σ are the strength of the dominant and scattered components, respectively; h is the altitude of the UAVs (both UAVs are assumed to have the same altitude); and with $a, b < 0$, and c being parameters to be fitted numerically according to the environment. Finally, we refer the reader to the survey in [93] for more detailed information about the air-to-air UAV communication channels.

C. Performance metrics

In CaTP, the communication aspects are taken into consideration in the optimization problem in either the target function or the constraints. This requires the use of metrics to quantify the performance of wireless communication. Next, we discuss the metrics that are most relevant to CaTP.

- 1) **Channel quality**: one way in which the channel quality can be assessed is by measuring its power by using the Channel-to-noise Ratio (CNR) and the Signal-to-Noise Ratio (SNR). The instantaneous CNR [5] at the receiver can be expressed as:

$$\text{CNR}(\mathbf{p}(t), \mathbf{q}(t), t) = \frac{|\mathcal{H}(\mathbf{p}(t), \mathbf{q}(t), t)|^2}{\sigma^2}, \quad (64)$$

where $\mathbf{p}(t)$ and $\mathbf{q}(t)$ are the positions of the transmitter and the receiver, respectively, and σ^2 is the power of the thermal noise generated at the receiver. The mean CNR is $\mathbb{E}[\text{CNR}(\mathbf{p}(t), \mathbf{q}(t), t)]$, where the expected value is taken w.r.t. small-scale fading and shadowing. The SNR is the CNR multiplied by the transmission power, which can be time-variant.

Another important metric is the Received Signal Strength (RSS) [105]. It measures the power of the received signal, with the reason behind its importance being that many receivers in the market provide the Received Signal Strength Index (RSSI) (a discretized version of the RSS). In practice, many algorithms resort to working with the RSSI.

- 2) **Error rate**: in some cases, one can be more interested in the performance of the communication system, rather than in the channel quality. The principal way of evaluating the performance of a communication system is by quantifying the errors that occurred in the transmission. This is done by calculating the Bit Error Rate (BER) or by the Packet Reception Ratio (PRR) [106], which measures how many packets were successfully received without errors. These metrics evaluate the performance of the communication system, and thus strongly depend on the specifications of the system, including the modulation scheme and the communication protocols.
- 3) **Channel capacity**: the channel capacity was first introduced by Claude Shannon in 1948 in [107]. It is an upper bound on the maximum bit rate, given channel conditions, for which an arbitrarily low BER can be reached. Its mathematical expression depends on the information that the transmitter and the receiver have about the channel, as well as on the power transmission strategy. When the channel is estimated at the receiver

and the transmitter uses constant transmission power, then the channel capacity is given by [108]:

$$C = B \int_0^\infty \log_2 (1 + \gamma) p(\gamma) d\gamma, \quad (65)$$

where γ is the SNR, $p(\gamma)$ is its p.d.f., and B is the bandwidth of the transmitted signal.

D. Energy consumption

Although often the MR's energy consumption is mostly due to motion, this is not always the case, as shown in the experiments presented in [49]. The μ controller, the CPU, and the sensing systems can consume an amount of energy which may be comparable to the amount of energy spent in motion. The same applies to the MR's communication system. The energy consumed by the communication system is mainly determined by the transmission power. Next, we discuss transmission strategies.

- 1) **Constant power transmission:** all signals are transmitted with constant average power. As a consequence, the transmitter's energy consumption depends on the transmission time, but is independent of the transmitter and receiver positions. In this scenario, the SNR depends on the positions of the transmitter and the receiver through the spatial variations of the channel.
- 2) **Adaptive power transmission:** the transmitter adapts its power to ensure a certain power P_{ref} for the received signal. The power is adapted as follows:

$$P = \frac{P_{ref}}{|\mathcal{H}(\mathbf{p}(t), \mathbf{q}(t), t)|^2}. \quad (66)$$

P_{ref} is selected to ensure a certain quality of service. The transmission power in (66) can take any arbitrarily large value. In practice, the transmission power is limited to a certain value P_{max} by the hardware limitations, or by legal regulations. If the intended transmission power is smaller than P_{max} , then the actual transmission power is (66). Alternatively, if the intended transmission power is larger than P_{max} (usually due to a poor channel gain), then it is not possible to satisfy the desired power P_{ref} at the receiver. The most common action in this scenario is to refrain from transmitting and say that an outage has occurred. Thus, the transmission power can be written as:

$$P = \begin{cases} \frac{P_{ref}}{|\mathcal{H}(\mathbf{p}(t), \mathbf{q}(t), t)|^2} & \text{for } \frac{P_{ref}}{|\mathcal{H}(\mathbf{p}(t), \mathbf{q}(t), t)|^2} \leq P_{max}, \\ 0 & \text{otherwise.} \end{cases} \quad (67)$$

A common practice for mathematical simplicity and tractability is to assume $P_{max} \rightarrow \infty$ (i.e. disregard the power limitation).

Finally, the energy consumption at the receiver is generally considered constant. It is usually significantly lower than that of the transmitter, and is hence often neglected in the analysis.

E. Final comments on communications models

We have provided an overview of communication systems and basic channel models for both ground MRs and UAVs. We also discussed the special characteristics of UAV channel models. Another special scenario that can be important for some CaTP applications, such as rescue and search operations, regards communication inside tunnels and underground mines. These types of channel models are outside the scope of this tutorial, although interested readers are referred to [109], [69], [110].

The models presented in this section are narrowband models, which are the most basic models. More complex and elaborate models include wideband communication channel models, which take into consideration how the channel varies w.r.t. the frequency. Also, we must mention that when one of the transceivers moves quickly, Doppler shift occurs and affects the received signals. This phenomenon can be of particular importance when dealing with fixed-wing UAVs as they are capable of high speed flight.

IV. COMMUNICATIONS-AWARE TRAJECTORY PLANNING

As mentioned in section I, Communications-aware Trajectory Planning (CaTP) is trajectory planning in the context of Communications-assisted Robotics (CaR) and Robotics-assisted Communications (RaC) applications. CaTP problems aim to design trajectories where both communications (e.g. communication energy consumption, quality of the communications link, number of transmitted bits) and robotics aspects (e.g. kinematic and dynamic constraints, motion energy consumption) are simultaneously considered. We begin with some preliminary concepts.

A particular case of CaTP is the Communications-aware Path Planning (CaPP) problem. The trajectory and path are defined as follows:

Definition 1 (Path). *The path followed by a robot from time instant t_1 to t_2 is defined as $\mathcal{P}(\mathbf{p}(t), t_1, t_2) \triangleq \{\mathbf{p}(t) | t \in [t_1, t_2]\}$, where $\mathbf{p}(t)$ is the position of the robot at time instant t .*

Definition 2 (Trajectory). *The trajectory followed by a robot from time instant t_1 to t_2 is the description of the robot's position at each instant $t \in [t_1, t_2]$ and can then be described as $\mathcal{T}(\mathbf{p}(t), t_1, t_2) = \{\mathbf{p}(t), t | t \in [t_1, t_2]\}$.*

The **path** consists of the collection of all the points visited by the MR without specifying when and without any velocity information. Alternatively, the trajectory gives not only information about the points visited by the MR, but also a temporal description of the change of the MR's position over time. The trajectory can also be considered as the combination of the path and the MR's velocity profile.

From the application point of view, a CaTP problem can be cast as either a CaR or a RaC task. We can also classify CaTP problems depending on what is being optimized into three categories. In the first category, the objective is to design the MR's full trajectory, i.e., path and velocity profile, see [4]. In the second category, the translational velocity is given (e.g. constant speed) and the objective is to design the MR's path,

see [111]; this is a CaPP problem. In the third category, the path is given and the objective is to design the translational speed profile with which the MR will follow the given path, see for example [106].

CaTP problems can also be divided according to two types of trajectories: **predetermined** trajectories and **adaptive** (also referred to as reactive) trajectories. Predetermined trajectories are designed before they are executed by the MR, e.g., [4]. Adaptive trajectories are created and modified as the robot executes them [97]; as such, the MR could use a predetermined trajectory as an initial guide and then implement an adaptive mechanism to adapt the trajectory in real-time in response to new information obtained from the environment, or the MR could create the trajectory in real-time while operating. In this section, we focus on predetermined trajectories, but we will briefly discuss the design of adaptive trajectories in the next section.

The optimization method and the optimum trajectory resulting from solving CaTP problems strongly depend on the information that is available about the wireless channel when solving the optimization problem. Some possible scenarios are described next.

- 1) **Physical map available:** in this scenario, we have full knowledge of the Radio Frequency (RF) map (or a good estimate of it). In other words, we have knowledge (or an estimate) of $\mathcal{H}(\mathbf{p}, \mathbf{q}(t), t)$ in (51) for all $\mathbf{p} \in \mathcal{W}$ and all $t \in [0, T]$ where \mathcal{W} is the workspace that the MR can move within and $\mathbf{q}(t)$ is the position of the other node.

For instance, in [112], the authors study the performance of different 3D path planners for a single UAV communicating over a cellular network. They resort to a realistic RF map to accurately evaluate the connectivity and the interference resulting from each path planning algorithm. This map is constructed as follows. First, a public 3D map of the region of Flanders, Belgium [113] is used. This map was generated by Lidar with centimetre precision, a latitude and longitude resolution of $1m \times 1m$, and each pixel containing the height of the surface. Then, the authors restricted the study to the city of Ghent. Using information from the Belgian Institute for Postal Services and Telecommunication, they located the position of nineteen BSs of the Belgian mobile provider, *Proximus*, within the area. Finally, this map was fed into the 3D radio coverage simulator [114].

This simulator models the 3D radiation pattern of the antennas observed. It uses both the 3D map and the location of the transmitter and receiver to check whether or not a LoS exists. By doing so, it takes into account any shadowing. To account for multipath fading, this simulator adds a Gaussian random process to the overall channel with variance dependent on the altitude of the UAV. In the end, the resulting 3D RF map allowed the authors to observe how changes in altitude of the UAV path planning can improve the communication performance.

If we have a physical 3D map of the workspace, then we can also obtain a 3D RF map implementing ray tracing

[71], [72], [73]. This type of RF map will capture the effect of shadowing (due to obstruction of the LoS), and can also capture multipath fading.

Note that, 2D physical maps can also be used to create 2D RF maps, which can be useful particularly for ground MRs operating indoors. These 2D RF maps will mainly be useful to precisely determine when walls obstruct the LoS.

- 2) **RF channel measurements available:** In this case, we do not have a physical map of the workspace where the MRs are operating, but we do have access to a number of RF channel measurements taken at different locations in the workspace. Thus, prior to solving the communications-aware trajectory planning, we feed the channel measurements available into a predictor to create an RF map that will be used by the trajectory planner.

In [115], the authors consider a ground MR that must visit a number of points of interest, gather data there, and then transmit all collected data to a BS. This must be done while minimizing the total energy consumed (the energy spent in motion plus the energy spent in transmission). The MR initially disposes of few channel measurements taken in the workspace. These measurements are then fed into the probabilistic channel assessment framework developed by the authors in [76] and [77]. This framework is used by the path planning algorithm to predict the channel gain throughout the workspace. The predicted probabilistic RF map is constructed relying on the pathloss model, the Probability Density Function (PDF) of the multipath fading, and the PDF of the shadowing, as well as its spatial correlation function. Note that, prediction requires making an assumption on the probabilistic distributions of the multipath fading and the shadowing.

- 3) **Mathematical model available:** In this case, we only dispose of a mathematical model of the communications channel.

In our previous work [4], we considered the problem of a multirotor UAV that must reach some goal while transmitting data to a BS. The only information about the communications channel used for solving the communications-aware trajectory planning was the pathloss model and the PDF of the shadowing. In [116], the authors considered the problem of optimizing the position of a UAV operating as a BS. To solve this, they considered the pathloss model, which is complemented by the PDF of the LoS.

In [117], we considered the problem of compensating the small-scale fading in an MR communications link. To solve this problem, we relied on the knowledge of the PDF and of the spatial correlation of the small-scale fading.

Now that we have introduced some preliminary concepts for CaTP problems, in the next subsection, we will discuss the mathematical structure of a generic CaTP optimization problem for obtaining a predetermined trajectory.

A. General Structure

The general structure of a CaTP optimization problem which aims to determine a predetermined trajectory of a single MR can be described as:

$$\begin{aligned} & \underset{\mathcal{C}, \mathcal{T}}{\text{minimize}} \quad J(\mathcal{C}, \mathcal{T}) \\ & \text{s.t.} \\ & \text{motion model,} \\ & \text{channel model,} \\ & \text{trajectory constraints,} \\ & \text{communications constraints,} \end{aligned} \quad (68)$$

where \mathcal{C} is the set of all communication related parameters to be optimized, such as modulation order or transmission power¹¹; and \mathcal{T} is the set of variables related to the trajectory of the robot, such as the completion duration of the trajectory or the waypoints that form the robot's path. For instance, the authors in [28] investigate aerial data aggregation and field estimation from a finite spatial field with a UAV. In this context, they look for the minimum time UAV trajectory completing a defined mission consisting of the collection of some minimal amount of data. In this optimization problem, the inputs forming \mathcal{T} are the number and 3D locations of the UAV hovering points, as well as the order in which they are visited. Further, there are no inputs related to the communications system, and thus $\mathcal{C} = \emptyset$. In [115], the authors consider the scenario where an MR is tasked with visiting a number of points of interest, gathering data, and then finding a good position to successfully transmit all of the collected data to a BS. The optimization problem consists of performing such a task while minimizing the total energy consumption, including the communication and motion components. In this optimization problem, the inputs forming \mathcal{T} are the set of waypoints forming the robot's path, and the input forming \mathcal{C} is the spectral efficiency (i.e. the bit rate normalized by the bandwidth) of the robot's transmitter. In [116], the authors consider the placement of a UAV acting as an aerial base station, seeking to maximize the number of users served while satisfying a minimum Quality of Service (QoS). In this optimization problem, the input forming \mathcal{T} is the 3D position of the UAV, and \mathcal{C} is the set of users who are provided communications by the UAV (i.e. the UAV decides to which users it will provide communication). In [14], the authors consider a fixed-wing UAV working as a communications relay between ground nodes and a BS. The optimization problem consists in maximizing the energy efficiency of the aerial relay (i.e. the total amount of data relayed over the energy consumed). Thus, the inputs forming \mathcal{T} are the position, velocity, and acceleration profiles of the UAV, where \mathcal{C} is the transmission power of the UAV and the transmission power of the BS. In [4], a UAV was required to reach a goal point in finite time while communicating with a BS. The optimization problem consisted of performing such a task efficiently from a communications and energy consumption perspective. The inputs forming \mathcal{T} were the control signals for the UAV motors, with no input related to the communications $\mathcal{C} = \emptyset$. In [118], the authors considered a multirotor UAV acting as an aerial BS

¹¹Note that if all of the communications parameters are fixed, then $\mathcal{C} = \emptyset$.

for ground users, where the UAV is equipped with a directional antenna of adjustable beamwidth. In the optimization problems considered by the users, the input forming \mathcal{T} is the altitude of the UAV, and the input forming \mathcal{C} is the beamwidth.

This generic CaTP problem (68) is composed of five elements: the optimization target $J(\mathcal{C}, \mathcal{T})$; a motion model for the MR describing how its *state* behaves according to the control signal \mathbf{u} ; a wireless channel model describing how the received and transmitted signals behave depending on the position and orientation of the MR; some trajectory related constraints; and finally, constraints related to the communication system performance and/or goals. We now discuss these five elements in more detail.

- 1) **Optimization target:** by convention, optimization problems are usually stated as minimization problems [119], as in (68). However, they are sometimes initially cast as maximization problems. One common instance of an optimization problem being cast as a maximization problem is when the focus is on energy efficiency [14] [12]; another example is the maximization of users served by an aerial relay [116]. Nevertheless, even if a problem is initially cast as a maximization problem, it can always be converted into an equivalent¹² minimization problem by proceeding as follows [119]:

$$\underset{\mathcal{C}, \mathcal{T}}{\text{maximize}} \quad J(\mathcal{C}, \mathcal{T}) \rightarrow \underset{\mathcal{C}, \mathcal{T}}{\text{minimize}} \quad -J(\mathcal{C}, \mathcal{T}). \quad (69)$$

There are other possible transformations of the optimization target to convert the maximization problem into a minimization problem. For example:

$$\underset{\mathcal{C}, \mathcal{T}}{\text{maximize}} \quad J(\mathcal{C}, \mathcal{T}) \rightarrow \underset{\mathcal{C}, \mathcal{T}}{\text{minimize}} \quad J^{-1}(\mathcal{C}, \mathcal{T}). \quad (70)$$

While the linear transformation in (69) maintains the same properties of the original optimization target regardless of its nature, the nonlinear transformation (70) deforms the original optimization target by expanding it for values in the region $[-1, 1]$ and compressing it outside of this interval. Furthermore, if the original optimization target $J(\mathcal{C}, \mathcal{T})$ can take a value of zero, then $J^{-1}(\mathcal{C}, \mathcal{T})$ will not be defined at this value. Nevertheless, note that if $J(\mathcal{C}, \mathcal{T}) > 0$ (or $J(\mathcal{C}, \mathcal{T}) < 0$), then the nonlinear transformation (70) is not necessarily an issue. For instance, the authors in [118] transform a minimization problem into a maximization problem by applying the nonlinear transformation (70) to a strictly positive optimization target. Related to this issue, the authors in [120] move in the opposite direction of the nonlinear transformation (70). Instead of minimizing the power consumption, they choose to maximize the inverse of the power consumption, as it makes their optimization problem easier to solve.

If the inputs of the optimization problem (i.e. \mathcal{C} and \mathcal{T}) are variables, then the optimization target is a function, as seen in the optimization problems of [121], [7]. On the other hand, if the inputs of the optimization

¹²Two optimization problems are equivalent if, and only if, they have exactly the same solution.

variable are functions, then the optimization target is a functional [122], as in [117], [21], [123]. Finally, if the optimization target is a function and the optimization problem is a minimization problem, then we refer to the optimization target as a cost function. Alternatively, if the optimization target is a function, but the optimization problem is a maximization problem, then we refer to the optimization target as the utility function [119]. Similarly, if the optimization target is a functional and the optimization problem is a minimization problem, then we refer to the optimization target as the cost functional [5], [8].

We must also mention that if the set of inputs $\{\mathcal{C}, \mathcal{T}\}$ contains continuous variables/functions and discrete variables/functions, then the optimization problem is referred to as mixed-integer. A very common class of mixed-integer optimization problems which often appears in CaPP is the Mixed-Integer Linear Programming (MILP) [115], [124], [125], [126].

We continue by reviewing some cases of functionals in the optimization targets. Let us start with the optimization target¹³ initially considered in [4] for a communications-aware trajectory planning problem for a multirotor UAV:

$$J = \lambda \int_0^{t_f} \|\mathbf{u}(t)\|_2^2 dt + (1 - \lambda)w(\mathbf{p}), \quad (71)$$

where t_f is the trajectory duration; the first term is the energy consumed by the UAV in motion, while the second term is a general communication term depending on the UAV bit rate over its whole trajectory. The parameter $\lambda \in [0, 1]$ determines the importance of one term over the other. The control signal for the UAV is $\mathbf{u}(t) \in \mathbb{R}^4$ defined in $t \in [0, t_f]$ (i.e. \mathbf{u} is a four dimensional vectorial function defined over a closed support). The 3D position of the UAV is then $\mathbf{p}(t) \in \mathbb{R}^3$ defined in $t \in [0, t_f]$ (i.e. \mathbf{p} is a three dimensional vectorial function defined over a closed support). The model in [4] that was used to describe the relationship between the UAV control signal \mathbf{u} and its position \mathbf{p} is the same as described in section II-B. Therefore, the optimization target J depends on two functions: the UAV control signal \mathbf{u} and the UAV position \mathbf{p} (which itself depends on \mathbf{u}). Furthermore, the optimization target is the convex combination of two functionals.

Another interesting example can be found in [123]. In this case, an MR disposes of a fixed finite time T to harvest radio energy from a BS. The channel experiences small-scale fading, and the radio energy harvested varies greatly over very small distances. Thus, the MR uses the following procedure divided in three phases: during the first phase, the MR moves along a line of length L for a duration of αT_s with $\alpha \in (0, 1)$ and $T_s < T$; during the second phase, the MR moves to the position in the line with the highest channel gain; lastly, the MR remains for the rest of the time (i.e. $T - T_s$) at that position

harvesting radio energy. The objective in cited paper is to optimize the velocity profile of the MR in order to maximize the expected value of the energy harvested. Therefore, the optimization target is:

$$\begin{aligned} J = & E_s(v_{L,\alpha,T_s}^I) + E_s(v_{L,\alpha,T_s}^{II}) + E_H(L, T_s) \\ & - E_m(v_{L,\alpha,T_s}^I) - E_m(v_{L,\alpha,T_s}^{II}), \end{aligned} \quad (72)$$

where v_{L,α,T_s}^I and v_{L,α,T_s}^{II} are the speed profiles of the MR for the first and second phases, respectively. They are both unidimensional, continuous functions parametrized over the variables L , α , and T_s . The support for v_{L,α,T_s}^I is $t \in [0, \alpha T_s]$ and the support for v_{L,α,T_s}^{II} is $t \in [\alpha T_s, T_s]$. The first term in (72) is the energy harvested during the first phase while using the speed profile v_{L,α,T_s}^I ; the second term is the energy harvested during the first phase while using the speed profile v_{L,α,T_s}^{II} ; the third term is the energy harvested at the optimum position found by the MR. This energy depends on the length L (the space where the MR searched for the position with the largest channel gain) and the time spent harvesting energy at the position with the largest channel gain; the fourth term is the energy spent by the MR in motion during the first phase; the fifth term is the energy spent by the MR in motion during the second phase. From the above description, we can observe that the optimization target (72) is the sum of four functionals ($E_s(v_{L,\alpha,T_s}^I)$, $E_s(v_{L,\alpha,T_s}^{II})$, $E_m(v_{L,\alpha,T_s}^I)$, and $E_m(v_{L,\alpha,T_s}^{II})$) and one function $E_H(L, T_s)$ (which depends on the variables L and T_s). In this problem, the functions v_{L,α,T_s}^I and v_{L,α,T_s}^{II} are actually parametrized on the variables L , α , and T_s . Nevertheless in [123], we use calculus of variations [127] to find the optimum shape of the speed profiles (i.e. the functions v_{L,α,T_s}^I and v_{L,α,T_s}^{II}) parametrized on L , α , and T_s . After this step, the functionals in (72) become functions of L , α , and T_s .

The general strategy for converting functionals into functions is to fix the shape of the function that constitutes the input to the functional. One way to do this is to actually find its optimum shape as described in the previous example. Regardless, this is not always possible due to the complexity of the problem, at least not in an analytical manner. In that case, we can proceed with the method used in [7] to transform a functional into a function. In [7], we considered a UAV acting as a data ferry between a source and a destination. The objective was to optimize its periodic trajectory with period T in order to maximize the upper bound of the number of bits transferred from the source to the destination via the UAV. During the first half of the trajectory, the UAV collects the data from the source and delivers it to the destination in the second half. The corresponding functional¹⁴ to maximize is:

$$J = \int_0^{T/2} r(x(t), y(t)) dt, \quad (73)$$

¹³We simplify the writing of the original equation for clarity purposes.

¹⁴Written in a simplified manner.

where the functions $x(t)$ and $y(t)$ represent the trajectory of the UAV at the time instant t in the $x - y$ plane, and the integrand of (73) is the maximum instantaneous bit rate achievable at (x, y) . The integral represents the maximum amount of bits collected by the UAV from the source (the number of bits delivered to the destination must be the same). Because of the constraints and the nature of the problem, the optimum trajectory of the UAV must be symmetric w.r.t. the middle point between the destination and the source. The functional (73) depends on the unidimensional continuous functions $x(t)$ and $y(t)$, with support $t \in [0, T]$. Since the problem indicates that the optimum UAV trajectory is periodic, then one way to transform the functional (73) into a function is by constraining the shape of the functions $x(t)$ and $y(t)$ with a Fourier series of order N :

$$\begin{aligned} x(t) &= \sum_{n=1}^N a_n \cos\left(\frac{n2\pi t}{T}\right) + \sum_{n=1}^N b_n \sin\left(\frac{n2\pi t}{T}\right), \\ y(t) &= \sum_{n=1}^N c_n \cos\left(\frac{n2\pi t}{T}\right) + \sum_{n=1}^N d_n \sin\left(\frac{n2\pi t}{T}\right). \end{aligned} \quad (74)$$

After adding the constraint (74) into the optimization problem, the functional (73) becomes a function of the Fourier series coefficients $\{a_n\}_{n=1}^N$, $\{b_n\}_{n=1}^N$, $\{c_n\}_{n=1}^N$, and $\{d_n\}_{n=1}^N$. Due to the constraint on the shape of the trajectory, the optimum trajectory resulting from this modified optimization problem will be a suboptimal trajectory for the original optimization problem. This suboptimal trajectory will get closer to the actual optimum trajectory as the order of the Fourier series grows, but so does the number of variables to optimize. In CaTP problems, the optimization target can contain two types of terms: communications-related terms and robotics-related terms.

Regarding the communications-related terms, we can find the following examples. In [128], the authors consider a multirotor UAV acting as a relay between a BS and a mobile ground node. The communications channel model suffers small-scale fading, and the cost function consists of the outage probability. In [116], the optimization target is the number of users served by a UAV operating as an aerial BS. In [129], the authors consider a Low-altitude aerial platform (LAP) acting as a BS to ground users in an urban environment. Therein, the problem was to optimize the LAP altitude to maximize the radius of coverage, i.e., the radius of the coverage area, which is defined therein as the area in which the path loss is lower than some specified threshold. In [118], the authors consider a multirotor providing communications to various ground users. In that paper, the authors consider various optimization problems. Among the communication-related terms appearing in the corresponding optimization targets we find the time that the UAV takes to transmit a certain amount of data, and also we find another term consisting

of the total amount of bits transmitted by the UAV to the ground users. In [117], we optimize the position of an MR that must communicate with a BS where the optimization target includes the expected value of the channel gain. In [115], the authors consider an MR that must visit various points of interest and then transmit the collected data to a BS. The communications term considered in the optimization target is the energy spent in transmitting all the collected data.

Regarding the robotics-related terms, we find the following examples. In [28], the authors consider a multirotor UAV. Their cost function has two robotics-related terms: the time that the UAV takes to complete a closed trajectory and the time that it spends hovering over ground nodes. In [115], the authors consider an MR moving at constant speed, where the cost function involved considers the energy spent in motion which takes the form (33). In [14], the authors aim at maximizing the efficiency of a fixed-wing UAV acting as a communications relay. The cost function considers the energy spent in propulsion for the UAV, which is the same formula as in (50).

In CaTP problems, the optimisation target can take different forms, however they can be divided into three classes. The first class includes communications and robotics terms, the second class has only robotics-related terms, and the third class has only communications-related terms. In subsections IV-B and IV-C, we will discuss in further detail the form and properties that this optimization target can take in different problems.

- 2) **Motion model:** this relates the state of the MR to the control signal \mathbf{u} . The motion model consists of kinematic or dynamic models like the ones discussed in section II. As mentioned in section II, many motion models are nonlinear with respect to the control signal \mathbf{u} , however they can also be linearized to simplify the control and the optimization procedure (although the solution would then become suboptimal).
- 3) **Channel model:** the selected channel model must take into account the physical environment where the MR and the nodes communicating with it are located (e.g. indoor or outdoor and urban or rural scenario). It is also important to consider if the links involved are ground-to-ground (the MR and the other node are located at ground level), air-to-ground (i.e. a UAV and a ground node), or air-to-air (i.e. communication between two UAVs).
- 4) **Trajectory constraints:** these constraints directly restrain the shape of the trajectory and the time in which it is completed.

One simple constraint in this category defines the area where the MR can operate. For example, the authors in [84] consider an MR with position $\mathbf{p}(t) \in \mathbb{R}^2$ at time instant t . They define the workspace $\mathcal{W} \subset \mathbb{R}^2$, and also define the set \mathcal{Q}_t which contains the set of points where the channel measurements have been taken up to the instant t . Then, they introduce the following constraint regarding the area where the MR can move at the time instant t :

$$\mathbf{p}(t) \in \mathcal{W} / \mathcal{Q}_t. \quad (75)$$

In [124], there is another similar constraint. The authors define the environment \mathcal{X} as a large convex polygonal subset of the 2-D Euclidean space \mathbb{R}^2 . Next, they define $\mathcal{X}_{obs} \subseteq \mathcal{X}$ as the regions in the environment occupied by polygon obstacles.

The shape of the trajectory can be constrained to polynomials [130] or splines [131]. One reason for using this type of constraint is that the resulting optimum trajectory can still be feasible for the real-life robot [97]. Various types of polynomials can be used, each with their own particular properties (e.g. Chebyishev polynomials [132], Laguerre polynomials [133]). The discussion of this particular type of constraint and their relation to a trajectory's feasibility and smoothness is a complex topic beyond the scope of this tutorial, but the interested reader can find more information in [134] and the references therein.

We can also constrain the initial and/or final positions of the robots [106], [12] by adding the trivial constraints:

$$\mathbf{p}(0) = \mathbf{p}_{ini}, \quad \mathbf{p}(t_f) = \mathbf{p}_{fin}. \quad (76)$$

If the initial and final positions are different (see [12], [135]), then we have an **open trajectory**. If they are the same ([136], [7]), then we have a **closed trajectory**. We find closed trajectories in repetitive tasks, such as a multirotor UAV operating as a data ferry [7], an MR doing persistent data collection from sensor nodes [126], or a fixed-wing UAV acting as a communications relay [136]. Note that, a multirotor UAV acting as a communications relay can simply hover and remain still at a specified position. However, a fixed-wing UAV must be moving at all times. Thus, when it operates as a communications relay, it will track a circular trajectory around a certain point, thereby executing a closed trajectory.

In the case of predetermined trajectories, $\mathbf{p}_{ini} = \mathbf{p}_{fin}$ implies that the trajectory is also periodic. Furthermore, if the trajectory is also smooth, then it can be well approximated using the Fourier series [7].

Another type of constraint aims at limiting the velocity and/or acceleration of the robot. In [137], the authors consider a group of N MRs with positions $\{\mathbf{x}_n\}_{n=1}^N$, where $\mathbf{x}_n \in \mathbb{R}^2$ and velocities $\{\mathbf{u}_n\}_{n=1}^N$, where $\mathbf{u}_n = \dot{\mathbf{x}}_n$. Next, they directly limit the speed of each MR by adding the following constraint:

$$\|\mathbf{u}_n\|_\infty \leq V_n, \quad (77)$$

where V_n is a design parameter. The authors mention that they used the H_∞ -norm to limit the MRs speed instead of the ℓ_2 -norm in order to keep their particular optimization problem as a linear program. Nevertheless, the use of the ℓ_2 -norm to directly limit the speed is very common [135], [11]. In the case of multirotor UAVs, it is also common to separately limit the horizontal speed and the vertical speed [138], [139]. To do this, we can add a constraint in the following manner:

$$\|\mathbf{v}_{xy}(t)\|_2 \leq V_{xy}, \quad |v_z(t)| \leq V_z, \quad (78)$$

where $\mathbf{v}_{xy}(t)$ is the horizontal velocity of the UAV and $v_z(t)$ is its vertical velocity. Then, V_{xy} and V_z are the horizontal and vertical speed limits. Sometimes it is possible to find constraints limiting not only the speed, but also the acceleration [29]. Furthermore, we can also have the following set of constraints [140]:

$$-\bar{\mathbf{v}} \leq \mathbf{v} \leq \bar{\mathbf{v}}, \quad -\bar{\mathbf{a}} \leq \mathbf{a} \leq \bar{\mathbf{a}}, \quad -\bar{\boldsymbol{\omega}} \leq \boldsymbol{\omega} \leq \bar{\boldsymbol{\omega}}, \quad (79)$$

where $\bar{\mathbf{v}} \in \mathbb{R}^3$ and $\bar{\mathbf{a}} \in \mathbb{R}^3$ are the upperbounds for the UAV translational velocity $\mathbf{v} \in \mathbb{R}^3$ and its translational acceleration $\mathbf{a} \in \mathbb{R}^3$. Similarly, $\bar{\boldsymbol{\omega}} \in \mathbb{R}^3$ is the upperbound for its attitude angular velocity $\boldsymbol{\omega} \in \mathbb{R}^3$. The inequalities in (79) act separately on each entry of the vectors \mathbf{a} , \mathbf{v} , and $\boldsymbol{\omega}$.

The constraints (77)-(79) directly limit the velocity of the UAV. There are other types of constraints which indirectly limit the velocity of the UAV by acting on the inputs to the dynamic model of the UAV. For instance, the authors in [141] tackle the optimum control of a multirotor UAV with n_r rotors. For this purpose, the authors consider the dynamic model of the rotors. From physical principles, the following constraints are added for each rotor:

$$\omega_{min} \leq \omega_i \leq \omega_{max}, \quad (80)$$

$$-\dot{\omega}_{max} \leq \dot{\omega}_i \leq \dot{\omega}_{max}, \quad (81)$$

where ω_i and $\dot{\omega}_i$ are the angular speed and angular acceleration of the i th rotor. Therefore, ω_{min} , ω_{max} , and $\dot{\omega}_{max}$ are their bounds.

5) **Communications constraints:** these act on the overall communication system performance or directly on the wireless channel experienced by the MR along the whole trajectory. When stochastic channel models are used, the constraints related to the wireless channel are probabilistic. For example, the authors in [28] consider the problem of a multirotor UAV collecting data from ground sensors in a dense Internet of Things (IoT) network. It moves around the region where the network is deployed and selects M hovering locations, collecting data at the nodes covered. The ground-to-air channels experience Nakagami- m fading. Thus, depending on the Signal-to-Interference-and-Noise Ratio (SINR) which itself depends on the hovering locations, the probability of successfully collecting data from the covered sensors can vary. Therefore, the authors add the following probabilistic constraint to their optimization problem:

$$\sum_{\mu=1}^M \mathbb{E}[K_\mu] \geq N, \quad (82)$$

where K_μ is the number of successfully collected observations at the μ th hovering location, and N is the minimum desired **average** number of successful observations that the UAV must collect from the IoT network. In [115], the authors consider the problem of an MR that must visit m Points of Interest (POI), gather their data, and then transmit it to a BS. The MR can transmit with n_r different spectral efficiencies. For every POI, the

MR can choose to transmit data from the current POI or from other n_s communication points close by in order to compensate for small-scaled fading. The authors include the following constraint:

$$\sum_2^m \sum_{j=1}^{n_s+1} \sum_{k=1}^{n_r} R_k t_{i,j,k} = V/B, \quad (83)$$

where R_k is the k th spectral efficiency, V is the total number of bits collected from the POIs, B is the bandwidth used in the transmission, and $t_{i,j,k}$ is the time spent by the MR transmitting at the j th communication point of the i th POI using the spectral efficiency R_k . Note that, even if both papers [28] and [115] consider a stochastic channel model, the constraint (82) is a stochastic while the constraint (83) is deterministic. This is due to the fact that the constraint (82) acts on the received bits, which is a stochastic process (due to the noise at the receiver and the stochastic channel model). However, the constraint (83) acts on the transmitted bits, which is a deterministic process. In [29], the authors consider a multirotor UAV equipped with solar panels acting as an aerial BS and providing communications to static ground users. The transmitter of the UAV disposes of a bandwidth \mathcal{W} , which is divided into N_F orthogonal subcarriers. Then, the authors include the following constraint in their optimization problem in order to ensure that each user is provided a minimum bit rate:

$$\sum_i^{N_F} s_k^i[n] B \log_2 (1 + \gamma_k^i[n]) \geq R_k^{req}, \quad \forall k, n \quad (84)$$

where $s_k^i[n] = 1$ if the k th user is assigned the i th subcarrier by the UAV at time n , and $s_k^i[n] = 0$ otherwise, B is the bandwidth of each subcarrier, $\gamma_k^i[n]$ is the SNR of the channel between the k th user and the UAV on the i th subcarrier at instant n , and R_k^{req} is the minimum bit rate required by the k th user, where $\gamma_k^i[n]$ depends on the position of the UAV (see [29] for a detailed mathematical description). The constraint (84) ensures that, at all times, the achievable data rate of each user is at least R_k^{req} . In [29], the optimization problem was formulated in discrete time. We can find similar constraints in [142] where a UAV is serving K users and a minimum bit rate for each one must be ensured, or in [143] where a UAV acts as a communications relay between a ground user and a BS and a constraint is added to ensure a minimum bit rate on each communications link.

We can constraint a robot to transmit along its trajectory an average of N bits or higher:

$$\int_0^T \mathbb{E}[R(\text{SNR}(\mathbf{p}(t), \mathbf{q}(t), t))] dt \geq N, \quad (85)$$

where $\text{SNR}(\mathbf{p}(t), \mathbf{q}(t), t)$ is the instantaneous SNR observed at time instant t over the link between the MR located at $\mathbf{p}(t)$ and the other node located at $\mathbf{q}(t)$. The function $R(\cdot)$ determines the bit rate transmission as a

function of the instantaneous SNR. This function $R(\cdot)$ depends on the modulation scheme as well as on the bandwidth of the transmitted signal. The expected value in (85) is taken w.r.t. the joint PDF of the shadowing and small-scale fading. To introduce this constraint, the designer needs to know the first order statistics of the wireless channel model. Because of the stochastic nature of the wireless channel, the constraint (85) does not ensure that the MR will be able to always transmit at least N bits, but rather that robots following the same trajectory in the same environment will transmit at least N bits on average. Note that (85) assumes that the transmission process is continuous (we observe this from the integral and the fact that the integrand is treated as a continuous function of time). Even if the transmission is not a continuous process (data is transmitted in packets and not in a continuous and uninterrupted flow), we can simply assume that it is a continuous process, since the dynamics of the motion process is generally much slower than the dynamics of the transmission process. When formulating the problem in discrete time and dealing with Decode-and-Forward (DF) relays, there is a special constraint that often appears called Information Causality Constraint (ICC) [144], [13], [14], [145]. At time slot n , the DF relay receives data from a source, processes it, and then transmits it at the next time slot to the destination. The ICC ensures that, at time slot n , the DF relay cannot transmit the data it received from the source to its destination in the same time slot. For instance, the authors in [144] consider a fixed-wing UAV acting as a relay between a source node and a destination node. The optimization problem is formulated in discrete time, and the ICC is included in the optimization problem as follows:

$$\sum_{i=2}^n \log_2 (1 + p_r[i] \gamma_{rd}[i]) \leq \sum_{i=1}^{n-1} \log_2 (1 + p_s[i] \gamma_{sr}[i]), \quad (86)$$

where $\gamma_{sr}[i]$ and $\gamma_{rd}[i]$ are the CNR at discrete time slot i of the source-to-relay and relay-to-destination links, respectively, and $p_s[i]$ and $p_r[i]$ are the transmission powers at discrete time slot i of the source and of the relay, respectively. The argument of the left term represents the achievable bit rate in the relay-to-destination at slot i , while the argument of the right term represents the achievable bit rate in the source-to-relay at slot i . The ICC (86) makes sure that at time slot n , the relay cannot transmit to the destination more bits than the maximum number of bits it had already processed from the source, hence the term *causality*. We must mention that the Amplify-and-Forward (AF) relays operate differently from the DF relays, and thus the ICC should be adapted accordingly.

There are also constraints acting directly on the wireless channel; the advantage of such constraints resides in the fact that it makes the optimisation problem more independent of the used communication system (e.g. modulation type, AF relay, or DF). For instance, when

the channel model is stochastic, we cannot ensure that the CNR will have a certain value γ_0 , but we can add a constraint to ensure that it achieves this value γ_0 with a desired probability η :

$$\Pr(\text{CNR}(\mathbf{p}(t), \mathbf{q}(t), t) \geq \gamma_0) = \eta, \quad \forall t \in [0, T], \quad (87)$$

where $\mathbf{p}(t)$ and $\mathbf{q}(t)$ are the positions of the transmitter and receiver at time instant t , and T is the time at which we want to maintain the constraint. We find a similar type of constraint in [120], [146] where the authors aim at ensuring a minimum SINR, however they use expected values rather than probabilities to deal with the stochasticity of the communications channels. In [147], the authors consider the placement of a UAV acting as an aerial BS. They introduce a constraint limiting the maximum path loss allowed, which acts only on the deterministic part of the wireless channel.

Another class of constraints act on the communications coverage. They can act either in the spatial domain [148], [116] or in the temporal domain [149]. For instance, the authors in [116] consider a UAV acting as an aerial BS for a group of ground users \mathcal{U} distributed in some area. Their objective is to maximize the number of users in \mathcal{U} served by the aerial BS. To solve this problem, the authors use the following constraint to determine which users are served:

$$R(h) \geq r_i - M(u_i - 1), \quad \forall i = 1, \dots, |\mathcal{U}|, \quad (88)$$

where $R(h)$ is the communications coverage radius of the UAV depending on its altitude h , r_i is the horizontal distance between the i th user and the BS, $\{u_i\}_{i=1}^{|\mathcal{U}|}$ are binary allocation variables to be optimized (if $u_i = 1$, then the i th user is served by the UAV and $u_i = 0$ otherwise), and $M > \max_i r_i$ is a design parameter. The constraint (88) works as follows. If we decide to allocate the i th user to the aerial BS (i.e. $u_i = 1$), then (88) enforces that this user has to be within the coverage area to satisfy the constraint. On the other hand, if we don't allocate the i th user to the aerial BS (i.e. $u_i = 0$), then the constraint (88) becomes satisfied regardless of its horizontal distance r_i to the aerial BS. In [149], the authors consider a UAV navigating in an area sparsely covered by ground BSs. The objective is to reach a final destination in minimum time T , but to ensure that the UAV does not spend more than τ_{max} continuous seconds outside of coverage by any of the BSs. To enforce this, the authors introduce the following constraint:

$$(\rho(t) - t - 1) \leq \tau_{max}, \quad (89)$$

where $\rho(t) = \text{argmin}_{\forall s > t} \{c_s = 1\}$ with:

$$c_t = \begin{cases} 1 & \text{if } \exists \mathbf{g}_k \in \mathcal{G} : \|\mathbf{g}_k - \mathbf{p}(t)\| \leq R, \\ 0 & \text{otherwise,} \end{cases} \quad (90)$$

where $\mathbf{p}(t)$ is the position of the UAV at time instant t , \mathcal{G} is set containing the positions of all the BSs, \mathbf{g}_k is the position of the k th BS, and R is the coverage range of the BSs.

Other types of constraints focus on the transmission power. The authors in [135] consider a UAV communicating with ground nodes that must reach a certain predefined goal. The transmitter of the UAV has power control capacities, i.e., it can vary the transmission power. In their optimization problem, the authors include a constraint to limit the average transmission power:

$$\frac{1}{N} \sum_{n=1}^N p[n] \leq P, \quad (91)$$

where $p[n]$ is the power transmitted by the UAV at discrete time n , N is the duration of the UAV trajectory, and P is the maximum average power allowed. It is also possible to constrain the maximum instantaneous transmission power. In [29], the authors consider a UAV with a transmitter with N_F subcarriers to serve K users. The authors limit the maximum instantaneous transmission power with the following constraint:

$$\sum_{i=1}^{N_F} \sum_{k=1}^K s_k^i[n] p_k^i[n] \leq P_{max}, \quad (92)$$

where $s_k^i[n]$ is a binary allocation variable. If at time n , the i th subcarrier is allocated to the k th user, then $s_k^i[n] = 1$; otherwise, $s_k^i[n] = 0$. The power transmitted by the UAV at time instant n to the k th user through the i th subcarrier is $p_k^i[n]$. Note that, the overall sum in the left term of (92) is the total power transmitted by the UAV at time n . We have to mention that both constraints (91) and (92) make sense for diverse reasons, among them we find the properties of the power amplifier of the RF transmitter. The RF amplifier is a nonlinear device, so it might be possible that the time average power of the signal transmitted operates within the linear region of the amplifier. However, if the maximum instantaneous power is unconstrained, then it is possible that this peak power is operating in the nonlinear region of the amplifier. Thus, the signal transmitted will be distorted by the nonlinearities of the power amplifier and will degrade the performance of the communication [150], [151].

The power consumed by the communications system can sometimes be comparable to the energy spent in motion by the robots. This is reflected in [29], where the authors consider a UAV equipped with solar panels for energy harvesting and providing communication to ground users. To ensure the continuous operation of the UAV, the authors include the following constraint:

$$\left(\frac{1}{\epsilon} P_{tx}[n] + P_{UAV}[n] + P_{static} \right) \Delta_T \leq q[n], \quad \forall n, \quad (93)$$

where $P_{tx}[n]$ is the power transmitted at discrete time n , $P_{UAV}[n]$ is the aerodynamic power consumption of the UAV at the time instant n , P_{static} denotes the static power consumed for maintaining the operation of the UAV, Δ_T is the sampling duration of the UAV controller, and $q[n]$ is the energy level of the battery.

Note that, the energy harvested from the sun does not appear in (93); this is because, in this system, the solar panels are only connected to the battery, so they cannot directly power the other systems of the UAV.

The constraints discussed above are **hard constraints**, i.e., either they are satisfied or they are not. In some cases, hard constraints can cause feasibility issues in the optimization problem [152]. It might be the case that some combination of parameter values makes it impossible to satisfy every single hard constraint in the optimization problem, rendering it unfeasible. In complex CaTP problems with many parameters and complicated constraints, it might be hard to identify this situation. One way to address this issue is by relaxing some hard constraints and transforming them into *soft constraints* [153], [154], [155]. The general idea behind a soft constraint is that it allows violation, but imposes a penalty depending on the extent of the violation.

In CaTP, some constraints are imposed by the physical world. For example, the energy constraint (93) states that the UAV cannot consume more energy than the energy stored within its battery, as this constraint is imposed by the laws of physics and cannot be relaxed. On the other hand, there are other types of constraints which are arbitrarily imposed by the designer. For the constraint in (76), the final position of the robot at the end of its trajectory is arbitrarily imposed by the designer. Thus, if the robot finishes its trajectory at $\mathbf{p}_{fin} + \epsilon$ with a small $\|\epsilon\|_2$, rather than at the arbitrary point \mathbf{p}_{fin} , there would most likely not be a problem. Similarly, in the constraint (84), the minimum achievable bit rate R_k^{req} is arbitrarily imposed by the designer. If a user experiences a bit rate slightly inferior to the minimum bit rate desired, it might pass unnoticed. These types of arbitrary constraints are the ones that can be relaxed and converted into soft constraints.

There are various methods to implement soft constraints, but we will discuss only three of them in this paper. The first method consists of the use of *slack variables* [154], [152], [119]. We can use them to relax inequality constraints. For instance, consider the following generic optimization problem with hard constraints:

$$\begin{aligned} & \underset{x}{\text{minimize}} && J(x) \\ & \text{s.t.} && \\ & && g(x) \leq 0, \\ & && f(x) = c, \end{aligned} \quad (94)$$

where $x, J(x), g(x), f(x), c \in \mathbb{R}$. We can relax the hard inequality constraint imposed on $g(x)$ with a slack variable s as follows:

$$\begin{aligned} & \underset{x,s}{\text{minimize}} && J(x) + k_1 s^2 \\ & \text{s.t.} && \\ & && g(x) \leq s, \\ & && f(x) = c, \\ & && s \geq 0 \end{aligned} \quad (95)$$

where $k_1 > 0$ is a design parameter. In (95), we can have $g(x) > 0$ since the slack variable s will take the necessary

value to satisfy the constraint $g(x) \leq s$. Nevertheless, this adds a penalty $k_1 s^2$ to the cost function. If $g(x) \leq 0$, then the slack variable takes the value of $s = 0$. The relaxed optimization problem needs to optimize not only the variable x from the original optimization problem, but also the slack variable s . In [12], we find an interesting example where a CaTP has its cost function exclusively composed of a single slack variable.

We can also use exponential penalty functions [156] to relax the inequality functions:

$$\begin{aligned} & \underset{x}{\text{minimize}} && J(x) + \frac{k_1}{k_2} (\exp(k_2 g(x)) - 1) \\ & \text{s.t.} && \\ & && f(x) = c, \end{aligned} \quad (96)$$

where $k_1, k_2 > 0$. If $g(x) = 0$, the penalization term becomes exactly zero. If $g(x) < 0$ and $k_2 \rightarrow +\infty$, then the penalization term tends to zero and its effect on the cost function becomes negligible. If $g(x) > 0$, then the effect of the penalization terms becomes larger depending on the values of k_1 and k_2 . In [4], we included this type of exponential penalization to avoid obstacles in a CaTP problem.

Another technique relies on moving the equality constraints into the optimization target as quadratic penalization terms [155], [153]:

$$\begin{aligned} & \underset{x}{\text{minimize}} && J(x) + k_1 |f(x) - c|^2 \\ & \text{s.t.} && \\ & && g(x) \leq 0, \end{aligned} \quad (97)$$

where $k_1 > 0$. The penalization term in (97) is small if $f(x)$ is close to the desired value c , and the farther $f(x)$ from c , the larger the penalization term. In [157], the authors consider a CaTP with multiple MRs. They use the same type of penalization in (97) to add penalization terms to their cost functional. These penalization terms are related to the number of bits transmitted, as well as to the final position and velocity of the MRs.

We can also simultaneously relax the inequality and equality constraints by combining the use of slack variables and the quadratic penalization terms:

$$\begin{aligned} & \underset{x,s}{\text{minimize}} && J(x) + k_1 |f(x) - c|^2 + k_2 s^2 \\ & \text{s.t.} && \\ & && g(x) \leq s, \\ & && s \geq 0, \end{aligned} \quad (98)$$

We must mention that if the original problem (94) is feasible, then all of its hard constraints are satisfied by the optimum solution x^* . Consequently, the relaxed problems (95), (97), and (98) are equivalent to (94), and (96) will tend to be equivalent to (94) as $k_2 \rightarrow +\infty$. Alternatively, if the original problem (94) is unfeasible, the relaxed problem (98) is still feasible; by tuning k_1 and k_2 , we can get as close as possible to satisfying the original hard constraints.

Not all of the five elements in (68) are essential in all CaTP optimization problems. Only the MR motion model (sometimes not explicitly mentioned when it is too simple), the channel model, and the optimization target are essential. Regarding the constraints, there are four different possibilities:

1) Case 1: the optimization target considers both communications and robotics aspects. In [5], we observe one instance of this case that is reproduced and analyzed in our Example 1.

Example 1. An MR is tasked to move in a finite time t_f from an initial position \mathbf{p}_{ini} to a final position \mathbf{p}_{fin} while transmitting a given number of bits c to a BS with a certain bit error probability. The objective is to optimize the trajectory and the instantaneous bit rate to balance the motion energy and the energy spent in motion.

The input to the MR is the control signal $\mathbf{u}(t) \in \mathbb{R}^2$, which directly controls its acceleration. The communications input is the instantaneous transmission bit rate $R(t) \in \mathbb{R}$. Note that, $\mathbf{u}(t)$ and $R(t)$ are both functions with support $[0, t_f]$.

In this example, the state vector of the system is $\mathbf{x}^T = [\mathbf{x}_1^T(t) \ \mathbf{x}_2^T(t) \ x_3(t)]$, where $\mathbf{x}_1(t) \in \mathbb{R}^2$ and $\mathbf{x}_2(t) \in \mathbb{R}^2$ are the MR position and velocity, respectively. Additionally, $x_3(t) \in \mathbb{R}$ is the number of bits transmitted by the MR since the start of the mission.

The optimization problem is cast as a maximization problem with the following cost functional:

$$\begin{aligned} J(\mathbf{x}, \mathbf{u}, R) = & \int_0^{t_f} \left(\frac{(2^{R(t)} - 1)s(\mathbf{x}_1(t))}{K} \right) dt \\ & + \gamma \int_0^{t_f} p_2(\|\mathbf{x}_2(t)\|_2, \|\mathbf{u}(t)\|_2) dt \\ & + C_1 \|\mathbf{x}_1(t_f) - \mathbf{p}_{fin}\|^2 + C_2 \|\mathbf{x}_2(t_f)\|^2 \\ & + C_3 \|x_3(t_f) - c\|^2. \end{aligned} \quad (99)$$

The first term in the functional corresponds to the energy spent in transmission, where the transmitter of the MR is equipped with a power control mechanism that adapts the transmission power automatically to ensure a p_b BER set with the constant $K = -1.5/\log(5p_b)$. The integrand of this first term corresponds to the power required to meet the targeted BER with the transmission bit rate $R(t)$, as well as the CNR estimation $s(\mathbf{x}_1(t))$ at position $\mathbf{x}_1(t)$. The second term is the energy spent in motion by the MR weighted by the parameter $\gamma > 0$, $p_2(a, b)$ is a second order polynomial on a and b , and the integrand of the second term is the power consumed at time t in motion by the MR. The last terms are quadratic penalties on the desired final states of the system. $C_1, C_2, C_3 > 0$ are design parameters that determine how important is to reach the desired final states. The first penalty tends to force the final MR position $\mathbf{x}_1(t_f)$ to the desired final position \mathbf{p}_{fin} . The second penalty tends to cause the MR arrive to the final position with the lowest possible speed. Lastly, the third penalty has the MR transmit data close to c bits by the end of its trajectory. The initial state value of the state variables is set with the following constraints:

$$\mathbf{x}_1(0) = \mathbf{p}_{ini}, \quad \mathbf{x}_2(0) = \mathbf{0}, \quad x_3(0) = 0, \quad (100)$$

and the inputs are bounded according to the following constraints:

$$0 \leq \|\mathbf{u}\|_2 \leq u_{max}, \quad 0 \leq R(t) \leq R_{max}. \quad (101)$$

The behaviour of the system is described by the linear dynamic model:

$$\dot{\mathbf{x}}_1(t) = \mathbf{x}_2(t), \quad (102)$$

$$\dot{\mathbf{x}}_2(t) = \mathbf{u}(t), \quad (103)$$

$$\dot{x}_3(t) = R(t), \quad (104)$$

The equations (102)-(103) constitute the MR. Regarding the communications model, we can say from a systems theory perspective that it is composed only of (104). However, if we interpret the communications model as the full mathematical description of how the communications system behaves, then the communications model is composed not only of (104), but also the bounds of the bit rate (104) and the transmitted power description in the first term of the functional (104), as well as the function $s(\mathbf{x}_1(t))$ describing how the CNR estimation varies with the position of the MR.

In summary, the optimization problem for this CaTP takes the following form:

$$\begin{aligned} \underset{\mathbf{u}, R}{\text{minimize}} \quad & J(\mathbf{x}, \mathbf{u}, R) \\ \text{s.t.} \quad & \dot{\mathbf{x}}_1(t) = \mathbf{x}_2(t), \\ & \dot{\mathbf{x}}_2(t) = \mathbf{u}(t), \\ & \dot{x}_3(t) = R(t), \\ & \mathbf{x}_1(0) = \mathbf{p}_{ini}, \quad \mathbf{x}_2(0) = \mathbf{0}, \quad x_3(0) = 0, \\ & 0 \leq \|\mathbf{u}\|_2 \leq u_{max}, \quad 0 \leq R(t) \leq R_{max}. \end{aligned} \quad (105)$$

This optimization problem has some interesting mathematical properties; the cost functional, with the exception of the first term, is quadratic w.r.t. the state vector \mathbf{x} and the input R . Additionally, the dynamic model is linear. ■

2) Case 2: the optimization target considers only robotics aspects. In [158], we observe one instance of this case that is reproduced and analyzed in our Example 2.

Example 2. An IoT sensor network is randomly deployed in a region \mathcal{A} according to a homogeneous Poisson Point Process (PPP) with density λ . Then, a multirotor UAV is tasked with collecting at least an expected amount of ζ successful transmissions from the nodes of the network.

The UAV is equipped with an antenna of a fixed beamwidth ϕ . It visits M Hovering Locations (HLs) to collect data from the sensor nodes. The coordinates of the HL- μ are $\ell_\mu = [x_\mu \ y_\mu \ h]$, where x_μ and y_μ are the $x-y$ coordinates of the HL- μ and h is its altitude, which is the same for all the HLs. When the UAV is at HL- μ , its communication system covers a circular area \mathcal{A}_μ with the coverage radius:

$$R = h \tan(\phi/2). \quad (106)$$

At the $\text{HL-}\mu$, the UAV spends a time T_{hover}^μ and the following process occurs. At $\text{HL-}\mu$, the UAV broadcasts a signal to activate the nodes in \mathcal{A}_μ . The nodes that are activated transmit, with a constant spectrum efficiency $\log_2(1 + \beta)$, over a common radio spectrum using a slotted ALOHA medium access scheme with transmission probability p_{tx} . The transmission of the n th node is successful if the SINR at the UAV is larger than β . This criterion comes from the definition of Shannon's channel capacity and its implications; if the SINR of the communications channel is β_0 , then the maximum bit rate ensuring that the data can be recovered without errors is $B \log_2(1 + \beta_0)$, where B is the bandwidth. Thus, if we try to transmit over this channel using a bit rate of $B \log_2(1 + \beta)$ with $\beta_0 < \beta$, then the transmission will fail. The set of all nodes in the region \mathcal{A}_μ that successfully transmit their data is $\tilde{\Psi}_\mu$.

The transmission of the node with the largest SINR is treated as the intended transmission by the UAV; the transmissions of other nodes are treated as interference. The SINR at the UAV receiver from the transmission of a node n in the set $\tilde{\Psi}_\mu$ is:

$$\text{SINR}_\mu^n = \frac{PG_n D_n^{-\eta}}{\sum_{x \in \tilde{\Psi}_\mu / \mathbf{x}_n} PG_x D_x^{-\eta} + \sigma^2}, \quad (107)$$

where P is the transmission power of the IoT nodes, η is the power path-loss coefficient, D_n is the distance between the UAV and the n th node in $\tilde{\Psi}_\mu$, G_n is the power gain due to small-scale fading (which in this case is considered to follow a Nakagami- m distribution), and σ^2 is the noise power at the receiver.

When the UAV moves from one HL to another HL, it moves in a straight line. Its acceleration rate is \hat{a} , its deceleration rate is \check{a} , and its maximum speed is v_{max} . Accordingly, the time that the UAV takes to travel between the μ th HL and the $\mu + 1$ th HL is:

$$\tau_\mu = \begin{cases} \sqrt{\frac{d_\mu}{\hat{a} + \check{a}}} & \text{if } d_\mu \leq \hat{d} + \check{d}, \\ \hat{t} + \check{t} + \frac{d_\mu - \hat{d} - \check{d}}{v_{max}} & \text{if } d_\mu > \hat{d} + \check{d}, \end{cases} \quad (108)$$

where d_μ is the distance between the $\text{HL-}\mu$ and the $\text{HL-}\mu + 1$, $\hat{t} = v_{max}/\hat{a}$, $\check{t} = v_{max}/\check{a}$, $\hat{d} = 1/2\hat{a}\hat{t}^2$, and $\check{d} = 1/2\check{a}\check{t}^2$. The first line in (108) is the time it takes for the UAV to move between the two HLs. If d_μ is too short, then the UAV cannot reach its maximum speed. The second line is the time it takes when the distance is adequately great, and the UAV can therefore reach its maximum speed.

The trajectory-related inputs in the optimization problem are the number M of total HLs, the 3D location of the M HLs given by $\mathbf{L} = [\ell_1, \ell_2, \dots, \ell_M]$ with $\ell_\mu \in \mathbb{R}^3$. The flight path of the UAV is encoded in the binary matrix $\mathbf{Z} \in \{0, 1\}^{M \times M}$ where $z_{i,j} = 1$ if the UAV departs from the i th HL to arrive to the j th HL, and $z_{i,j} = 0$ otherwise.

The communications-related input is the coverage radius R . Nevertheless, given that in this scenario the beamwidth ϕ of the UAV antenna is fixed then the

altitude of the HLs uniquely determines the coverage radius R , see (106). Thus, the inputs R and \mathbf{L} cannot be chosen independently.

The path constraints of the optimization problem are the following. Each HL must be reached from only one HL:

$$\sum_{i=1, i \neq j}^M z_{i,j} = 1, \quad \forall j \in [1, M]. \quad (109)$$

At each HL, the UAV can only reach one HL:

$$\sum_{j=1, i \neq j}^M z_{i,j} = 1, \quad \forall i \in [1, M]. \quad (110)$$

Note that constraints (109) and (110) imply that the path for the UAV must be closed. The last path constraint is the Miller-Tucker-Zemlin (MTZ) constraint [159] which ensures that the path does not include subloops :

$$\begin{aligned} \phi_i - \phi_j + Mz_{i,j} &\leq M - 1 \\ 2 \leq i \neq j &\leq M. \end{aligned} \quad (111)$$

where $\phi = [\phi_2, \phi_3, \dots, \phi_M] \in \mathbb{R}^{M-1}$ are auxiliary variables for the MTZ constraint exclusively.

The communications constraints imposed are the following. The expected value of the number of successful transmissions collected in all the M HLs by the UAV must be at least ζ :

$$\sum_{\mu=1}^M \mathbb{E}[K_\mu] \geq \zeta, \quad (112)$$

where K_μ is the number of successful transmissions collected in the μ th HL. Then, the UAV must cover the full region \mathcal{A} where the IoT sensor network is deployed:

$$\mathcal{A} \subseteq \bigcup_{\mu=1}^M \mathcal{A}_\mu. \quad (113)$$

The cost function is the total flying time of the UAV to perform one full round of the collection process:

$$T_{total} = \sum_{\mu=1}^M T_{\text{hover}}^\mu + T_{travel}, \quad (114)$$

where T_{hover}^μ is the time that the UAV hovers over the $\text{HL-}\mu$, this time depends on the number of HLs, the channel capacity, and the probability of receiving a successful transmission, see [158] for the details. T_{travel} is the time that the UAV spends in motion which depends mainly on \mathbf{L} and on \mathbf{Z} .

In summary, the optimization problem for this CaTP takes the following form:

$$\begin{aligned}
& \underset{M, R, \mathbf{L}, \mathbf{Z}, \phi}{\text{minimize}} && T_{total} \\
& \text{s.t.} && \\
& \sum_{\mu=1}^M \mathbb{E}[K_\mu] \geq \zeta && \mathcal{A} \subseteq \cup_{\mu=1}^M \mathcal{A}_\mu, \\
& \sum_{i=1, i \neq j}^M z_{i,j} = 1, && \forall j \in [1, M], \\
& \sum_{j=1, j \neq i}^M z_{i,j} = 1, && \forall j \in [1, M], \\
& \phi_i - \phi_j + M z_{i,j} \leq M - 1, && 2 \leq i \neq j \leq M, \\
& R = h \tan(\phi/2). && \quad (115)
\end{aligned}$$

Note that in this optimization problem we have continuous variables (\mathbf{L} , ϕ and R) and discrete variables (M and \mathbf{Z}). Thus, this is a Mixed-Integer Programming (MIP) problem. Note that the discrete variables in this problem are used to determine the UAV path. ■

3) Case 3: the optimization target considers only the communications aspects. In [29], we observe one instance of this case that is reproduced and analyzed in our Example 3.

Example 3. In [29], a multirotor UAV is equipped with solar panels and with a multicarrier transmitter, having N_F subcarriers, tasked with providing communications to K ground users. The solar panels allow the UAV to recharge energy. This problem is formulated as a discrete time problem and considers the joint optimization of the 3D UAV trajectory and the wireless resources allocation for maximization of the system sum throughput over a given time period of time. The time is divided into N_T time slots of duration Δ_T .

The inputs to the UAV in this optimization problem is its 3D position $\mathbf{r} \in \mathbb{R}^{N_T \times 3}$, and its 3D velocity $\mathbf{v} \in \mathbb{R}^{N_T \times 3}$ over all the time duration considered. Another input in this problem is the energy level of the UAV battery $\mathbf{q} \in \mathbb{R}^{N_T \times 1}$.

The communications inputs are the power transmitted by the UAV and the subcarriers allocation schedule. The power transmitted to the k th user through the i th subcarrier at time slot n is denoted $p_k^i[n]$, if the i th subcarrier is allocated to the k th user at time slot n , then $s_k^i[n] = 1$, and $s_k^i[n] = 0$ otherwise.

The UAV motion model is a first order model:

$$\mathbf{r}[n+1] = \mathbf{r}[n] + \mathbf{v}[n+1]\Delta_T, \quad (116)$$

where $\mathbf{r}[n] \in \mathbb{R}^3$ is the position of the UAV at time slot n , and $\mathbf{v}[n] \in \mathbb{R}^3$ is the velocity of the UAV at time slot n . The UAV model also includes the aerodynamic

power consumption model at time slot n :

$$\begin{aligned}
P_{UAV}[n] &= \frac{k_1}{\sqrt{v_{x,y}^2[n] + \sqrt{v_{x,y}^4[n] + 4k_2^4}}} \\
&+ k_3 v_z[n] + k_4 v_{x,y}^3[n], \quad (117)
\end{aligned}$$

where $v_{x,y}[n]$ and $v_z[n]$ are the horizontal and vertical speeds of the UAV, where k_1 , k_2 , k_3 , and k_4 are constants, see [29] for more details. The power generated by the solar panel is upper bounded according to:

$$P_{solar}[n] = \frac{c_1}{1 + \exp(-c_2(z[n] - c_3))} + c_4, \quad (118)$$

The communications model is described by the following equations. The signal received by the user k assigned to the i th subcarrier at time slot n is:

$$u_k^i[n] = \frac{\sqrt{\zeta p_k^i[n]} h_k^i[n]}{\|\mathbf{r}[n] - \mathbf{r}_k\|} d_k^i[n] + n_k^i[n], \quad (119)$$

where $\mathbf{r}_k \in \mathbb{R}^3$ is the position of the k th user, ζ captures the antenna gain, $h_k^i[n] \in \mathbb{C}$ is the channel gain between the UAV and the user k on the subcarrier i during time slot n and it accounts for the effects of the multipath fading and of the shadowing, $n_k^i[n] \in \mathbb{C}$ is noise generated at the k th user receiver on the subcarrier i , and $d_k^i[n] \in \mathbb{C}$, denotes the symbol transmitted from the UAV to the k th user through the subcarrier i . Note that since $d_k^i[n]$, and $n_k^i[n]$ are stochastic processes then (119) is an incomplete description of the channel model if their statistics are not indicated. Thus, the paper indicates that: 1) $\mathbb{E}[d_k^i[n]] = 1$; 3) $n_k^i[n]$ is zero-mean Additive White Gaussian Noise (AWGN) with constant variance σ^2 . We also have to mention that in [29], the authors describe an offline trajectory planning problem and also its online version. In this example we are discussing the offline version, and in this version the authors assume a non-causal knowledge¹⁵ of $h_k^i[n]$, thus making this term deterministic, see [29] for the details of this issue.

The communications model is completed with the description of the achievable bit rate for the k th user during time slot n through the i th subcarrier:

$$R_k^i[n](\mathbf{p}, \mathbf{s}, \mathbf{r}) = s_k^i[n] B \log_2 \left(1 + \frac{\zeta^2 |h_k^i[n]|^2 p_k^i[n]}{\sigma^2} \right), \quad (120)$$

where B is the bandwidth of the subcarrier.

This optimization problem is cast as a maximization problem, and the utility function of this optimization problem is the total throughput averaged over the number of subcarriers N_F :

$$J(\mathbf{p}, \mathbf{s}, \mathbf{r}) = \frac{1}{N_F B} \sum_{n=1}^{N_T} \sum_{i=1}^{N_F} \sum_{k=1}^K R_k^i[n](\mathbf{p}, \mathbf{s}, \mathbf{r}). \quad (121)$$

¹⁵Thus making its offline trajectory problem of theoretical interest only, but in their online version the authors consider a causal knowledge of this term which is a more realistic and practical assumption.

Then, the acceleration, the speeds, and the altitude of the UAV are constrained:

$$\|\mathbf{v}[n+1] - \mathbf{v}[n]\|_2 \leq a_{max} \Delta_T, \quad (122)$$

$$v_{x,y}[n] \leq V_{max}^{x,y}, \quad (123)$$

$$v_z[n] \leq V_{max}^z, \quad (124)$$

$$Z_{min} \leq z[n] \leq Z_{max}. \quad (125)$$

The energy level of the UAV battery is constrained as follows:

$$0 \leq q[n] \leq q_{max}, \quad (126)$$

$$q[1] = q_0, \quad q[N_T + 1] = q_{end}, \quad (127)$$

where q_0 is the initial state of the battery and q_{end} is the final state desired for the battery.

The communications constraints are now described. Since $p_k^i[n]$ represent power they must be positive:

$$p_k^i[n] \geq 0. \quad (128)$$

In the UAV transmitter, all the subcarriers are combined and pass through the same amplifier, and so at time slot n the maximum power transmitted via all the subcarriers together is limited:

$$\sum_{i=1}^{N_F} \sum_{k=1}^K s_k^i[n] p_k^i[n] \leq P_{max}, \quad (129)$$

where P_{max} is the maximum transmission power at any time. Then the subcarriers allocation should be done so that each subcarrier is allocated to only one user at most:

$$\sum_{k=1}^K s_k^i[n] \leq 1, \quad s_k^i[n] \in \{0, 1\}, \quad (130)$$

also, the UAVs must ensure that each user experiences a minimum bit rate over all the service time:

$$\sum_{i=1}^{N_F} R_k^i[n](\mathbf{p}, \mathbf{s}, \mathbf{r}) \geq R_k^{req}, \quad (131)$$

where R_k^{req} is the minimum bit rate required by user k . Then we have the energy consumption constraints. The total energy consumed at time slot n cannot be superior to the energy stored in the battery at time slot n :

$$\left[\sum_{i=1}^{N_F} \sum_{k=1}^K \frac{1}{\epsilon} s_k^i[n] p_k^i[n] + P_{UAV}[n] + P_{static} \right] \Delta_T \leq q[n], \quad (132)$$

where $\epsilon \in (0, 1)$ is the efficiency of the power amplifier of the transmitter of the UAV, and P_{static} denote the constant power to maintain the UAV operational. Then, the increase of energy in the battery between consecutive time slots is bounded according to the following constraint:

$$\begin{aligned} q[n+1] &\leq q[n] + P_{solar}[n] \Delta_T - P_{static} \Delta_T \\ &\quad - \left[\sum_{i=1}^{N_F} \sum_{k=1}^K \frac{1}{\epsilon} s_k^i[n] p_k^i[n] + P_{UAV}[n] \right] \Delta_T. \end{aligned} \quad (133)$$

This constraint limits the maximum energy level increase of the battery between consecutive slots, it implies that depending on the level of the batter $q[n]$ the UAV might not store in the battery all the power generated by its solar panel.

In summary, the optimization problem for this CaTP takes the following form:

$$\begin{aligned} &\text{maximize}_{\mathbf{p}, \mathbf{s}, \mathbf{r}, \mathbf{v}, \mathbf{q}} \quad J(\mathbf{p}, \mathbf{s}, \mathbf{r}) \\ &\text{s.t.} \end{aligned} \quad (134)$$

$$\begin{aligned} &\|\mathbf{v}[n+1] - \mathbf{v}[n]\|_2 \leq a_{max} \Delta_T, \\ &v_{x,y}[n] \leq V_{max}^{x,y}, \\ &v_z[n] \leq V_{max}^z, \\ &Z_{min} \leq z[n] \leq Z_{max}, \end{aligned}$$

$$\begin{aligned} R_k^i[n](\mathbf{p}, \mathbf{s}, \mathbf{r}) &= s_k^i[n] B \log_2 \left(1 + \frac{\zeta^2 |h_k^i[n]|^2 p_k^i[n]}{\sigma^2} \right) \\ p_k^i[n] &\geq 0, \\ \sum_{i=1}^{N_F} \sum_{k=1}^K s_k^i[n] p_k^i[n] &\leq P_{max}, \\ \sum_{k=1}^K s_k^i[n] &\leq 1, \quad s_k^i[n] \in \{0, 1\}, \\ \sum_{i=1}^{N_F} R_k^i[n](\mathbf{p}, \mathbf{s}, \mathbf{r}) &\geq R_k^{req}, \end{aligned}$$

$$\begin{aligned} &\text{(133), (134),} \\ &0 \leq q[n] \leq q_{max}, \quad q[1] = q_0, \quad q[N_T + 1] = q_{end}. \end{aligned} \quad (135)$$

Note that in this optimization problem we have continuous variables (\mathbf{p} , \mathbf{r} , \mathbf{v} and \mathbf{q}) and discrete variables (\mathbf{s}). Thus, this is a MIP problem. Note that the discrete variables in this problem are used to determine the allocation of the subcarriers of the UAV transmitter to the users served by the UAV. In addition, the problem is formulated in discrete time, where the time between two consecutive discrete instants corresponds to the duration of the symbols transmitted by the multicarrier transmitter of the UAV. This assumes that the communications channel remains more or less constant during the slot time, i.e., it assumes that the coherence time of the communications channel is larger than the time slot duration Δ_T . ■

Now that we have described the structure of a generic CaTP problem, we will next discuss in more detail the different types of CaTP problems, which we classify into loose categories according to their application.

B. Minimum Energy Trajectories

The **Minimum Energy Trajectory with Communications Objectives** problem is one of the most illustrative CaTP problems. It considers an MR that accomplishes a certain task involving both motion and communications. The objective is to design the MR's trajectory so as to perform the desired task while minimizing the overall energy consumption (i.e. communications energy plus motion energy). This is important since MRs usually draw their energy from an onboard battery which feeds not only their locomotion system, but their communications system as well. By minimizing the overall

energy consumption, we may either reduce the MR's battery size (and thus its cost) or increase the MR's operational time, allowing it to fulfil more and longer tasks. Note that this problem may be irrelevant for tethered MRs since they receive energy from an external source [160].

At first glance, we could say that the energy spent by the MR in communications is negligible compared to the energy spent in motion, but as mentioned in section III-D, this is not always true. As shown in [161], the energy consumed by the communication system may be comparable to the energy spent in motion. This depends on various aspects, such as the amount of data transmitted, the distance to the node communicating with the MR, and the adopted power transmission strategy. In addition, as mentioned in [23], the size of the MR also determines how significant the communication power consumption is against the motion power consumption. For a small MR, the power spent in communications can be significant w.r.t. the power consumed in motion; however, for larger and heavier robots, the communication power might be negligible w.r.t. the power consumed in motion.

Mathematically, the Minimum Energy Trajectory with Communications Objectives problem is stated as an optimization problem with the following optimization target:

$$J = E_{\text{motion}}(\mathbf{u}, 0, T) + E_{\text{comm}}(\mathbf{u}, 0, T), \quad (136)$$

where $E_{\text{motion}}(\mathbf{u}, 0, T)$ and $E_{\text{comm}}(\mathbf{u}, 0, T)$ are the energies spent by the MR in motion and in communications, respectively, from time instant 0 up to time T using the control signal \mathbf{u} , and T is the task completion time that can be either a fixed parameter or an optimization variable. We must mention that the power transmission policy selected (see section III-D) drastically affects the optimum trajectory and the complexity of the problem.

If a constant transmission power strategy is selected for the MR and a continuous transmission is considered, then communication energy consumption becomes:

$$E_{\text{comm}}(\mathbf{u}, 0, T) = PT. \quad (137)$$

If the task completion time T and the constant transmission power P are fixed, then the communication energy becomes a constant term in the cost function (136) and the problem becomes that of a minimum motion energy trajectory design subject to communications constraints, which are often related to the quality of the received signal. Since the transmission power is constant, the received power will depend on the channel gain, which depends on the actual MR's trajectory itself.

On the other hand, if a transmission power control mechanism is used by the MR (see section III-D), then the communication energy consumption in (136) depends on the particular trajectory followed by the MR. If the transmission power is given by (66), the received power is always P_{ref} , and thus the quality of the signal received is independent of the trajectory. However, (66) assumes no bound on the maximum transmission power. If we consider maximum transmission power, then the actual transmission power consumption is given by (67). Additional constraints are needed to ensure that the robot can communicate. We illustrate this with the

following example: an MR must depart from a point A and arrive at a point B while communicating with a base station using the power control strategy (67). We want to optimize its trajectory so that total energy (136) is minimized. If the channel observed along the minimum motion energy path between points A and B is so poor that no transmission is possible along this path (i.e. $E_{\text{comm}}(\mathbf{u}, 0, T) = 0$), this would be the optimum path for our problem, however the issue is that no communication would occur. Therefore, when using the transmission power policy in (67), we must also include constraints to ensure that communication requirements are satisfied.

We can find one instance of this problem in [48] where the authors consider the problem of a ground MR that needs to communicate with a base station and must reach a predefined target point. The path is optimized so that the total energy consumption is minimized while completing the entire task. In [5], the authors consider the problem of minimizing the total energy consumption of a ground MR that must reach a target point in a predefined time and transmit a certain amount of data to a base station. In [162], [163], we consider the problem of a ground MR that must communicate with a BS through a communication channel experiencing small-scale fading. We design the trajectory so that the MR can find a good location for transmission. We optimize this trajectory so that the total energy (i.e. communications and motion energies) is minimized.

C. Energy Efficient Trajectories

In the previous subsection, we discussed the Minimum Energy Trajectory with Communications Objectives problem. We now discuss a more general CaTP optimization problem where the communications aspect considered in the optimization target is different from the communication energy consumption. This type of problem can be applied to an MR whose motion power consumption is significantly larger than the communication power consumption. In this scenario, the objective is usually to use as little energy in motion as possible to complete a communication related task, which depends on the performance of the communication system and/or the channel quality. In other words, the objective is to complete a task in an energy efficient manner. We refer to these types of trajectories as Energy Efficient Communications-aware trajectories.

One way to achieve this is to use the following optimization target:

$$J = \theta E_{\text{motion}}(\mathbf{u}, 0, T) + (1 - \theta) f_{\text{comm}}(\mathbf{u}, 0, T) \quad (138)$$

where $E_{\text{motion}}(\mathbf{u}, 0, T)$ is the motion energy consumed by the MR, $f_{\text{comm}}(\mathbf{u}, 0, T)$ is a communication metric to be minimized, and $\theta \in [0, 1]$ is a design parameter that determines the importance of one objective with respect to the other. Since both terms have generally different physical units, we need to normalize them to ensure that they vary, more or less, in the same numerical range. This is highly convenient for avoiding problems when solving the CaTP optimization

problem numerically. We used this approach to construct the objective function in [4]. Another way of formulating an energy efficient communications-aware trajectories problem is by maximizing the following objective function:

$$J = \frac{g_{comm}(\mathbf{u}, 0, T)}{E_{motion}(\mathbf{u}, 0, T)} \quad (139)$$

where $g_{comm}(\mathbf{u}, 0, T)$ is a communications metric to be maximized. Here, (139) maximizes the ratio of two metrics. The advantage of doing this is that we can easily combine metrics having different units and do not need to normalize them, nor to select an adequate weight parameter. Nevertheless, with the fact that there is no weight parameter, this optimization target lacks flexibility by being able to produce only a single trajectory, rather than a whole Pareto front of possible trajectories. We used this approach to construct the objective function in [164].

Yet another way to tackle energy efficient communications-aware trajectories is to select the optimization target as the motion energy and then introduce the communications objective as constraints. By doing this, the MR will reach the communications objective using as minimal motion energy possible. The complementary form is also possible, where the cost function is a communications metric and constraints are imposed on the motion energy. In this approach, the MR expends a certain amount of energy as efficiently as possible to optimize the communications metric.

For instance, in [84], the authors considered the problem of a MR that must sense some area while maintaining communication with a base station. The objective is to design a trajectory to complete this task while maintaining appropriate channel quality throughout the entire trajectory. In [165], the authors considered the problem of a MR that must find a position in which the channel gain is high enough to allow for communication with a certain quality of service, while using as minimal motion energy possible. In [166], the authors considered a problem in which a team of MRs all have a copy of the same message and need to transmit the message to a base station, which combines the signals received from all the MRs. The objective is to maximize the total received signal power. To achieve this, the MRs need to find positions where the channel gain is high enough using as little energy as possible. In [111], the authors considered the problem of designing the path for an energy-limited UAV that must reach a certain target point. During the whole trajectory, it must also satisfy certain channel constraints in order to transmit video while moving. In [112], the authors highlight the importance of considering the wireless communication links for UAVs when designing paths; they considered the notion of communication coverage of a UAV's path. In [167], [168], we considered the problem of an MR that must reach a certain target point and transmit data to a base station; the trajectory is optimized so as to spend as little energy in motion as possible, while transmitting as much data as possible. The objective function in [167], [168] takes the form of (138) where the communication-related term represents the number of bits transmitted by the MR. In [4], we extended

this by considering a general communications term that could represent various types of communications-related criteria.

D. Other Trajectory Design Strategies

In the previous subsections, we addressed minimum energy CaTP and energy efficient CaTP problems. For completeness, we will next briefly discuss some other types of CaTP problems that represent interesting and exciting research opportunities. Some additional examples of problems related to CaTP can be found in [169].

- 1) **Trajectory design for Robotic relays.** A robotic relay is an MR that relays data between communicating nodes. They can be used to establish communication between two nodes, A and B (which may be either static or mobile), which cannot communicate directly as the channel between them is too weak. This can happen if both nodes are too far away from each other or if there are various obstacles between them. In this case, one or more robotic relays can be used to establish communication between nodes A and B . The advantage of using MRs as mobile relays instead of static relays is that they can adapt their positions to maintain or improve the performance of the system, regardless of any change in the environment or in the positions of the nodes A and B . This type of problem might be of particular interest to researchers working in multirobot systems.

In this problem, the objective is to optimize the trajectory of one or more MRs acting as robotic relays in order to have good end-to-end communication performance. For instance, in [137], the authors considered the scenario in which a chain of robotic relays must ensure communication between a static robot and a robot that is exploring a certain area. In [170], the authors addressed the problem of designing trajectories for robotic routers to ensure communication within an indoor environment. In [171], the authors considered the problem of a fixed-wing UAV relay for helping a terrestrial robot. In [144], the authors also considered a fixed-wing UAV relay between ground nodes and optimized its trajectory to maximize the end-to-end throughput. The authors of [172] developed an experimental platform for robotic relays. In [173], we considered the problem of optimizing the position of a robotic relay to transfer data from various sensors to a fusion center.

- 2) **Trajectory Design for Data Ferries.** Robotic data ferries operate similarly to robotic relays, except that they move between the nodes in order to physically transport data. Data ferries are suitable only in scenarios where the application using data to be transferred tolerates the delay introduced by the movement of the data ferry. In some cases, the source node produces data continuously, which requires designing a periodic (or quasi-periodic) trajectory. These periodic trajectories are generally optimized by maximizing the end-to-end throughput or maximizing the energy efficiency of the data transfer process (i.e. minimizing the energy cost of transferring one bit of data).

In [87], the authors considered the problem of designing a closed trajectory for a UAV acting as a data ferry between two nodes. The objective was to maximize the end-to-end throughput. In [121], we studied the problem of a ground MR acting as a ferry that must gather data from various sensors and then move towards a fusion center to deliver the data. We studied the tradeoff between the energy consumption of the MR and the end-to-end throughput. In [7], we considered the problem of a UAV acting as a data ferry between two nodes. We optimized its closed trajectory to maximize the end-to-end throughput. To do this, we parametrized the trajectory using Fourier series and then optimized the coefficients.

In [12], the authors optimize the trajectory of a UAV that collects the data from sensor nodes in an energy efficient manner for the network. In [164], we optimized a 3D closed trajectory for a quadrotor UAV to collect data in an energy efficient manner from various sensor nodes. Interestingly, as the UAV in this scenario increases its altitude, the region that it covers grows, but the channel losses also grow. Thus, a careful optimization of the UAV altitude must be performed.

In [174], the authors consider a scenario where a multirotor UAV must collect data from a sensor network at some collections points. First, the authors optimize the location of the collection points and the 2D UAV trajectory in order to minimize the average Age of Information (AoI) of the data collected. Then, they also solve the problem of minimizing the maximum AoI from all the sensor nodes. The AoI is a *freshness measure of the data*, it essentially measures the time since its generation up to its delivery to the intended recipient. In [175], the authors consider a similar problem where UAV must collect data from some nodes located at specific points of interest and then deliver the data to a fusion center via a cellular network. Since the cellular network is designed for ground users, then it does not have coverage everywhere in the sky. And the UAV will encounter various coverage holes at the altitude where it operates. In this problem the authors optimize the UAV trajectory in order to minimize the worst AoI from all the nodes.

3) **Communications-aware Trajectory for PV equipped robots.** Recently, there has been an interest in adding solar PV panels to UAVs. One of the main motivations for adding PV panels to the UAVs is to extend their flying time as much as possible. This addition converts the UAVs into agents that can perform three main actions: transmit data, move, and recharge batteries through their solar panels. Interestingly, both the solar power production of the UAV's PV panels and the quality of its communications are a function of the UAV position. By giving the UAV the ability to produce energy, the CaTP problem becomes more complex. Indeed, we now have to consider not only the motion and communications aspects, but the energy generation aspect as well.

In [29], the authors consider the problem of optimizing the 3D trajectory of a UAV equipped with a PV solar panel that must provide a wireless communication service to ground users. The trajectory is optimized to maximize the overall throughput provided to the users during a certain amount of time, while also simultaneously taking into account the communications, the solar power production, and the motion-induced energy consumption. In [176], the authors addressed this same problem of how the UAV can produce energy for self-consumption, but can also sell it. In addition, the users are charged by the amount of data processed by the UAV. The objective is to optimize the UAV trajectory to maximize the overall revenue. In this problem, the energy and data transmitted are both translated into money, and thus the optimization target representing the revenue is a weighted sum of the data received by the UAV from the users, the energy consumed, and the energy sold. Note that this particular problem is a mixture of a CaTP problem and a smart-grid problem. The authors in [177] consider a framework in which UAVs equipped with transceivers and PV panels forming part of a heterogeneous network must optimize their behaviour in order to minimize the overall energy consumption of the network, while providing certain service to the users.

4) **Trajectory Design for Small-Scale Fading Compensation.** As mentioned in section III-A, the small-scale fading provokes large variations in the channel gain over small distances (compared to the wavelength used). These variations can significantly degrade the performance of the communication system. Thus, it is important to compensate for this phenomenon. One way to perform this compensation is to control the position of the robot's antenna, which is done by controlling the position of the robot itself. By doing this, the robots can leverage the spatial variations of small-scale fading to improve in a smart fashion the channel gain observed. This problem can take two forms. In the first, the objective is to find a static position from which the robot will transmit its data. The robot explores a small region (compared to the wavelength) in order to find a suitable point for transmission. A trajectory planner is designed for such a task. In its second form, the robot must follow a certain path and can only control its linear velocity. In this case, a speed controller is designed to adequately compensate for the small scale fading. Broadly speaking, the general strategy that such controllers follow is to reduce the speed when the channel gain is high and increase the speed otherwise. The authors in [106] considered a problem where a robot has to follow a predefined closed path and is able to stop at some points. A speed controller is designed so that the robot stops for a certain time at positions with high channel gain to communicate with a remote node. In [178], the authors experimentally show how by controlling the position of the robot, they can com-

pensate for the small-scale fading. They designed short trajectories to perform this task. In [179], the authors also experimentally demonstrate this same principle by means of an antenna mounted on a turntable. In [123], we considered a ground MR harvesting RF energy and developed a trajectory planner that exploits small-scale fading to maximize the amount of energy harvested. The path explored by the MR in this technique is restricted to a straight line whose length is optimized. In [180], we extended this trajectory planner by optimizing not only the length of the path, but also its shape. Furthermore, in [117], we developed a predetermined trajectory planner that allows a ground MR to find points with high channel gain in its vicinity in an energy efficient manner. In this technique, the MR explores a set of stopping points to determine the best position for communication. These stopping points are close to each other and the small-scale fading at those locations presents low spatial correlation. This ensures the obtainment of high channel gains while minimizing the amount of energy spent in motion for the exploration of the stopping points. We expanded upon this work in [21] by making the trajectory planner adaptive. The locations of the points are determined on the fly and in an iterative manner. At each time, the next point to be visited by the MR is calculated as a function of the channel measured in the current and previous points. Results show that this technique outperforms the technique presented in [117], but requires an estimate of the shadowing as well. We further investigated this technique in [181] by considering the problem in which an MR equipped with an antenna mounted on a rotary platform has to follow a predefined trajectory while communicating with a BS through a fading channel. We developed a feedback controller that continuously optimizes the position of the antenna and operates under time-varying fading. In [173], [121], we further extended this technique to optimize the position of a ground MR to compensate for the small-scale fading of multiple communication channels simultaneously.

5) **Communications-aware UAV Placement.** In the previously described problems, the main focus was on the robot's trajectory. In Communications-aware UAV placement problems, the focus is on the stopping (or final) positions of the UAV to provide a communication service to ground users, rather than on the full trajectory. Although in some cases, the energy required by the UAV to reach a convenient final position was also of interest. For these problems, the wireless channel model usually consider the effect of the altitude and uses similar models to the ones described in section III-B1. With 5G, it is expected that drones will become a part of the cellular networks in order to improve their performance. Therefore, this particular problem is of high interest. Note that, even if this is not a CATP problem, it requires similar tools and models. For this reason and its importance to future cellular networks, we will next briefly describe some instances of this problem.

For example, the authors in [182] considered the problem of positioning UAVs for improving a cellular network. In [183], the authors optimize the altitude of a UAV to provide service to a cellular network. The authors of [148] address the problem of optimizing the 3D position of a UAV to maximize the number of covered users. In [116], the problem of optimizing the 3D position of UAV to maximize the number of users covered by the network is considered, which maximizes the revenue of the network. In [147], optimization of the position of a UAV giving communications service to a user inside a vertical building is evaluated. The problem of a distributed algorithm is considered in [184] for the purpose of the iterative optimization of a position of a team of UAVs giving service to other users in a network.

6) **UAVs and physical security.** A recent and interesting application is the implementation of physical layer techniques [185] through the use of UAV to solve cybersecurity issues in cellular networks [186]. One interesting example of this type of problem is the joint optimization of the UAV's trajectory and communications strategy to improve the security of the network against eavesdroppers. The general strategy to achieve this is to use one or more UAVs to either (i) jam the eavesdropper to degrade its signal-to-noise ratio or (ii) act as relays between the BS and the targeted node so that the latter reduces its transmission power, thus decreasing the strength of the signals captured by eavesdroppers.

For example in [187], the authors consider the following problem. A source node A must transmit data to a destination node B via a UAV acting as a relay, but a malicious node E is acting as an eavesdropper. The problem addressed by the authors is the joint optimization of the UAV trajectory and the communications parameters (such as bandwidth and transmission power) in order to maximize the secrecy rate. The general strategy consists of degrading the communications channel between the UAV and the eavesdropper while improving the quality of the end-to-end communication between nodes A and B . The same authors addressed a more elaborate version of this problem in [188], [186]. In [189], the authors optimize the trajectory and communication parameters of a UAV that operates exclusively as a jammer. The setup consists of a source node S , a destination node D , an eavesdropper E , and a UAV jammer. The authors optimize the trajectory of the UAV jammer and its power in order to significantly degrade the strength of the signal received by the eavesdropper, while simultaneously minimising the impact on the node S . The reader may find more information about the optimization of the UAV trajectory to improve the cybersecurity of cellular networks in [190], [191], [192].

E. CaTP Formalization and Final Comments

The description (68), presented at the beginning of this section, provided the reader with a *bird's eye view* on the CaTP problem. This allowed us to then discuss in

detail every single aspect and let (68) act as a high level map for the reader to understand how all the components fit together without getting lost in the details discussed. But now, after having discussed the details of the main components of the CaTP and having presented various examples we proceed to conclude this tutorial with a mathematical formalization of (68). This formalization is more precise and is described as follows:

$$\underset{\mathcal{C}, \mathcal{T}}{\text{minimize}} \quad J(\mathcal{C}, \mathcal{T}) \quad (140)$$

s.t.

$$\dot{\mathbf{x}} = \mathbf{f}_{dyn}(\mathbf{x}, \mathcal{T}), \quad (141a)$$

$$\mathbf{f}_{kyn}(\mathbf{x}) = \mathbf{0}, \quad (141b)$$

$$\mathbf{f}_{lim}(\mathcal{T}) = \mathbf{0}, \quad (141c)$$

$$\mathbf{g}_{lim}(\mathcal{T}) \leq \mathbf{0}, \quad (141d)$$

$$E_{mech} = \mathbf{f}_{mech}(\mathbf{x}, \mathcal{T}), \quad (141e)$$

$$\mathbf{r} = \mathbf{f}_{chan}(\mathbf{p}, \mathbf{q}, \mathbf{h}, \mathbf{n}_{com}, t, \mathcal{C}), \quad (142a)$$

$$\Gamma = \mathbf{f}_{pr}(\mathbf{p}, \mathbf{q}, \mathbf{h}, t, \mathcal{C}), \quad (142b)$$

$$\mathbf{d}_{rx} = \int_0^{t_f} \mathbf{f}_{rate}(\Gamma, \mathcal{C}) dt, \quad (142c)$$

$$\mathbf{f}_{rep}(\mathbf{h}) = \mathbf{f}_{desc}(\mathbf{p}, \mathbf{q}, t) \quad (142d)$$

$$\mathbf{f}_{rep}(\mathbf{n}_{com}) = \mathbf{f}_{nc}, \quad (142e)$$

$$\mathbf{f}_{lim}(\mathcal{C}) \leq \mathbf{0}, \quad (142f)$$

$$E_{comm} = \mathbf{f}_{comm}(\Gamma, \mathcal{C}), \quad (142g)$$

$$\mathbf{f}_{traj}(\mathbf{x}, \mathcal{T}) = \mathbf{0}, \quad (143a)$$

$$\mathbf{g}_{traj}(\mathbf{x}, \mathcal{T}) \leq \mathbf{0}, \quad (143b)$$

$$\mathbf{f}_{comm}(\mathbf{r}, \Gamma, \mathbf{d}_{rx}, \mathbf{p}, \mathbf{q}, \mathcal{C}) = \mathbf{0}, \quad (144a)$$

$$\mathbf{g}_{comm}(\mathbf{r}, \Gamma, \mathbf{d}_{rx}, \mathbf{p}, \mathbf{q}, \mathcal{C}) \leq \mathbf{0}. \quad (144b)$$

Let us proceed to discuss each element of the optimization problem (140)-(144b). We divide the optimization problem into the optimization target (140), and four blocks of constraints.

In (140) we have the optimization target which, as discussed before, can be either a cost function or a cost functional depending on the particular problem as discussed in sections IV-A, IV-B, IV-C and IV-D.

The first block constitutes the model of the robot and it is composed of (141a)-(141e).

In (141a), the function \mathbf{f}_{dyn} describes the dynamic model of the robot used, and \mathbf{x} is the state vector that describes the robot, for example it can be similar to the models discussed in section II-A3, section II-B, or section II-C. Note that, in the particular case of the communications-aware UAV placement problem, discussed in section IV-D, the dynamic model is not needed.

The equality constraint (141b) describes the forward kinematic model of the robot. We can obtain \mathbf{f}_{kyn} by algebraically manipulating the robot's kinematic models, like the ones described in section II-A1, in the standard form of (141b). If the robot has no kinematic constraints due to its design then we can put aside this constraint. The constraints (141c) and (141d) introduce the direct constraints on the input related to the robot's control. Some examples of the function \mathbf{g}_{lim} for inequality constraints can be obtained from (77)-(81). One example of the function \mathbf{f}_{lim} for equality constraints can be found in the Example 2 for the variable \mathbf{Z} that determines the robot's path.

The equation (141e) describes the mechanical energy consumption of the robot, it can be described by models like the ones described in section II-A4, section II-B, or section II-C. This model is not always necessary, but it becomes essential if we are interested in the total operation time of the robot or we are interested in energy efficiency.

The second block constitutes the model of the communications channel and it is composed of (142a)-(142g). In (142a), the function \mathbf{f}_{chan} represents the communications channel model. \mathbf{r} represents the signal (or signals) received at the robot's receiver, \mathbf{p} and \mathbf{q} represent the robot's position and attitude respectively, \mathbf{h} represents the contribution of the small-scale fading and shadowing to the channel gain, \mathbf{n}_{comm} is the noise generated at the receiver, and t represents the time. This type of model can take for example the form shown in (119), or like the ones discussed in section III-A. If the communications channel is time invariant we drop the dependency on t in the function \mathbf{f}_{chan} .

In (142b), Γ represents the SNR (or SINR depending on the particular problem) at the robot's receiver, (107) is one example of how the function \mathbf{f}_{pr} can look. We have to mention that (142b) can be calculated from (142a), and so it is not always essential to add this model if we already have included (142a). But, sometimes the optimization problem directly includes the model (142b) and leaves out the model (142a) like in Example 2.

In (142c), \mathbf{d}_{rx} represents the data received from the start to the final instant t_f , and the function \mathbf{f}_{rate} is a representation of the data rate. Here, *data* can mean different things depending on how the optimization problem is formulated, for example it can be the number of bits received like in Example 1 and Example 3, or the number successful transmissions (or data packets) like in Example 2.

The equation (142d) describes the model of the shadowing and/or small-scale fading, i.e. \mathbf{h} . If the channel model selected is stochastic then the function \mathbf{f}_{rep} is the statistical representation chosen for \mathbf{h} , and \mathbf{f}_{desc} is the actual description for $\mathbf{f}_{rep}(\mathbf{h})$. For example, let $h \in \mathbb{R}$ be the small-scale fading, and then we can choose to represent h with his mean and his variance. Then, $\mathbf{f}_{rep}(h) = [\mathbb{E}[h], \text{Var}[h]]^T$ and then, in the r.h.s. of (142d), \mathbf{f}_{desc} would be the actual expressions chosen for

the vector $[\mathbb{E}[h], \text{Var}[h]]$ appearing on the l.h.s.. But we could also choose to represent h with its PDF and its temporal correlation as well. If we are not using a stochastic model and h is time-invariant, then we could, for example, represent h with a 2D RF map. In this case, we could have $\mathbf{f}_{rep}(h) = h(\mathbf{p}, \mathbf{q})$ and \mathbf{f}_{desc} could be a numerical function that returns the corresponding value of h for each pair $\{\mathbf{p}, \mathbf{q}\}$, see section III-A and the references therein for more information. Note that if the channel model used in (142a) disregards the small-scale fading and the shadowing then (142d) is not required, this occurs when the designer uses a deterministic channel model, see section III-A1.

The equation (142e) is the statistical description of the noise generated at the receiver. It acts similarly as (142d) with the exception that the description for the noise is always statistical, and its representation is always the PDF and the temporal autocorrelation. Nevertheless, this model is rarely explicitly written in the equations, and the authors rather mention that the noise at the receiver is zero-mean AWGN with power σ^2 . That description implies that the PDF is Gaussian with zero-mean, variance σ^2 , and that its temporal autocorrelation is $C(n_{com}(t_1), n_{com}(t_2)) = \sigma^2\delta(t_1 - t_2)$ where $\delta(t)$ is the Dirac delta distribution.

The constraint (142f) acts directly on the communications-related inputs. In Example 3 we find an instance of this type of constraint to limit the instantaneous transmission power, see section IV-A for more examples of this inequality constraints.

The constraint (142g) describes the energy consumption model for the communications system. In section III-D we can find various examples of this type of energy consumption models. This model is not always needed, but is convenient to be added when the energy consumption of the communications system is not negligible in comparison to the energy consumed by the motion of the robot. See section IV-B for examples of CaTP where this model is needed. On the other hand, in scenarios where the energy consumed in motion is far greater, then the energy consumption model for the communications system is not needed.

The third block constitutes the constraints introduced by the designer on the trajectory/path, excluding the constraints on the input due to physical reasons, and it is composed of (143a) and (143b). We can see in section IV-A various examples of different types of this class of constraints.

The fourth block constitutes the constraints introduced by the designer on the communications system, excluding the constraints on the input due to physical reasons, and it is composed of (144a) and (144b). We can see in section IV-A various examples of different types of this class of constraints.

The CaTP problem formulation presented above does not intend to be a *one model fits all*, but rather a guide to the reader about how to mathematically construct and organize its own CaTP problem. Depending on the spe-

cific needs this formulation would require adjustments. For instance, (140)-(144b) is formulated in continuous time, but an equivalent discrete time formulation¹⁶ is also possible. A battery model could also be included in (140)-(144b), see Example 3.

As mentioned in the text above some models and constraints are not always essential and can be absent depending on the specific problem. But what is always essential for (140)-(144b) to be a CaTP problem is:

- a) Either (142a) or (142b) are present.
- b) The function \mathbf{f}_{chan} or the function \mathbf{f}_{pr} , if the former is not present, should depend on the position of the robot.
- c) The cost function (140) actually depends on \mathcal{C} or there is at least one constraint in (144a)-(144b) that depends on \mathcal{C} .

If (140)-(144b) does not satisfy all three conditions then it is not a (140)-(144b). Those two conditions provide a bridge that links the robotic block (i.e., (141a)-(141e) and (143a)-(143b)) with the communications block (i.e., (142a)-(142g) and (144a)-(144b)). In other words, we can say that TP problem is a CaTP problem if it includes a communications channel model that depends on the position of the agent and if at least one communications-related term appears either in the optimization target or in any constraint.

V. DISCUSSION AND CONCLUDING THOUGHTS

The growing interest for merging ground MRs and UAVs with communication systems is gaining momentum in both industry and academia. One of the main reasons for this occurrence is the surge of 5G technologies, which aim to integrate UAVs into the cellular networks. Another important reason involves the growing popularity of multi-robot systems where the MRs must maintain communication links. In these applications, the communications and robotics aspects are closely interrelated. In section I, we discussed some of the consequences of addressing these problems without an interdisciplinary approach.

Due to the strong entanglement between the robotics and communications aspects, an interdisciplinary approach is fundamental to fully exploit the maximum potential of this research area. In the hope of contributing to the quantity of material and quality of this research area, this tutorial has provided the basic theory behind this still underdeveloped, yet promising research area. We have described different motion models for various types of ground and aerial MRs, as well as various channel models for different scenarios relevant to the CaTP problems. Additionally, we have provided a general mathematical formulation for CaTP problems for predetermined trajectories. Different ways have been shown in which the robotic motion models and the communications channel models can interact with each other within the formulation of CaTP problems. Finally, we have provided a brief application-oriented classification of different CaTP problems and other related problems.

¹⁶This type of CaTP problems are common, see Example 3.



Daniel Bonilla Licea received his M.Sc. degree in 2011 from the Centro de Investigación y Estudios Avanzados (CINVESTAV), Mexico City. From May 2011 until June 2012, he worked as an intern in the signal processing team of Intel Labs in Guadalajara, Mexico. He received his PhD degree in 2016 from the University of Leeds, U.K. In 2016, he was invited for a short research visit at the Centre de Recherche en Automatique de Nancy (CRAN), France. In 2017, he collaborated in a research project with the Centro de Investigación en Computación (CIC) in Mexico.

From 2017 to 2020, he held a postdoctoral position at the International University of Rabat, Morocco. Currently, he holds a postdoctoral position at the Czech Technical University in Prague, Czech Republic. His research interests are signal processing and communications-aware robotics.



Dr Ghogho (F'18) received the M.Sc. degree in 1993 and the PhD degree in 1997 from the National Polytechnic Institute of Toulouse, France. He was an EPSRC Research Fellow with the University of Strathclyde (Scotland), from Sept 1997 to Nov 2001. In Dec 2001, he joined the school of Electronic and Electrical Engineering at the University of Leeds (England), where he was promoted to full Professor in 2008. While still affiliated with the University of Leeds, in 2010 he joined the International University of Rabat (Morocco) where he is currently Dean of

Doctoral College and Director of TICLab (ICT Research Laboratory). He is also a co-founder and co-director of the CNRS-Associated International Research Lab DataNet. He was awarded the UK Royal Academy of Engineering Research Fellowship in 2000 and the IBM Faculty Award in 2013. He was elevated to the grade of IEEE Fellow in 2018. His research interests are in signal processing, machine learning, and wireless communication. In the past, he served as an associate editor of the Signal Processing Magazine, the IEEE Transactions on Signal Processing, the IEEE Signal Processing Letters, and the Elsevier Digital Signal Processing journal, and a member of the IEEE Signal Processing Society SPCOM Technical Committee, the IEEE Signal Processing Society SPTM Technical Committee, and the IEEE Signal Processing Society SAM Technical Committee. He is currently a member of the steering committee of the IEEE Transactions of Signal and Information Processing over Networks. He held invited scientist/professor positions at Telecom Paris-Tech (France), NII (Japan), BUPT (China), University Carlos 3rd of Madrid (Spain), ENSICA (Toulouse), Darmstadt Technical University (Germany), and Minnesota University (USA).



Martin Saska received his MSc. degree at Czech Technical University in Prague, 2005, and his Ph.D. degree at University of Wuerzburg, Germany, within the PhD program of Elite Network of Bavaria, 2009. Since 2009, he is a research fellow at Czech Technical University in Prague, where he founded and heads the Multi-robot Systems lab (<http://mrs.felk.cvut.cz/>) and co-founded the Center for Robotics and Autonomous Systems with more than 70 researchers cooperating in robotics (<https://robotics.fel.cvut.cz/cras/>). He was a visiting scholar at the University of Illinois at Urbana-Champaign, USA in 2008, and at University of Pennsylvania, USA in 2012, 2014, and 2016, where he worked with Vijay Kumar's group within GRASP lab. He is an author or co-author of >150 publications in peer-reviewed conferences with multiple best paper awards and more >40 publications in impacted journals, including IJRR, AURO, JFR, ASC, EJC, with >4000 citations indexed by Scholar and H-index 35. His team won multiple robotic challenges in MBZIRC 2017, MBZIRC 2020, and DARPA SubT competitions (<http://mrs.felk.cvut.cz/projects/mbzirc>, <http://mrs.felk.cvut.cz/mbzirc2020>, <http://mrs.felk.cvut.cz/projects/darpa>).

REFERENCES

- [1] A. Gasparri, L. Sabattini, and G. Ulivi, "Bounded Control Law for Global Connectivity Maintenance in Cooperative Multirobot Systems," *IEEE Transactions on Robotics*, vol. 33, no. 3, pp. 700–717, 2017.
- [2] Y. Gao, H. Chen, Y. Li, C. Lyu, and Y. Liu, "Autonomous wi-fi relay placement with mobile robots," *IEEE/ASME Transactions on Mechatronics*, vol. 22, no. 6, pp. 2532–2542, 2017.
- [3] V. S. Varadharajan *et al.*, "Swarm Relays: Distributed Self-Healing Ground-and-Air Connectivity Chains," *IEEE Robotics and Automation Letters*, vol. 5, no. 4, pp. 5347–5354, 2020.
- [4] D. Bonilla Licea, M. Bonilla, M. Ghogho, S. Lasaulce, and V. S. Varma, "Communication-aware energy efficient trajectory planning with limited channel knowledge," *IEEE Transactions on Robotics*, vol. 36, no. 2, pp. 431–442, 2020.
- [5] U. Ali, Hong Cai, Y. Mostofi, and Y. Wardi, "Motion and communication co-optimization with path planning and online channel prediction," in *2016 American Control Conference (ACC)*, 2016, pp. 7079–7084.
- [6] A. Muralidharan and Y. Mostofi, "First passage distance to connectivity for mobile robots," in *2017 American Control Conference (ACC)*, 2017, pp. 1517–1523.
- [7] D. Bonilla Licea, M. Bonilla, M. Ghogho, and M. Malabre, "Uav trajectory planning for delay tolerant communications," in *2019 IEEE 58th Conference on Decision and Control (CDC)*, 2019, pp. 4166–4171.
- [8] U. Ali, H. Cai, Y. Mostofi, and Y. Wardi, "Motion-Communication Co-Optimization With Cooperative Load Transfer in Mobile Robotics: An Optimal Control Perspective," *IEEE Transactions on Control of Network Systems*, vol. 6, no. 2, pp. 621–632, 2019.
- [9] Y. Kantaros, M. Guo, and M. M. Zavlanos, "Temporal logic task planning and intermittent connectivity control of mobile robot networks," *IEEE Transactions on Automatic Control*, vol. 64, no. 10, pp. 4105–4120, 2019.
- [10] Y. Zeng and R. Zhang, "Energy-efficient uav communication with trajectory optimization," *IEEE Transactions on Wireless Communications*, vol. 16, no. 6, pp. 3747–3760, 2017.
- [11] Q. Wu, Y. Zeng, and R. Zhang, "Joint Trajectory and Communication Design for Multi-UAV Enabled Wireless Networks," *IEEE Transactions on Wireless Communications*, vol. 17, no. 3, pp. 2109–2121, 2018.
- [12] C. Zhan, Y. Zeng, and R. Zhang, "Energy-efficient data collection in uav enabled wireless sensor network," *IEEE Wireless Communications Letters*, vol. 7, no. 3, pp. 328–331, 2018.
- [13] X. Liu *et al.*, "Throughput Optimization of Blocked Data Transmission: A Mobile-Relay-UAV-Assisted Approach," in *IEEE International Conference on Computer and Communications*, 2019, pp. 792–796.
- [14] S. Ahmed, M. Z. Chowdhury, and Y. M. Jang, "Energy-Efficient UAV Relaying Communications to Serve Ground Nodes," *IEEE Communications Letters*, vol. 24, no. 4, pp. 849–852, 2020.
- [15] M. T. Dabiri and S. M. S. Sadough, "Optimal Placement of UAV-Assisted Free-Space Optical Communication Systems With DF Relaying," *IEEE Communications Letters*, vol. 24, no. 1, pp. 155–158, 2020.
- [16] M. I. Khalil, "Energy Efficiency Maximization of Relay Aerial Robotic Networks," *IEEE Transactions on Green Communications and Networking*, vol. 4, no. 4, pp. 1081–1090, 2020.
- [17] A. Zhou, S. Xu, S. Wang, J. Huang, S. Yang, T. Wei, X. Zhang, and H. Ma, "Robotic Millimeter-Wave Wireless Networks," *IEEE/ACM Transactions on Networking*, vol. 28, no. 4, pp. 1534–1549, 2020.
- [18] M. Debachisha and N. Enrico, "A survey on cellular-connected UAVs: Design challenges, enabling 5G/B5G innovations, and experimental advancements," *Computer Networks*, vol. 182, pp. 1–25, 2020.
- [19] Y. Zeng, Q. Wu, and R. Zhang, "Accessing from the sky: A tutorial on uav communications for 5g and beyond," *Proceedings of the IEEE*, vol. 107, no. 12, pp. 2327–2375, 2019.
- [20] S. Chung, A. A. Paranjape, P. Dames, S. Shen, and V. Kumar, "A survey on aerial swarm robotics," *IEEE Transactions on Robotics*, vol. 34, no. 4, pp. 837–855, 2018.
- [21] D. Bonilla Licea, D. McLernon, and M. Ghogho, "Mobile robot path planners with memory for mobility diversity algorithms," *IEEE Transactions on Robotics*, vol. 33, no. 2, pp. 419–431, 2017.
- [22] J. Fink, A. Ribeiro, and V. Kumar, "Robust control of mobility and communications in autonomous robot teams," *IEEE Access*, vol. 1, pp. 290–309, 2013.
- [23] M. Coppola, K. N. McGuire, C. De Wagter, and G. C. H. E. de Croon, "A survey on swarming with micro air vehicles: Fundamental challenges and constraints," *Frontiers in Robotics and AI*, vol. 7, p. 18, 2020. [Online]. Available: <https://www.frontiersin.org/article/10.3389/frobt.2020.00018>

[24] M. Calvo-Fullana, A. Pyattaev, D. Mox, S. Andreev, and A. Ribeiro, "Communications and robotics simulation in uavs: A case study on aerial synthetic aperture antennas," *IEEE Communications Magazine*, vol. 59, no. 1, pp. 22–27, 2021.

[25] M. Calvo-Fullana, D. Mox, A. Pyattaev, J. Fink, V. Kumar, and A. Ribeiro, "Ros-netsim: A framework for the integration of robotic and network simulators," *IEEE Robotics and Automation Letters*, vol. 6, no. 2, pp. 1120–1127, 2021.

[26] M. Guo and M. M. Zavlanos, "Multirobot data gathering under buffer constraints and intermittent communication," *IEEE Transactions on Robotics*, vol. 34, no. 4, pp. 1082–1097, 2018.

[27] M. Lindhe and K. H. Johansson, "Using robot mobility to exploit multipath fading," *IEEE Wireless Communications*, vol. 16, no. 1, pp. 30–37, 2009.

[28] O. M. Bushnaq, A. Celik, H. Elsawy, M. Alouini, and T. Y. Al-Naffouri, "Aeronautical data aggregation and field estimation in iot networks: Hovering and traveling time dilemma of uavs," *IEEE Transactions on Wireless Communications*, vol. 18, no. 10, pp. 4620–4635, 2019.

[29] Y. Sun, D. Xu, D. W. K. Ng, L. Dai, and R. Schober, "Optimal 3d-trajectory design and resource allocation for solar-powered uav communication systems," *IEEE Transactions on Communications*, vol. 67, no. 6, pp. 4281–4298, 2019.

[30] H. Kim and B. K. Kim, "Minimum-energy trajectory planning and control on a straight line with rotation for three-wheeled omni-directional mobile robots," in *2012 IEEE/RSJ International Conference on Intelligent Robots and Systems*, 2012, pp. 3119–3124.

[31] P. F. Muhl and C. P. Neuman, "Kinematic modeling of wheeled mobile robots," *Journal of Robotic Systems*, vol. 4, no. 2, pp. 281–340, 1987.

[32] ———, "Kinematic modeling of wheeled mobile robots," *Journal of Robotic Systems*, vol. 8, no. 2, pp. 281–340, 1987.

[33] B. Siciliano, L. Sciavicco, L. Villani, and G. Oriolo, *Robotics: Modelling, Planning and Control*. Springer-Verlag London Limited, 2010.

[34] H. Kim and B. K. Kim, "Minimum-energy translational trajectory generation for differential-driven wheeled mobile robots," in *J Intell Robot Syst*, vol. 49, 2007, pp. 367–383.

[35] A. J. Weinstein and K. L. Moore, "Pose estimation of ackerman steering vehicles for outdoors autonomous navigation," in *2010 IEEE International Conference on Industrial Technology*, 2010, pp. 579–584.

[36] H. J. Kim and B. K. Kim, "Minimum-energy trajectory planning on a tangent for battery-powered three-wheeled omni-directional mobile robots," in *ICCAS 2010*, 2010, pp. 1701–1706.

[37] N. Tan, Z. Zhu, and P. Yu, "Neural-network-based control of wheeled mobile manipulators with unknown kinematic models," in *2020 International Symposium on Autonomous Systems (ISAS)*, 2020, pp. 212–216.

[38] A. P. Andrews and M. S. Grewal, *Kalman filtering: Theory and Practice Using MATLAB*. John Wiley & Sons, 2008.

[39] U. Ali, Y. Yan, Y. Mostofi, and Y. Wardi, "An optimal control approach for communication and motion co-optimization in realistic fading environments," in *2015 American Control Conference (ACC)*, 2015, pp. 2930–2935.

[40] H. Kim and B. K. Kim, "Minimum-energy cornering trajectory planning with self-rotation for three-wheeled omni-directional mobile robots," in *Int. J. Control Autom. Syst.*, vol. 15, 2017, p. 1857–1866.

[41] P. Tokekar, N. Karnad, and V. Isler, "Energy-optimal trajectory planning for car-like robots," *Autonomous Robots*, vol. 37, p. 279–300, 2014.

[42] S. Liu and D. Sun, "Minimizing energy consumption of wheeled mobile robots via optimal motion planning," *IEEE/ASME Transactions on Mechatronics*, vol. 19, no. 2, pp. 401–411, 2014.

[43] Yongguo Mei, Yung-Hsiang Lu, Y. C. Hu, and C. S. G. Lee, "Energy-efficient motion planning for mobile robots," in *IEEE International Conference on Robotics and Automation, 2004. Proceedings. ICRA '04. 2004*, vol. 5, 2004, pp. 4344–4349 Vol.5.

[44] ———, "Deployment of mobile robots with energy and timing constraints," *IEEE Transactions on Robotics*, vol. 22, no. 3, pp. 507–522, 2006.

[45] Guiling Wang, M. J. Irwin, P. Berman, Haoying Fu, and T. La Porta, "Optimizing sensor movement planning for energy efficiency," in *ISLPED '05. Proceedings of the 2005 International Symposium on Low Power Electronics and Design*, 2005., 2005, pp. 215–220.

[46] F. El-Moukademy, E. Tornig, and G. Xing, "Mobile relay configuration in data-intensive wireless sensor networks," *IEEE Transactions on Mobile Computing*, vol. 12, no. 2, pp. 261–273, 2013.

[47] Chiping Tang and P. K. McKinley, "Energy optimization under informed mobility," *IEEE Transactions on Parallel and Distributed Systems*, vol. 17, no. 9, pp. 947–962, 2006.

[48] C. C. Ooi and C. Schindelhauer, "Minimal energy path planning for wireless robots," *Mobile Networks and Applications*, vol. 14, no. 3, pages=309–321, doi=10.1007/s11036-008-0150-5, 2009.

[49] Y. Mei, Y. Lu, Y. C. Hu, and C. G. Lee, "A case study of mobile robot's energy consumption and conservation techniques," in *2th International Conference on Advanced Robotics*, 2005.

[50] W. Youn and S. Andrew Gadsden, "Combined quaternion-based error state kalman filtering and smooth variable structure filtering for robust attitude estimation," *IEEE Access*, vol. 7, pp. 148 989–149 004, 2019.

[51] G. Michieletto, A. Cenedese, L. Zaccarian, and A. Franchi, "Hierarchical nonlinear control for multi-rotor asymptotic stabilization based on zero-moment direction," *Automatica*, vol. 117, p. 108991, 2020. [Online]. Available: <https://www.sciencedirect.com/science/article/pii/S0005109820301898>

[52] J. Diebel, "Representing attitude: Euler angles, unit quaternions, and rotation vectors," 2006.

[53] R. Mahony, V. Kumar, and P. Corke, "Multirotor aerial vehicles: Modeling, estimation, and control of quadrotor," *IEEE Robotics Automation Magazine*, vol. 19, no. 3, pp. 20–32, 2012.

[54] F. Morbidi, R. Cano, and D. Lara, "Minimum-energy path generation for a quadrotor uav," in *2016 IEEE International Conference on Robotics and Automation (ICRA)*, 2016, pp. 1492–1498.

[55] C. M.V, *Flight Dynamics: Principles. A Linear Systems Approach to Aircraft Stability and Control*. Elsevier Ltd., New York, 2013.

[56] F. Yacef, N. Rizoug, L. Degaa, O. Bouhali, and M. Hamerlain, "Trajectory optimisation for a quadrotor helicopter considering energy consumption," in *2017 4th International Conference on Control, Decision and Information Technologies (CoDIT)*, 2017, pp. 1030–1035.

[57] W. Green and P. Oh, "Autonomous hovering of a fixed-wing micro air vehicle," in *Proceedings 2006 IEEE International Conference on Robotics and Automation, 2006. ICRA 2006.*, 2006, pp. 2164–2169.

[58] R. W. Beard and T. W. McLain, *Small Unmanned Aircraft: Theory and Practice*. USA: Princeton University Press, 2012.

[59] I. Lugo-Cárdenas, G. Flores, S. Salazar, and R. Lozano, "Dubins path generation for a fixed wing uav," in *2014 International Conference on Unmanned Aircraft Systems (ICUAS)*, 2014, pp. 339–346.

[60] J. W. Langelaan, N. Alley, and J. Neidhoefer, "Wind field estimation for small unmanned aerial vehicles," *Journal of Guidance, Control, and Dynamics*, vol. 34, no. 4, pp. 1016–1030, 2011. [Online]. Available: <https://doi.org/10.2514/1.52532>

[61] R. W. Beard, J. Ferrin, and J. Humphreys, "Fixed wing uav path following in wind with input constraints," *IEEE Transactions on Control Systems Technology*, vol. 22, no. 6, pp. 2103–2117, 2014.

[62] T. A. Johansen, A. Cristofaro, K. Sørensen, J. M. Hansen, and T. I. Fossen, "On estimation of wind velocity, angle-of-attack and sideslip angle of small uavs using standard sensors," in *2015 International Conference on Unmanned Aircraft Systems (ICUAS)*, 2015, pp. 510–519.

[63] K. T. Borup, B. N. Stovner, T. I. Fossen, and T. A. Johansen, "Kalman filters for air data system bias correction for a fixed-wing uav," *IEEE Transactions on Control Systems Technology*, vol. 28, no. 6, pp. 2164–2176, 2020.

[64] P. J. Nguyen-Tuong D., "Model learning for robot control: a survey," *Cognitive Process*, vol. 12, p. 319–340, 2011.

[65] A. F. Molisch, *Wireless Communications*. John Wiley & Sons Ltd, 2011.

[66] P. Liu, D. W. Matolak, B. Ai, and R. Sun, "Path loss modeling for vehicle-to-vehicle communication on a slope," *IEEE Transactions on Vehicular Technology*, vol. 63, no. 6, pp. 2954–2958, 2014.

[67] B. Sklar, "Rayleigh fading channels in mobile digital communication systems .i. characterization," *IEEE Communications Magazine*, vol. 35, no. 7, pp. 90–100, 1997.

[68] A. F. Molisch, F. Tufvesson, J. Karedal, and C. F. Mecklenbrauker, "A survey on vehicle-to-vehicle propagation channels," *IEEE Wireless Communications*, vol. 16, no. 6, pp. 12–22, 2009.

[69] A. E. Forooshani, S. Bashir, D. G. Michelson, and S. Noghanian, "A survey of wireless communications and propagation modeling in underground mines," *IEEE Communications Surveys Tutorials*, vol. 15, no. 4, pp. 1524–1545, 2013.

[70] T. Rappaport, *Wireless communications: Principles and practice*, 2nd ed., ser. Prentice Hall communications engineering and emerging technologies series. Prentice Hall, 2002, includes bibliographical references and index.

[71] N. ryul Jeon, C. hoon Lee, N. gyoung Kang, and S. cheol Kim, "Performance of channel prediction using 3d ray-tracing scheme compared to conventional 2d scheme," in *Asia-Pacific Conference on Communications*, 2006.

[72] R. Zentner and A. K. Micalo, "Ray tracing interpolation for continuous modeling of double directional radio channel," in *Eurocon*, 2013.

[73] O. Stabler and R. Hoppe, "Mimo channel capacity computed with 3d ray tracing model," in *3rd European Conference on Antennas and Propagation*, 2009.

[74] S. Y. Seidel and T. S. Rappaport, "914 mhz path loss prediction models for indoor wireless communications in multifloored buildings," *IEEE Transactions on Antennas and Propagation*, vol. 40, no. 2, pp. 207–217, 1992.

[75] Kwok-Wai Cheung, J. H. . Sau, and R. D. Murch, "A new empirical model for indoor propagation prediction," *IEEE Transactions on Vehicular Technology*, vol. 47, no. 3, pp. 996–1001, 1998.

[76] Y. Mostofi, M. Malmirchegini, and A. Ghaffarkhah, "Estimation of communication signal strength in robotic networks," in *2010 IEEE International Conference on Robotics and Automation*, 2010, pp. 1946–1951.

[77] M. Malmirchegini and Y. Mostofi, "On the spatial predictability of communication channels," *IEEE Transactions on Wireless Communications*, vol. 11, no. 3, pp. 964–978, 2012.

[78] M. Gudmundson, "Correlation model for shadow fading in mobile radio systems," *Electronics Letters*, vol. 27, pp. 2145–2146(1), November 1991.

[79] F. Baccelli and X. Zhang, "A correlated shadowing model for urban wireless networks," in *2015 IEEE Conference on Computer Communications (INFOCOM)*, 2015, pp. 801–809.

[80] R. D. A. Timoteo, D. C. Cunha, and G. D. C. Cavalcanti, "A proposal for path loss prediction in urban environments using support vector regression," in *ICT 2014*, 2014.

[81] N. C. Beaulieu and M. Naseri, "A circuit theory model for shadow fading autocorrelation in wireless radio channels," *IEEE Wireless Communications Letters*, vol. 8, no. 1, pp. 161–164, 2019.

[82] Xiaodong Cai and G. B. Giannakis, "A two-dimensional channel simulation model for shadowing processes," *IEEE Transactions on Vehicular Technology*, vol. 52, no. 6, pp. 1558–1567, 2003.

[83] M. K. Simon and M.-S. Alouini, *Digital Communication over Fading Channels*. John Wiley & Sons Ltd, 2005.

[84] A. Ghaffarkhah and Y. Mostofi, "Communication-aware motion planning in mobile networks," *IEEE Transactions on Automatic Control*, vol. 56, no. 10, pp. 2478–2485, 2011.

[85] W. C. Jakes, *Microwave Mobile Communications*. IEEE Press, 1974.

[86] Yahong Rosa Zheng and Chengshan Xiao, "Simulation models with correct statistical properties for rayleigh fading channels," *IEEE Transactions on Communications*, vol. 51, no. 6, pp. 920–928, 2003.

[87] A. J. Carfang, N. Wagle, and E. W. Frew, "Improving data ferrying by iteratively learning the radio frequency environment," in *2014 IEEE/RSJ International Conference on Intelligent Robots and Systems*, 2014, pp. 1182–1188.

[88] S. K. Goudos and G. Athanasiadou, "Application of an ensemble method to uav power modeling for cellular communications," *IEEE Antennas and Wireless Propagation Letters*, vol. 18, no. 11, pp. 2340–2344, 2019.

[89] J. Chen, U. Yatnalli, and D. Gesbert, "Learning radio maps for uav-aided wireless networks: A segmented regression approach," in *2017 IEEE International Conference on Communications (ICC)*, 2017, pp. 1–6.

[90] Y. Egi and C. E. Otero, "Machine-learning and 3d point-cloud based signal power path loss model for the deployment of wireless communication systems," *IEEE Access*, vol. 7, pp. 42 507–42 517, 2019.

[91] E. Ostlin, H. Zepernick, and H. Suzuki, "Macrocell path-loss prediction using artificial neural networks," *IEEE Transactions on Vehicular Technology*, vol. 59, no. 6, pp. 2735–2747, 2010.

[92] P. S. Bithas, E. T. Michailidis, N. Nomikos, D. Vouyioukas, and A. G. Kanatas, "A survey on machine-learning techniques for uav-based communications," *Sensors*, vol. 19, no. 23, 2019. [Online]. Available: <https://www.mdpi.com/1424-8220/19/23/5170>

[93] A. Khuwaja, Y. Chen, N. Zhao, M. Alouini, and P. Dobbins, "A survey of channel modeling for uav communications," *IEEE Communications Surveys Tutorials*, vol. 20, no. 4, pp. 2804–2821, 2018.

[94] W. Khawaja, I. Guvenc, D. W. Matolak, U. C. Fiebig, and N. Schneckenburger, "A survey of air-to-ground propagation channel modeling for unmanned aerial vehicles," *IEEE Communications Surveys Tutorials*, vol. 21, no. 3, pp. 2361–2391, 2019.

[95] M. Asadpour, B. Van den Berg, D. Giustiniano, K. A. Hummel, S. Pollin, and B. Plattner, "Micro aerial vehicle networks: an experimental analysis of challenges and opportunities," *IEEE Communications Magazine*, vol. 52, no. 7, pp. 141–149, 2014.

[96] E. Yanmaz, R. Kuschnig, and C. Bettstetter, "Channel measurements over 802.11a-based uav-to-ground links," in *2011 IEEE GLOBECOM Workshops (GC Wkshps)*, 2011, pp. 1280–1284.

[97] D. Bonilla Licea, G. Silano, M. Ghogho, and M. Saska, "Optimum trajectory planning for multi-rotor uav relays with tilt and antenna orientation variations," in *2021 29th European Signal Processing Conference (EUSIPCO)*, 2021, pp. 1586–1590.

[98] N. Ahmed, S. S. Kanhere, and S. Jha, "On the importance of link characterization for aerial wireless sensor networks," *IEEE Communications Magazine*, vol. 54, no. 5, pp. 52–57, 2016.

[99] C. Cheng, P. Hsiao, H. T. Kung, and D. Vlah, "Performance measurement of 802.11a wireless links from uav to ground nodes with various antenna orientations," in *Proceedings of 15th International Conference on Computer Communications and Networks*, 2006, pp. 303–308.

[100] E. Yanmaz, R. Kuschnig, and C. Bettstetter, "Achieving air-ground communications in 802.11 networks with three-dimensional aerial mobility," in *2013 Proceedings IEEE INFOCOM*, 2013, pp. 120–124.

[101] J. Chen, D. Raye, W. Khawaja, P. Sinha, and I. Guvenc, "Impact of 3d uwb antenna radiation pattern on air-to-ground drone connectivity," in *2018 IEEE 88th Vehicular Technology Conference (VTC-Fall)*, 2018, pp. 1–5.

[102] Q. Zhang, M. Mozaffari, W. Saad, M. Bennis, and M. Debbah, "Machine learning for predictive on-demand deployment of uavs for wireless communications," in *2018 IEEE Global Communications Conference (GLOBECOM)*, 2018, pp. 1–6.

[103] H. E. Hammouti and M. Ghogho, "Air-to-ground channel modeling for uav communications using 3d building footprints," in *Ubiquitous Networking*, N. Boudriga, M.-S. Alouini, S. Rekhis, E. Sabir, and S. Pollin, Eds. Cham: Springer International Publishing, 2018, pp. 372–383.

[104] N. Goddemeier and C. Wietfeld, "Investigation of air-to-air channel characteristics and a uav specific extension to the rice model," in *2015 IEEE Globecom Workshops (GC Wkshps)*, 2015, pp. 1–5.

[105] A. Zanella, "Best practice in rss measurements and ranging," *IEEE Communications Surveys Tutorials*, vol. 18, no. 4, pp. 2662–2686, 2016.

[106] M. Lindhe and K. H. Johansson, "Communication-aware trajectory tracking," in *2008 IEEE International Conference on Robotics and Automation*, 2008, pp. 1519–1524.

[107] C. E. Shannon, "A mathematical theory of communication," *The Bell System Technical Journal*, vol. 27, no. 3, pp. 379–423, 1948.

[108] A. Goldsmith, *Wireless Communications*. Stanford University, 2004.

[109] S. Yarkan, S. Guzelgoz, H. Arslan, and R. R. Murphy, "Underground mine communications: A survey," *IEEE Communications Surveys Tutorials*, vol. 11, no. 3, pp. 125–142, 2009.

[110] A. Hrovat, G. Kandus, and T. Javornik, "A survey of radio propagation modeling for tunnels," *IEEE Communications Surveys Tutorials*, vol. 16, no. 2, pp. 658–669, 2014.

[111] A. Mardani, M. Chiaberge, and P. Giaccone, "Communication-aware uav path planning," *IEEE Access*, vol. 7, pp. 52 609–52 621, 2019.

[112] S. De Bast, E. Vinogradov, and S. Pollin, "Cellular coverage-aware path planning for uavs," in *2019 IEEE 20th International Workshop on Signal Processing Advances in Wireless Communications (SPAWC)*, 2019, pp. 1–5.

[113] Geopunt, "DHMV II," <http://www.geopunt.be/actualiteit/2016/april/dhmvi-volledig>, [Online; accessed 17-January-2023].

[114] A. Colpaert, E. Vinogradov, and S. Pollin, "Aerial coverage analysis of cellular systems at lte and mmwave frequencies using 3d city models," *Sensors*, vol. 18, no. 12, 2018. [Online]. Available: <https://www.mdpi.com/1424-8220/18/12/4311>

[115] Y. Yan and Y. Mostofi, "Communication and path planning strategies of a robotic coverage operation," in *2013 American Control Conference*, 2013, pp. 860–866.

[116] R. I. Bor-Yaliniz, A. El-Keyi, and H. Yanikomeroglu, "Efficient 3-d placement of an aerial base station in next generation cellular networks," in *2016 IEEE International Conference on Communications (ICC)*, 2016, pp. 1–5.

[117] D. Bonilla Licea, M. Ghogho, D. McLernon, and S. A. R. Zaidi, "Mobility diversity-assisted wireless communication for mobile robots," *IEEE Transactions on Robotics*, vol. 32, no. 1, pp. 214–229, 2016.

[118] H. He, S. Zhang, Y. Zeng, and R. Zhang, "Joint altitude and beamwidth optimization for uav-enabled multiuser communications," *IEEE Communications Letters*, vol. 22, no. 2, pp. 344–347, 2018.

[119] S. Boyd and L. Vandenberghe, *Convex Optimization*. Cambridge University Press, 2004.

[120] D. S. Kalogerias and A. P. Petropulu, "Mobile beamforming and spatially controlled relay communications," in *2016 IEEE International Conference on Acoustics, Speech and Signal Processing (ICASSP)*, 2016, pp. 6405–6409.

[121] E. Nurellari, D. B. Licea, and M. Ghogho, "Optimum trajectory planning for robotic data ferries in delay tolerant wireless sensor networks," in *2019 27th European Signal Processing Conference (EUSIPCO)*, 2019, pp. 1–5.

[122] D. G. Luenberger, *Optimization by vector space methods*. John Wiley and Sons, 1969.

[123] D. Bonilla Licea, S. A. Raza Zaidi, D. McLernon, and M. Ghogho, "Improving radio energy harvesting in robots using mobility diversity," *IEEE Transactions on Signal Processing*, vol. 64, no. 8, pp. 2065–2077, 2016.

[124] Z. Liu, B. Wu, J. Dai, and H. Lin, "Distributed communication-aware motion planning for multi-agent systems from stl and spatei specifications," in *2017 IEEE 56th Annual Conference on Decision and Control (CDC)*, 2017, pp. 4452–4457.

[125] E. F. Flushing, L. M. Gambardella, and G. A. Di Caro, "On using mobile robotic relays for adaptive communication in search and rescue missions," in *2016 IEEE International Symposium on Safety, Security, and Rescue Robotics (SSRR)*, 2016, pp. 370–377.

[126] A. Ghaffarkhah and Y. Mostofi, "Optimal motion and communication for persistent information collection using a mobile robot," in *2012 IEEE Globecom Workshops*, 2012, pp. 1532–1537.

[127] D. Kirk, *Optimal Control Theory: An Introduction*. Dover Publications, Inc., 2004, includes bibliographical references and index.

[128] S. Zhang, H. Zhang, Q. He, K. Bian, and L. Song, "Joint trajectory and power optimization for uav relay networks," *IEEE Communications Letters*, vol. 22, no. 1, pp. 161–164, 2018.

[129] A. Al-Hourani, S. Kandeepan, and S. Lardner, "Optimal lap altitude for maximum coverage," *IEEE Wireless Communications Letters*, vol. 3, no. 6, pp. 569–572, 2014.

[130] I. D. Cowling, O. A. Yakimenko, J. F. Whidborne, and A. K. Cooke, "A prototype of an autonomous controller for a quadrotor uav," in *2007 European Control Conference (ECC)*, 2007, pp. 4001–4008.

[131] C. Richter, A. Bry, and N. Roy, *Polynomial trajectory planning for aggressive quadrotor flight in dense indoor environments*, ser. Springer Tracts in Advanced Robotics, 2016, vol. 114, cited By :333. [Online]. Available: www.scopus.com

[132] J. Vlassenbroeck and R. Van Dooren, "A chebyshev technique for solving nonlinear optimal control problems," *IEEE Transactions on Automatic Control*, vol. 33, no. 4, pp. 333–340, 1988.

[133] M. Huzmezan, G. Dumont, W. Gough, and S. Kovac, "Multivariable laguerre-based indirect adaptive predictive control a reliable practical solution for process control," in *IASTED Modeling and Control Conf*, 2001, pp. 18–21.

[134] D. Brescianini and R. D'Andrea, "Computationally efficient trajectory generation for fully actuated multirotor vehicles," *IEEE Transactions on Robotics*, vol. 34, no. 3, pp. 555–571, 2018.

[135] Y. Huang, J. Xu, L. Qiu, and R. Zhang, "Cognitive uav communication via joint trajectory and power control," in *2018 IEEE 19th International Workshop on Signal Processing Advances in Wireless Communications (SPAWC)*, 2018, pp. 1–5.

[136] F. Ono, H. Ochiai, and R. Miura, "A wireless relay network based on unmanned aircraft system with rate optimization," *IEEE Transactions on Wireless Communications*, vol. 15, no. 11, pp. 7699–7708, 2016.

[137] E. Stump, A. Jadbabaie, and V. Kumar, "Connectivity management in mobile robot teams," in *2008 IEEE International Conference on Robotics and Automation*, 2008, pp. 1525–1530.

[138] C. You and R. Zhang, "3d trajectory optimization in rician fading for uav-enabled data harvesting," *IEEE Transactions on Wireless Communications*, vol. 18, no. 6, pp. 3192–3207, 2019.

[139] M. Hua, L. Yang, Q. Wu, and A. L. Swindlehurst, "3d uav trajectory and communication design for simultaneous uplink and downlink transmission," *IEEE Transactions on Communications*, vol. 68, no. 9, pp. 5908–5923, 2020.

[140] K. Liu, L. Ma, H. Zhou, S. Li, K. Zhang, D. Huang, B. Li, and D. Zhao, "Optimal time trajectory generation and tracking control for over-actuated multirotors with large-angle maneuvering capability," *IEEE Robotics and Automation Letters*, vol. 7, no. 3, pp. 8339–8346, 2022.

[141] J. A. Bezerra and D. A. Santos, "Optimal exact control allocation for under-actuated multirotor aerial vehicles," *IEEE Control Systems Letters*, vol. 6, pp. 1448–1453, 2022.

[142] Z. Xiao, H. Dong, L. Bai, D. O. Wu, and X.-G. Xia, "Unmanned aerial vehicle base station (uav-bs) deployment with millimeter-wave beamforming," *IEEE Internet of Things Journal*, vol. 7, no. 2, pp. 1336–1349, 2020.

[143] J. Chen and D. Gesbert, "Optimal positioning of flying relays for wireless networks: A los map approach," in *2017 IEEE International Conference on Communications (ICC)*, 2017, pp. 1–6.

[144] Y. Zeng, R. Zhang, and T. J. Lim, "Throughput maximization for uav-enabled mobile relaying systems," *IEEE Transactions on Communications*, vol. 64, no. 12, pp. 4983–4996, 2016.

[145] X. Hu, K.-K. Wong, K. Yang, and Z. Zheng, "Uav-assisted relaying and edge computing: Scheduling and trajectory optimization," *IEEE Transactions on Wireless Communications*, vol. 18, no. 10, pp. 4738–4752, 2019.

[146] M. Mozaffari, W. Saad, M. Bennis, and M. Debbah, "Mobile unmanned aerial vehicles (uavs) for energy-efficient internet of things communications," *IEEE Transactions on Wireless Communications*, vol. 16, no. 11, pp. 7574–7589, 2017.

[147] H. Shakhatreh, A. Khereishah, A. Alsarhan, I. Khalil, A. Sawalmeh, and N. S. Othman, "Efficient 3d placement of a uav using particle swarm optimization," in *2017 8th International Conference on Information and Communication Systems (ICICS)*, 2017, pp. 258–263.

[148] Y. Chen, N. Li, C. Wang, W. Xie, and J. Xv, "A 3d placement of unmanned aerial vehicle base station based on multi-population genetic algorithm for maximizing users with different qos requirements," in *2018 IEEE 18th International Conference on Communication Technology (ICCT)*, 2018, pp. 967–972.

[149] E. Bulut and I. Guevenc, "Trajectory optimization for cellular-connected uavs with connectivity constraint," in *2018 IEEE International Conference on Communications Workshops (ICC Workshops)*, 2018, pp. 1–6.

[150] L. Ding, G. Zhou, D. Morgan, Z. Ma, J. Kenney, J. Kim, and C. Giardina, "A robust digital baseband predistorter constructed using memory polynomials," *IEEE Transactions on Communications*, vol. 52, no. 1, pp. 159–165, 2004.

[151] D. Morgan, Z. Ma, J. Kim, M. Zierdt, and J. Pastalan, "A generalized memory polynomial model for digital predistortion of rf power amplifiers," *IEEE Transactions on Signal Processing*, vol. 54, no. 10, pp. 3852–3860, 2006.

[152] M. Askari, M. Moghavvemi, H. A. F. Almurib, and A. M. A. Haidar, "Stability of soft-constrained finite horizon model predictive control," *IEEE Transactions on Industry Applications*, vol. 53, no. 6, pp. 5883–5892, 2017.

[153] H. Schepker, S. Nordholm, and S. Doclo, "Acoustic feedback suppression for multi-microphone hearing devices using a soft-constrained null-steering beamformer," *IEEE/ACM Transactions on Audio, Speech, and Language Processing*, vol. 28, pp. 929–940, 2020.

[154] E. C. Kerrigan and J. M. Maciejowski, "Soft constraints and exact penalty functions in model predictive control," in *UKACC International Conference, Cambridge*, 2000, pp. 1–6.

[155] Q. Chen, P. Liu, Q. Shen, and J. Liu, "Soft-constrained random walk propagation for hierarchical image matting," in *2016 3rd International Conference on Information Science and Control Engineering (ICISCE)*, 2016, pp. 626–630.

[156] S. DorMohammadi and M. Rais-Rohani, "Exponential penalty function formulation for multilevel optimization using the analytical target cascading framework," *STRUCTURAL AND MULTIDISCIPLINARY OPTIMIZATION*, vol. 47, no. 4, pp. 599–612, APR 2013.

[157] U. Ali, H. Cai, Y. Mostofi, and Y. Wardi, "Motion-communication co-optimization with cooperative load transfer in mobile robotics: An optimal control perspective," *IEEE Transactions on Control of Network Systems*, vol. 6, no. 2, pp. 621–632, 2019.

[158] O. M. Bushnaq, A. Celik, H. Elsawy, M.-S. Alouini, and T. Y. Al-Naffouri, "Aeronautical data aggregation and field estimation in iot networks: Hovering and traveling time dilemma of uavs," *IEEE Transactions on Wireless Communications*, vol. 18, no. 10, pp. 4620–4635, 2019.

[159] C. E. Miller, A. W. Tucker, and R. A. Zemlin, "Integer programming formulation of traveling salesman problems," *J. ACM*, vol. 7, no. 4, p. 326–329, oct 1960. [Online]. Available: <https://doi.org/10.1145/321043.321046>

[160] E. Rossi, M. Bruschetta, R. Carli, Y. Chen, and M. Farina, "Online nonlinear model predictive control for tethered uavs to perform a safe and constrained maneuver," in *2019 18th European Control Conference (ECC)*, 2019, pp. 3996–4001.

[161] Y. Yan and Y. Mostofi, "To go or not to go: On energy-aware and communication-aware robotic operation," *IEEE Transactions on Control of Network Systems*, vol. 1, no. 3, pp. 218–231, 2014.

[162] D. B. Licea, D. McLernon, M. Ghogho, and S. A. R. Zaidi, "An energy saving robot mobility diversity algorithm for wireless communications," in *21st European Signal Processing Conference (EUSIPCO 2013)*, 2013, pp. 1–5.

[163] D. Bonilla Licea, D. McLernon, and M. Ghogho, "Designing optimal trajectory planners for robotic communications," in *IET Intelligent Signal Processing Conference 2013 (ISP 2013)*, 2013, pp. 1–6.

[164] D. Bonilla Licea, E. Nurellari, and M. Ghogho, "Energy-efficient 3d uav trajectory design for data collection in wireless sensor networks," in *ICASSP 2020 - 2020 IEEE International Conference on Acoustics, Speech and Signal Processing (ICASSP)*, 2020, pp. 8329–8333.

[165] A. Muralidharan and Y. Mostofi, "Path planning for a connectivity seeking robot," in *2017 IEEE Globecom Workshops (GC Wkshps)*, 2017, pp. 1–6.

[166] ———, "Distributed beamforming using mobile robots," in *2016 IEEE International Conference on Acoustics, Speech and Signal Processing (ICASSP)*, 2016, pp. 6385–6389.

[167] D. B. Licea, V. S. Varma, S. Lasaulce, J. Daafouz, and M. Ghogho, "Trajectory planning for energy-efficient vehicles with communications constraints," in *2016 International Conference on Wireless Networks and Mobile Communications (WINCOM)*, 2016, pp. 264–270.

[168] D. B. Licea, V. S. Varma, S. Lasaulce, J. Daafouz, M. Ghogho, and D. McLernon, "Robust trajectory planning for robotic communications under fading channels," in *Ubiquitous Networking*, E. Sabir, A. García Armada, M. Ghogho, and M. Debbah, Eds. Cham: Springer International Publishing, 2017, pp. 450–460.

[169] A. Muralidharan and Y. Mostofi, "Communication-aware robotics: Exploiting motion for communication," *Annual Review of Control, Robotics, and Autonomous Systems*, vol. 4, no. 1, pp. 115–139, 2021. [Online]. Available: <https://doi.org/10.1146/annurev-control-071420-080708>

[170] O. Tekdas and V. Isler, "Robotic routers," in *2008 IEEE International Conference on Robotics and Automation*, 2008, pp. 1513–1518.

[171] H. Oh, H. Shin, S. Kim, P. Ladosz, and W. Chen, "Communication-aware convoy following guidance for uavs in a complex urban environment," in *2016 24th Mediterranean Conference on Control and Automation (MED)*, 2016, pp. 1230–1235.

[172] K. Kim, K. G. Shin, and D. Niculescu, "Mobile autonomous router system for dynamic (re)formation of wireless relay networks," *IEEE Transactions on Mobile Computing*, vol. 12, no. 9, pp. 1828–1841, 2013.

[173] D. Bonilla Licea, E. Nurellari, and M. Ghogho, "Energy balancing for robotic aided clustered wireless sensor networks using mobility diversity algorithms," in *2018 26th European Signal Processing Conference (EUSIPCO)*, 2018, pp. 1815–1819.

[174] J. Liu, P. Tong, X. Wang, B. Bai, and H. Dai, "Uav-aided data collection for information freshness in wireless sensor networks," *IEEE Transactions on Wireless Communications*, vol. 20, no. 4, pp. 2368–2382, 2021.

[175] G. Chen, C. Cheng, X. Xu, and Y. Zeng, "Minimizing the age of information for data collection by cellular-connected uav," *IEEE Transactions on Vehicular Technology*, pp. 1–5, 2023.

[176] L. Chiaravaglio, F. D'andrea Giovanni, R. Choo, F. Cuomo, and S. Colonese, "Joint optimization of area throughput and grid-connected microgeneration in uav-based mobile networks," *IEEE Access*, vol. 7, pp. 69 545–69 558, 2019.

[177] A. Alsharoa, H. Ghazzai, A. Kadri, and A. E. Kamal, "Spatial and temporal management of cellular hetnets with multiple solar powered drones," *IEEE Transactions on Mobile Computing*, vol. 19, no. 4, pp. 954–968, 2020.

[178] W. Burgard, O. Brock, and C. Stachniss, *An Experimental Study of Exploiting Multipath Fading for Robot Communications*. MIT press, 2008, pp. 289–296.

[179] D. Puccinelli and M. Haenggi, "Spatial diversity benefits by means of induced fading," in *2006 3rd Annual IEEE Communications Society on Sensor and Ad Hoc Communications and Networks*, vol. 1, 2006, pp. 128–137.

[180] D. B. Licea, D. McLernon, M. Ghogho, E. Nurellari, and S. A. Raza Zaidi, "Robotic mobility diversity algorithm with continuous search space," in *2018 26th European Signal Processing Conference (EUSIPCO)*, 2018, pp. 702–706.

[181] D. B. Licea, M. Ghogho, D. McLernon, and S. A. R. Zaidi, "Antenna controller for low-latency and high reliability robotic communications over time-varying fading channels," in *2019 27th European Signal Processing Conference (EUSIPCO)*, 2019, pp. 1–5.

[182] G. Geraci, A. Garcia-Rodriguez, L. G. Giordano, D. Lopez-Perez, and E. Bjoernson, "Supporting uav cellular communications through massive mimo," in *2018 IEEE International Conference on Communications Workshops (ICC Workshops)*, 2018, pp. 1–6.

[183] A. Farajzadeh, O. Ercetin, and H. Yanikomeroglu, "Uav data collection over noma backscatter networks: Uav altitude and trajectory optimization," in *ICC 2019 - 2019 IEEE International Conference on Communications (ICC)*, 2019, pp. 1–7.

[184] H. El Hammouti, M. Benjillali, B. Shihada, and M. Alouini, "Learn-as-you-fly: A distributed algorithm for joint 3d placement and user association in multi-uavs networks," *IEEE Transactions on Wireless Communications*, vol. 18, no. 12, pp. 5831–5844, 2019.

[185] L. J. Rodriguez, N. H. Tran, T. Q. Duong, T. Le-Ngoc, M. Elkashlan, and S. Shetty, "Physical layer security in wireless cooperative relay networks: state of the art and beyond," *IEEE Communications Magazine*, vol. 53, no. 12, pp. 32–39, 2015.

[186] X. Sun, D. W. K. Ng, Z. Ding, Y. Xu, and Z. Zhong, "Physical layer security in uav systems: Challenges and opportunities," *IEEE Wireless Communications*, vol. 26, no. 5, pp. 40–47, 2019.

[187] X. Sun, C. Shen, T.-H. Chang, and Z. Zhong, "Joint resource allocation and trajectory design for uav-aided wireless physical layer security," in *2018 IEEE Globecom Workshops (GC Wkshps)*, 2018, pp. 1–6.

[188] X. Sun, C. Shen, D. W. K. Ng, and Z. Zhong, "Robust trajectory and resource allocation design for secure uav-aided communications," in *2019 IEEE International Conference on Communications Workshops (ICC Workshops)*, 2019, pp. 1–6.

[189] A. Li, Q. Wu, and R. Zhang, "Uav-enabled cooperative jamming for improving secrecy of ground wiretap channel," *IEEE Wireless Communications Letters*, vol. 8, no. 1, pp. 181–184, 2019.

[190] Y. Cai, F. Cui, Q. Shi, M. Zhao, and G. Y. Li, "Dual-uav-enabled secure communications: Joint trajectory design and user scheduling," *IEEE Journal on Selected Areas in Communications*, vol. 36, no. 9, pp. 1972–1985, 2018.

[191] Y. Zhou, P. L. Yeoh, H. Chen, Y. Li, R. Schober, L. Zhuo, and B. Vucetic, "Improving physical layer security via a uav friendly jammer for unknown eavesdropper location," *IEEE Transactions on Vehicular Technology*, vol. 67, no. 11, pp. 11 280–11 284, 2018.

[192] C. Liu, J. Lee, and T. Q. S. Quek, "Safeguarding uav communications against full-duplex active eavesdropper," *IEEE Transactions on Wireless Communications*, vol. 18, no. 6, pp. 2919–2931, 2019.